UNIVERSITÀ DEGLI STUDI DI TRIESTE

P.le Europa, 1 – I-34127 – TRIESTE

XX CICLO DEL

DOTTORATO DI RICERCA IN

NANOTECNOLOGIE

ELECTRICAL CHARACTERIZATION OF ORGANIC MONOLAYERS AT THE NANOSCALE: A DIFFERENTIAL SCANNING CONDUCTIVE TIP AFM INVESTIGATION

Dottorando

DENIS SCAINI

Coordinatore del Collegio dei Docenti

Chiar.mo Prof. ***MAURIZIO FERMEGLIA***

(Università di Trieste)

Tutor

Chiar.mo Prof. ***GIACINTO SCOLES***

Relatore

Dott.sa. ***LOREDANA CASALIS***

To Me and You and Everyone We Know

Miranda Joly

Acknowledgement

I am foremost grateful to my advisor, Prof. Giacinto Scoles, for his unlimited support and guidance throughout this work. His encouragement, enthusiasm and integrity provoked me and were essential for the completion of this work. But, most of all, I am very grateful to him for providing me with the freedom to pursue my own ideas with his definite support.

I would like to express my deepest gratitude to my co-advisor, Dr. Loredana Casalis, for her suggestions, confidence and support. I am truly grateful to her for helpful discussions and encouragement whenever I struggled with some difficulties. I also thank Prof. Sandro Scandolo for helpful discussions.

The members of the group, Dr. Robert Hudej, Dr. Christian Grunwald, Fabian Herberg, Matteo Castronovo, Martina Dell'Angela, Elham Mirmomtaz, Fouzia Bano, Mauro Melli, Barbara Sanavio, Francesca Toma were an amazing source of knowledge, enthusiasm and fun.

I am also thankful to our collaborators, Dr. Marco Lazzarino, Dr. Silvano De Franceschi and Dr. Jian Liang for helpful discussions.

Most of all, my deepest gratitude goes to my parents and my sister for their abundant love and support and guidance. It is only with their wide and complete confidence in me that I could manage to complete this work and have a pleasant stay in Trieste. For all this, I will always be obliged to them.

Special thanks to my friends, in particular to Luca, Marco, Cristina, Cornelia, Alessia and Elisabetta, for their lively company and boundless support. I never forget the opportunity to enjoy life with them. They gave me the strength to face hard times and always made me feel at home.

Abstract

CT-AFM (Conductive Tip AFM) is commonly used for electrical characterization of organic and inorganic surface systems. Understanding electron transfer at the molecular level may lead to the development of molecular assemblies with unique properties and is of great importance for the advancement of both organic, molecular and bio-electronics. In this work we follow an approach to the study of Metal-molecule-Metal surface junctions that uses a combination of different AFM-based techniques. We first use nanografting to build nanopatches of the molecules of interest into a hosting reference self assembled monolayer (SAM) typically made of alkane and aromatic thiols. After the tip is changed to a conductive one, CT-AFM is used to characterize electrically the whole system recording, at the same time, the system topography. Some of the advantages of this approach are the possibility to build and study a wide range of different monolayers side-by-side on the same sample and the in-situ control of the quality both of the hosting monolayer and that of the grafted patches. Results will be presented on saturated and unsaturated thiols self-assembled and nanografted on Au(111) surfaces. We will also show a clear correlation between the contrast in current images and the quality of molecular packing inside the nanopatches.

Table of Contents

1 Introduction

Introduction

Self-Assembled Monolayers (SAMs) are organic thin films grown on different substrates using molecules with an active head group that has high vertical affinity to the surface but high lateral mobility that allows the lateral packing of the molecules to be stabilized by intermolecular van der Waals forces. Many SAMs on different surfaces have been prepared and investigated, among which monolayers of alkanethiol radicals on gold are probably the most intensively studied to date.[1] [2-3]

Proved and potential applications of SAMs include their use as resist to protect underlying substrates from etching or corrosion;[4] as coating agent to prevent aggregation of nanoparticles; [5] as well-defined, controllable, mask for lithographic techniques with nanometer scale resolution;[6] to modify the wettability and other surface properties;[7-8] as building blocks for fabricating surface-bound architectures, such as biosensors,[9] nanoelectronic devices[10] and, finally, as substrates for crystallization.[11]

Many spectroscopic and microscopic techniques have been applied to studying SAMs, including X-ray photoelectron spectroscopy,[12] infrared spectroscopy,[13] high-resolution electron energy loss spectroscopy,[14] near-edge X-ray adsorption fine structure spectroscopy,[15] low energy electron diffraction,[16] mass spectroscopy,[17] electrochemistry,[18] NMR spectroscopy,[19] helium scattering[20] and scanning probe miscroscopy.[21] These methods, with various viewing angles, can explore into the structures, growth kinetics, and chemical reactions of SAMs from the macroscopic scale down to the molecular level.

Standing out from the many techniques mentioned above, scanning probe microscopy (SPM), including scanning tunneling microscopy (STM) and atomic force microscopy (AFM), has been one of the most popular methods to characterize SAMs. The strength of SPM is its capability of imaging and manipulating surface structures at nanometer scale or even at the atomic/molecular scale *in-situ*. STM, probing into the local density of states on the sample surface,[22] usually offers better spatial resolution than AFM because interaction (the tunneling current) is localized at the outmost atom of the tip and, moreover, because the strong dependency of tunneling current versus tip/sample distance. However, AFM can explore into many force-related properties such long range electrostatic and magnetic forces exerted by the surface,[23] short-range adhesive forces,[24] elasticity and plasticity,[25] charge transport,[26] polarizability[27] and thermal characterization and stimulation[28] are only some of the possible branch of application of AFM on surfaces. Besides, AFM does not require conductive samples, which results in its flexibility of examining various samples in different environments.

It is worth noting that when the AFM tip is coated with metal thin film and can measure the tunneling current through the tip-sample gap, AFM is called conductive-tip AFM (CT-AFM). Unlike STM, in which tunneling current is used as the feedback signal to control the movement of the piezo, CP-AFM is still an AFM based technique because the force between the sample and the tip (i.e. the cantilever deflection) is detected during scanning and used in the feedback loop. That means the measured signal (current in CT-AFM) and the feedback signal are, in this case, independent.

Understanding charge transport at the molecular level is of crucial importance for developing molecular assemblies with uncommon properties for novel applications, such as molecular

electronic devices and sensors.[22,29-30] Precise measurements of the charge transport and tunneling at the contacts and through the molecules are likely to provide crucial insight into the electronic couplings within and between molecules and with the interface[30]. While, after Ratner's pioneering work in 1974,[31] this field has made steady progress, the direct measurement of the electrical characteristics of individual molecules is still very problematic.[32] The possible applications that this work may have in the field of drug detection and health care are, however, strongly pushing for progress in molecular electronics studies.

One of the basic questions that has remained open is about the mechanism through which charge is transported through molecules. Although the charge transport mechanism may be very different from the well-established ones for metals and semiconductors,[33] experimentally measuring the "conductance" of molecules follows the well established procedure, in which the molecules are bridged between two electrodes, and then a bias is added to the electrodes and the current passing through the junction is measured.[34] Strategies for fabricating M-m-M junctions include assembling of molecules into metal-capped nanopores[35-36] or between a semiconductor surface and a mercury drop.[37-38] Also, mechanically controlled break junctions[39-41] and nanofabricated electrodes[42] or crossed wires[43] have been used. Of particular interest is the use of the metallic tip of a scanning probe microscope to form and characterize M-m-M junctions.[26,44-46]

All the methods can be classified into two categories. The first is for measuring *single* molecule conductivity,[40,47][44] while the second is aiming at measuring conductance of molecular *assemblies*,[33-34] typically the small number of molecules within the contact region of two electrodes. In single-molecule conductivity measurement, inserting and confirming the only molecule between the two electrodes has been, and perhaps still is, a huge challenge to the scientists.[40,47-48] Besides, there has been evidence that the molecular conformation can dramatically affect on the measured current intensities.[49-50] To obtain the reliable value of conductivity for a single molecule, the measurements have to be repeated hundred of thousand of times to start a reliable statistical analysis.[40] On the other hand, measuring the SAM conductance under AFM tip contact area involves hundred to thousand molecules whose conformation is stabilized by the intermolecular van der Waals forces. The reproducibility of the results in the

same experimental setup is usually better than the single molecule measurement because it is actually averaging over a large number of molecules in each measurement. However, when measuring the SAM conductivity, precisely determining the number of molecules involved remains problematic.

SPM, including STM and conductive-tip atomic force microscopy (CT-AFM), has been widely used to explore the transport of charge through SAMs.[45,51-53] In these experiments the metallic substrate and the conductive probe act as the two electrodes. By adding a small bias to the electrodes and measuring the current tunneling through the gap filled with the organic medium, the conductivity of the nanometer scale Metal-molecule-Metal junction is obtained. This experimental setup is popular because the probe of SPM is intrinsically at nanoscale and does not require lithographic fabrication methods to prepare the nanojunction. Moreover, besides being the electrode, the probe of SPM offers a powerful tool for imaging the sample surface and for many other spectroscopic and microscopic characterizations and lithographic applications. [54-55]

When measuring the electron transport properties of SAMs, however, controlling the nature of the contact between the SPM tip and the SAM is difficult. In particular, the nanometer scale interactions, the contact area (in AFM), and the thickness of the vacuum barrier between the tip and the SAM (in STM) are all quite hard to estimate with good precision. To determine the number and configurations of the molecules in the nanojuncitons and the presence of contaminants covering the tip is very difficult. Molecular dimensions (and so, indirectly, the distance between the two electrodes), molecular HOMO-LUMO energy gaps, molecular ionization potentials, metal work functions, molecule-substrate bonding and functional group architectures, contact properties (i.e., the number of molecules involved), all have a strong impact on the transport characteristics.[56-59] The discrepancies of current-per-molecule values between different CT-AFM data for the same alkanethiol can reach up to three orders of magnitude [34,60] or more and, apparently, cannot be reduced by statistical methods. This is a major issue, not only from the purely experimental point of view but also because it makes the comparison between theory and experiment quite problematic, which is clearly an obstacle to further advances in this field.

Since we still lack an experimental method of measuring the number of molecules involved in the electrical measurements and of describing the tip contact properties with precision, it is difficult to determine the absolute value of each molecule. However, we try to circumvent this difficulty by fabricating two or more SAMs *side-by-side* in the nanometer scale, then measuring their "resistance" in a single experiment, so as to determine their relative current flows. Moreover, simultaneously determined molecular resistances may be used to determine a ratio-dependent property, as the tunneling current decay constant, for homologous molecules.

Nanografting, an AFM based nanolithographic technique which was first introduced by Liu and her co-workers,[61] offers precisely this opportunity. In nanografting, the AFM tip is used to shear away the thiols of the monolayer from the gold substrate by applying a relatively large force load while scanning over a flat region of interest in the presence of molecules different than those of the initial SAM, which are solvated in a neighboring solution.[62-63] As revealed by a lower force scan, a new patch of SAM composed of the new molecules is then formed by exchange of the hydrogen atom from the incoming thiols and the thiol radicals that are being displaced from the surface. Using this method, two or more nanopatches of SAMs composed of different molecules can be placed as close as possible, and their properties can be compared using the same tip and in the same scan. Consequently, the uncertainties induced by the fact that probes may change between two different runs, mentioned above, can be minimized.

After nanografting is performed, a new and, at least initially, clean metal-coated tip (at a given bias voltage with respect to the surface) is scanned above the surface region where adjacent patches of different SAMs are present, so that the current flowing through these monolayers can be recorded in a single experiment in a bidimensional image where color contrast is representative to the amount of flowing current. The current map, together with the topography image, acquired by the conventional AFM laser-deflection feedback, are simultaneously obtained. The topography image differentiates the two molecules by their heights and the current image differentiates the two molecules by their conductivities. If we use as the reference SAM that hosts nanopatches a well know molecule, as a short alkanethiol, well characterized experimentally and theoretically, all obtained value of current or resistance may be referred to it. This allows to normalize all the data using the reference matrix removing from the measurements the

contribution of the tip/molecules contact. In particular the unknown contamination state of the tip will be overcome.

There is evidence in the literature[61,64] that nanografting can accelerate the kinetics of SAM growth and prepare SAMs with fewer defects than those prepared by self-assembly. Moreover, numerous experiments confirm that molecules in SAMs fabricated by nanografting assume well-predictable conformations.[65] As reliable absolute topographic measurements on SAMs are difficult due to the intrinsic lack of a reference level, the matrix (the initial SAM) in nanografting provides an easily available reference height for this type of measurements. The topography images, through which the vertical height of the molecules in the SAMs can be deduced, play a crucial role in determining the conformation of the molecules and the following current measurement because the conductivity is extremely sensitive to the molecular conformation. For instance, the vertical (standing-up) configuration of molecules ensures that the electron transport goes through the backbone (long axis) of the molecules. If the molecules adopt a lying-down conformation on the surface, the resulting current can be totally different. Zhao et al.[66-67] have prepared nano-sized patterns by adding a sufficient bias to the conductive tip to remove the molecules in the initial SAM and fill in the new ones, followed by measurements of the conductivity distribution and current-bias relation by the CP-AFM in solution. But the height of their patterns did not agree well with a close-packed SAM model so the results are not quite conclusive.

Unlike those experiments in which new molecules were inserted into an existing monolayer by exchange reactions, nanografting, however, is a better nanolithographic method which can offer well-addressable control of the molecules and can make monolayers of at least the same quality as that prepared by self-assembly. In our experiments, multiple patches are made and their topographic images are collected and analyzed to ensure the molecules in the monolayers are forming a “standing up” instead of a “lying down” phase. Other useful information, such as the frictional images in contact mode AFM are also collected and discussed where necessary.

In summary, nanografting offers the opportunity of comparing various properties of SAMs at the nanoscale. It also offers a versatile method of fixing thiol molecules with observable conformations onto gold surfaces. Taking advantage of this technique, we carried out a series of nanograft-

ing experiments during the past three years to explore the properties of nanostuctured SAMs composed of different molecules, mainly thiols on gold surfaces.[30,46,68-72]

Outline Contents of Chapters 2 to 8

Chapter 2 gives a detailed description of self-assembled monolayers (SAMs) focusing, in particular, on thermodynamic and energetic aspects. The complete procedure used for SAM formation from liquid phase is described. The chapter places particular emphasis on the factors that influence SAM quality as molecular concentration, kind of solvent, immersion time and temperature. Characteristic morphology and structure assumed by molecules on the supporting metallic substrate are also discussed.

In Chapter 3, an introduction to the techniques used in the thesis is presented. After a description about AFM working principle and operative modes, a short excursus on the capability of the instrument to work in many different environments, in particular water, is done. Starting from this, the nanolithographic AFM assisted technique called nanografting is introduced.[62] The capability of this method to immobilize different molecules in highly ordered nanopatch, side-by-side, into a reference SAM is demonstrated. Characterization of the obtained molecular structures is performed using CT-AFM. The advantages of the technique compared with other molecular transport investigations (i.e. STM) are demonstrated. The chapter concludes discussing many variables that influence the real force applied by the tip on the surface.

In Chapter 4 we present a differential approach based on the combination of CT-AFM measurements and AFM-driven nanolithography to the study of Metal-molecule-Metal junctions. By using nanografting, we build nano-patches of alkanethiol molecules of different chain length in a reference matrix made by a self-assembled monolayer of other alkanethiol molecules, and by CT-AFM we measure the transport properties of the different molecules on the same surface with the same tip, simultaneously controlling the morphology of each molecular assembly through AFM topographic images. This method, as shown here, allows for a direct comparison between the values of current measured through the different molecules, eliminating the contribution of the tip-molecule contact resistance to the measurements. The validity of this approach is demonstrated for molecules belonging to the alkanethiol family, for which the tunneling decay constant

β is estimated with unprecedented precision. A model sketching a double bi-layered junction is also proposed to explain the theoretical motivation at the base of differential current measurements.

In Chapter 5, we try to describe the most important factor that shifts the measured current value from the "real" one. There have been many reports in the literature on the current-voltage characteristics of thiol SAMs on gold surfaces. However the published results from different groups are often inconsistent with one another and the underlying causes are not clear. Many factors, including the substrate/tip roughness, degree of order of the SAMs, contaminants on the tip, applied load, contact area and environmental humidity, may play important roles in the electrical measurements. During our experiments, some clues are observed, and described here, which provides valuable insights into the problem.

In Chapter 6, the differential CT-AFM technique on which we focused in Chapter 4 is extended to molecules that don't belong to the same family (non-homologous molecules) such as aliphatic and aromatic thiols. In particular, using a reference SAM layer of a well-characterized molecular family (as the case of alkanethiols) a normalization of electrical properties for all the molecules under investigation is possible. Doing that a value for the resistance of a short aromatic thiol (2-Benzene Ethanethiol) is determined. An indirect comparison of this value with values coming from literature shows that the order of magnitude for resistance is the correct one. Some practical difficulty of obtaining absolute values of "resistance" and about the possibility to extrapolate single molecule values of resistance from "massive" measurements are also discussed at the end of this chapter.

Chapter 7 starts from the evidence that mechanical properties of self-assembled molecules, such as the compressibility of the chains, and electrical properties, as charge transport through them, depend strongly by the molecular packing. The question that will be addressed in this section of the thesis is if the molecular order in a nanografted structure is comparable with that present in a spontaneously formed SAM. To do that, rictional force and conductive tip AFM investigations are performed systematically on different nanografted SAMs. Defects reduction is observable in the nanostructured area compared with the spontaneous formed hosting SAMs. This is an important result as it has allowed to understand why DNA hybridization proceeds unhindered in

dense nanografted patches (results obtained in our laboratory) while it is highly hindered in dense SAMs.

In chapter 8 a summary of the main results coming out from all the work described in this thesis is described along with an outlook on future applications of the CT-AFM technique. Future directions in the fields of surface immobilization of proteins and of the electrophysiology of neurons will be briefly discussed that have, in our opinion, great potential for applications to *in vitro* diagnostics and for fundamental studies in neuroscience.

(For sake of simplicity, the author has opted for gathering all the references at the end of the thesis).

2

Self-Assembled Monolayers of Organic Molecules

1. Self-Assembled Monolayers

Self-assembled monolayers (SAMs) are distinguished from ordinary surfactant monolayers by the fact that one end of the molecule is designed to have a favorable and specific interaction with the surface of interest (substrate). SAMs may be so described as ordered molecular assemblies formed by the spontaneous adsorption of an active surfactant on a surface.

This simple process makes SAMs inherently manufacturable and thus technologically for surface engineering. Although the area is not limited to long-chain molecules, SAMs of functionalized long-chain hydrocarbons are most frequently used as building blocks of supermolecular structures.

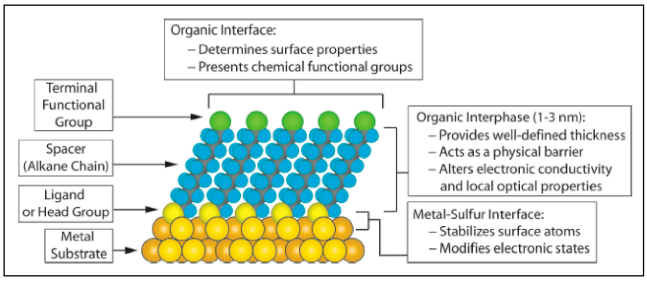

Figure 2.1. Schematic diagram of an ideal, single-crystalline SAM of alkanethiolates supported on a gold surface with a (111) texture. The anatomy and characteristics of the SAM are highlighted.

2. Alkanethiol SAMs on Au(111)

The structure of SAMs and the mechanisms by which they assemble are subjects that have evolved considerably over the past two decades because there have been substantial advances made in the characterization methods. The development of scanning probe microscopy (AFM, STM, etc.) provided powerful new capacities to study both the structural organization of SAMs and the assembly process at a molecular level. These techniques have greatly extended the initial structural understandings derived mainly from spectroscopic techniques (RAIRS, XPS, ellipsometry, etc.) and physical methods (most notably, studies of wetting). High resolution X-Ray diffraction beamlines at new generation synchroton radiation facilities, fully devoted to studies of surfaces and interfaces have been developed in the last 10 years. With such incidence X-Ray diffraction (GIXRD) set-up, new insights into the nature of the SAMs structure have made possible.

SAMs naturally exhibit a high degree of structural order due to the interplay between substrate-head group chemisorption forces and chain-chain long-range attraction forces. However, despite the well defined structure formed by the molecules in the SAM is, from a crystallographic point of view, well known, the true atomistic picture of such organization is still debated, even for the

most extensively studied alkanethiols on Au(111). Only recently, has the role of the underlying Au substrate on the chemisorptio of thiols been realized,[73] and it is now clear that the presence of adatoms and vacancies plays a crucial role in this process.[73] Defects, both of intrinsic and extrinsic types, are present in the SAM at the thermodynamic equilibrium. Dynamic aspects of SAMs that need to be taken into account are coverage-driven ordering transitions, conformational isomerism, lateral diffusion, and environmentally responsive reconstructions of them. The mechanisms of formation of SAMs and the limiting structures obtained by both solution and gas-phase adsorption have been studied extensively. The literature on the structural and physical characterization of SAMs and the structural evolution during assembly has been described in several excellent reviews.[74-75] The general understanding provided in the extensive body of work on SAMs of thiols on metals is summarized here; in particular, we emphasize some of the unresolved questions regarding the structure and dynamics of SAMs and discuss the intrinsic and extrinsic elements that complicate the common representation of SAMs. The discussion begins most naturally with the chemistry of the metal-sulfur bonding interactions.

Nature of the Gold-SAM Interface

Most SAMs of practical interest are formed at a reactive interface, that is, the adsorbate and the substrate undergo a reaction that lead to the formation of the SAM. The chemistry involved for the chemisorption of thiols on gold is, in principle, the most straightforward but remains the most enigmatic. Even less is known about SAM formation from organosulfur compounds (thiols, disulfides, sulfides) on other metals, such as palladium, silver, copper, and mercury. All these systems have been studied in some detail, but each metal has a different structural surface chemistry and a different reactivity toward organosulfur compounds. These variations impact the assembly process in significant ways and lead to a variety of structures. The structural details of the metal-sulfur interface are only understood in qualitative terms at a level that makes it possible to rationalize many of the details seen in the organizations of the organic groups they support. Consideration of the bonding arrangements formed at the metal-sulfur interfaces for several representative examples does suggest, however, a common motif: SAM molecules tend to adopt structural arrangements that are similar to simple adlayer structures formed by elemental sulfur on that metal.[76-77] We provide here an analysis of the stabilization energy for gold-sulfur

bonds and a brief summary of the current knowledge regarding the structural ordering for SAMs of n-alkanethiolates on gold.

Thermodynamic Analysis of Gold-Thiolate Bonds

The formation of a thiolate requires the chemical activation of the S-H bond of the thiol (or the S-S bond of the disulfide). The energetics involved in this bond activation (the bonding energy between the adsorbate molecules of the SAM and the gold substrate) were first examined in studies carried out in 1987: using temperature-programmed desorption as a kinetic measure of the SAM binding energy, Dubois et al. established that the adsorption of dimethyl disulfide on Au(111) occurs dissociatively.[78] The reaction is fully reversible, and recombinative desorption of the disulfide is an activated process with a barrier lying near 30 kcal/mol. This energy suggests that a fairly significant degree of charge transfer to sulfur must occur in the thiolates, an inference that has been supported by the results of theoretical calculations.[79] Using different experimental protocols, Scoles and co-workers also investigated the bonding energies of various organosulfur adsorbates on Au, and their studies suggest, for the case of SAMs involving thiolate structures, bonding energies similar to those cited above.[80] Other kinetic treatments reveal the complex nature of the thermodynamics of the metal-sulfur bonding interactions. For example, Whitesides et al. and Liu and co-workers both reported the results of desorption experiments that employed SAMs immersed in a solvent.[81-82] The kinetics of these processes can be modeled using conventional rate equations, and these models suggest barriers for desorption that are somewhat lower than the values obtained from desorption rate measurements made in UHV (~20÷25 kcal/mol). Schlenoff et al. used electrochemical measurements to provide a detailed analysis of the thiol/thiolate/disulfide bond energies and desorption barriers for SAMs on gold.[83] Of particular interest was the estimation that the barrier for the bimolecular recombinative desorption of an alkanethiolate from a SAM on gold in the form of a dialkyl disulfide is ~15 kcal/mol. This value is approximately a factor of 2 less than that deduced in the gas-phase studies. We note here, though, that the two energies are not directly comparable given that one also contains contributions from the heats of dissolution of the adsorbate as well as the heat of immersion of the substrate in the solvent. The latter energies can, in fact, be quite large; for example, the segmental heat of interaction of a hydrocarbon on gold is ~1.5 kcal/ mol for a methylene group. In this context, the range of reported values appears to be one that follows

directly from the different forms of the measurements used to assess the strength of the Au-S bonding interaction. As the vacuum measurements are most easily interpreted, we believe it is reasonable to conclude that the Au-S bond that anchors the SAM is, in fact, a reasonably strong one (Au-S bond strength on the order of ca. 50 kcal/mol).

Where does the Hydrogen Go?

The fate of the hydrogen of the S-H groups still has not been determined unambiguously. It seems probable that adsorption in a vacuum leads to loss of the hydrogen in the form of dihydrogen. The reductive elimination of H_2 from Au(111) is a weakly activated process. In solution, another possibility exists. If the thiol hydrogen is not lost in the form of H_2, the presence of oxygen in the reaction medium might also lead to its oxidative conversion to water. In either case, the Au-S bonding interaction in the thiolate is sufficient to retain the chains at the surface in a durable fashion and preclude a recombinative desorption of a disulfide product at room temperature.

Surface Structure of Aliphatic and Aromatic Thiolates on Gold

High-coverage thiol phases on Au(111) are generally accepted to form a (√3×√3)R30° with respect to the underlying Au.[1,74,84-85] The literature also strongly confirms that this organization adopts a superstructure of the (√3×√3), namely a c(4×2) superlattice.[85-86]

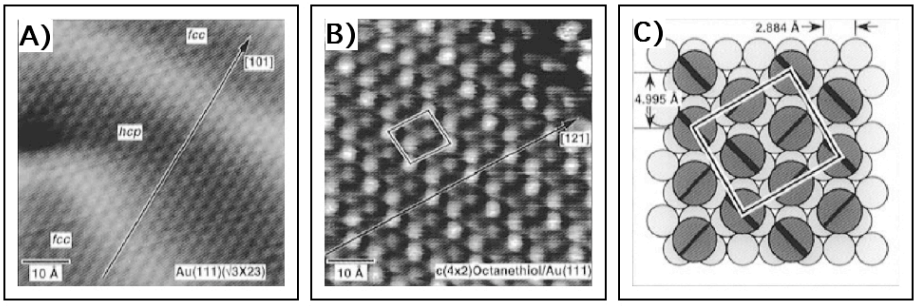

Figure 2.2. (A) Constant-current STM topograph of reconstructed Au(111) surface showing quasi-hexagonal arrangement of Au atoms and bright ridges due to variations in registry between surface and subsurface layers. Atomic rows deviate from linearity due to partial stacking fault in hcp regions (ABA stacking). (B) Constant-current STM topograph of octanethiol monolayer on Au(111). Au reconstruction is lifted and alkanethiols adopt commensurate crystalline lattice characteriized by a c(4×2) superlattice of a (√3×√3)R30°. (C) Model of commensuration condition between alkanethiol monolayer (large circles) and bulk-terminated Au surface (small circles). Diagonal slash in large circles represents azimuthal orientation of plane defined by all-trans hydrocarbon chain.

Figure 2.2B shows this structure schematically. The SAMs formed by n-alkanethiols were originally described as thiolate overlayers (chemisorbed structures formed by the activation of the S-H bond at the gold surface).[78] Diffraction experiments and STM imaging suggested a structure involving some degree of S-S bonding between pairs of adjacent adsorbates on the surface of the gold (a disulfide model).[87] Alternative interpretations have been presented, and this quasi-disulfide model has now been largely abandoned in favor of the original thiolate model.[79] The latter is a simple adlayer model of the Au-S bonding interactions. Within this model there has been considerable discussion of the surface sites involved in this bonding.[87] Bonding of the thiolates at both 3-fold hollows and bridge sites has been suggested on the basis of both experiment and theory.[88] More recently, experimental works have identified on-top and quasi-on-top adsorption sites as preferred sites,[73] while the 3-fold hollow site has been generally abandoned. This aspect of the structure is still debated as of this writing.

Mechanisms of Assembly

SAMs can form from either liquid or vapor phase. Films created by vapour phase (e.g. molecular beam) deposition of thiols on gold share many structural characteristics with solution-deposited films. Studies on these films have the advantages of ultra-high-vacuum (UHV) substrate cleanliness and the availability of traditional in situ surface characterization techniques. On the other hand assembly from solution on the laboratory bench is convenient and sufficient for most applications of SAMs, especially for those requiring contact with other solution in subsequent experiments (for example, support for cell culture, wetting studies, AFM assisted nanolithography[89]). For the purposes of the work presented in this thesis, only solution prepared SAMs are taken under consideration.

Bulk Transport and Adsorption

Many processes are involved in SAM growth. A first step is clearly the solution-phase transport of adsorbate molecules to the solid-liquid interface, which can involve some combination of diffusive and convective transport. This is followed by adsorption on the substrate with some adsorption rate (related to a "sticking" probability). The overall adsorption dynamics may be diffusion-controlled, adsorption-rate controlled, or in an intermediate mixed-kinetic regime. This part of the self-assembly process is closely related to the adsorption of surface-active molecules at the liquid-vapor interface, an area that has been thoroughly studied. Although the typical quantity of interest at the liquid-vapor interface is surface tension rather than surface concentration (or coverage), the two quantities are related by the surface equation of state. In fact, most dynamic adsorption models are actually written in terms of surface concentration and translated into dynamic surface tension predictions, using an equation of state determined by applying the Gibbs equation to equilibrium surface tension data. The dynamics of surfactant adsorption were thoroughly reviewed by Chang and Franses,[90] and most of the mathematical development presented by them is directly relevant to the initial adsorption stage of SAM formation.

Self-Organization on the Surface

During the formation of SAMs there is an evolution of the molecular order as adsorption progresses and the surface coverage increases. For example, the very early stages of adsorption can be pictured as isolated adsorbed molecules, conformationally disordered and randomly distributed on the substrate. The final film involves close-packed adsorbate molecules with relatively uniform molecular orientation and conformation. Although one might imagine a continuous path from the former structure to the latter, experimental evidence points to a step-wise process that can be thought of as an isothermal path through a quasi-equilibrium 2D-phase diagram like the one schematically illustrated in Figure 2.3. Possible states alluded to in this phase diagram include (a) a low-density "vapor" phase in which isolated, mobile adsorbate molecules are randomly deposited on the surface, (b) an intermediate-density phase that could involve conformationally disordered molecules or ones lying flat on the surface, and (c) a final, high-density "solid" phase in which the molecules are conformationally ordered, close packed, and standing approximately normal to the surface plane with a possible polar tilt angle of about $\leq 30°$. As discussed below, other states are, of course, possible.

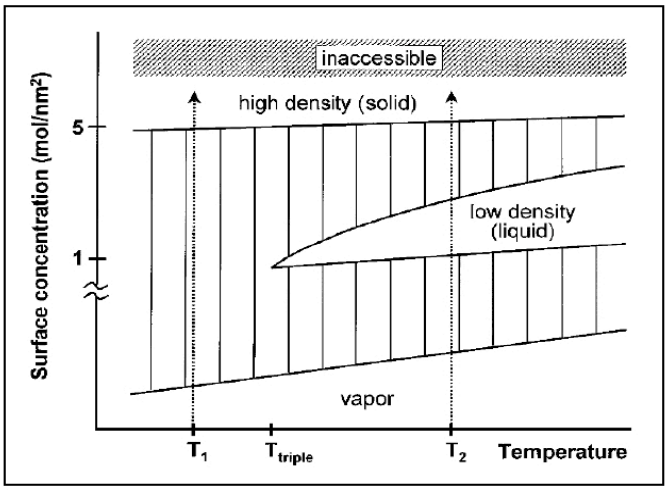

Figure 2.3. Schematic quasi-equilibrium 2D-phase diagram for a generic SAM system. The dotted lines represent hypothetical isothermal paths of SAM growth at temperatures below (*T1*) and above (*T2*), the triple point (T_{triple}).

In a hypothetical situation in which the adsorption rate is much slower than any other process, the monolayer system would follow the equilibrium phase diagram. There are two qualitatively different growth processes suggested by the lines at temperatures *T1* and *T2* in Figure 2.3, below

and above the triple point respectively. If the temperature is lower than the triple point (e.g. *T1*), the growth sequence will be similar to the one shown in Figure 2.4A. Initially, adsorbed molecules will form a dilute 2D-vapor phase. At a relatively low surface concentration, the monolayer will enter a coexistence region between the vapor and the high-density condensed (solid) phase. Domains (islands) of solid phase will nucleate and grow, surrounded by isolated adsorbate molecules in the vapor phase. Eventually, these domains will grow to cover the entire substrate. This mechanism is analogous to the three dimensional (3D) process of crystal nucleation and growth from a vapor phase precursor, and the 2D scenario is typical for epitaxial film growth from the vapor phase (e.g. molecular-beam epitaxy). At a temperature above the triple point (e.g. *T2* in Figure 2.3), a more complicated progression will occur as illustrated in Figure 4B. When the vapor phase reaches a certain surface concentration, islands of an intermediate, low-density condensed phase will nucleate and grow. This phase may be a disordered 2D-liquid phase or an ordered phase with lower density than the solid phase (e.g. a "lying-down" phase where the molecular axis is parallel to the surface plane). Eventually the vapor phase is completely converted to the low-density condensed phase. As adsorption continues, a second transition occurs involving nucleation, growth, coalescence, etc, of solid-phase islands surrounded by the low-density condensed phase. Note that, at any temperature, a snapshot of an incomplete film during growth will often involve islands of one phase surrounded by another, in particular, islands of solid phase surrounded by either liquid or vapor phase. It is important to recognize that the picture painted in the previous paragraph is somewhat oversimplified. For example, the adsorption rate will not always be much slower than other surface processes, and, therefore, partial monolayers may be quite far from equilibrium. If the nucleation and growth of condensed-phase domains do not keep up with the deposition rate, the less condensed phase will become "super concentrated" (i.e. it will have a density greater than the equilibrium coexistence concentration), and, thus, its density may vary considerably during the growth of the more condensed phase. This behavior is well known in vapor phase thin-film deposition, where the surface concentration of free adsorbate atoms is understood to vary during island nucleation and growth, and is likely to occur during SAM growth at ambient conditions as well. However, the surface concentration in the vapor phase will always be small and amount to a negligible fraction of the molecules on the surface. In the case of a 2D-liquid phase, however, the surface density is not negligible, and,

in fact, the film thickness is directly related to the surface concentration. Therefore, variation of the surface density in a 2D liquid in coexistence with solid-phase islands will have a significant effect on the appearance of the partial-monolayer film.

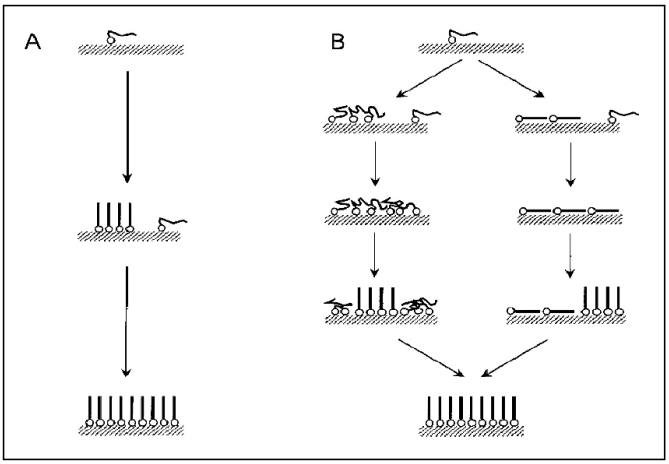

Figure 2.4. Cartoons depicting typical sequences of a self-assembled monolayer structure during growth below (A) and above (B) a triple point like that shown in Figure 2.3. (A) Below the triple point, growth proceeds from a 2D-vapor phase, through a solid-vapor coexistence region, to the solid phase. (B) Above the triple point, the SAM must pass through three phases and two coexistence regions. The intermediate low-density phase may be disordered (liquid) phase, a "lying-down" phase, etc.

The molecules used to create SAMs have numerous degrees of freedom, and, therefore, it is quite possible that the equilibrium phase diagram could be more complicated and involve a greater number of condensed phases than implied in Figure 2.3. It could include a lying-down phase and a disordered-liquid phase, for example. However, there are numerous other possibilities. Langmuir monolayers of long-chain fatty acids, for example, are known to display a variety of liquid crystalline and crystalline phases [91] that differ in the polar tilt angle, the azimuthal direction of molecular tilt (i.e. nearest-neighbor *vs.* next-nearest-neighbor direction), and rotational freedom (herringbone *vs.* rotator). To date there is no firm experimental evidence for liquid-crystalline phases, transient or equilibrium, in SAMs. Given their ubiquity in Langmuir monolayers and Langmuir-Blodgett films, however, one would not be surprised if they were observed in SAMs with the appropriate experimental studies. Therefore, although it is certainly overly simplistic, the phase diagram of Figure 2.3 will be used as a conceptual framework to describe the experimentally observed growth mechanisms of various SAM systems discussed in the following sections. Two general experimental strategies have been used to study monolayer

growth: (a) in situ studies under actual deposition conditions in real time and (b) studies on quenched partial monolayers removed from solution and possibly rinsed to remove loosely attached adsorbate molecules. Although in situ experiments have become increasingly important in recent years, many publications in the literature report experiments that used quenched films. The clear advantage of in situ experiments is that one avoids the issue of whether the film structure is altered by the quenching process. This is not a trivial matter, since there is clear evidence that quenching can alter the film coverage and morphology in some molecular systems. On the other hand, working with quenched films permits the use of certain techniques not applicable *in situ*, such as contact angle and X-Ray photoelectron spectroscopy. Furthermore, one can work over a longer range of time scales (i.e. concentrations). Although experiments on quenched films often report reliable and useful information (particularly on qualitative issues), one must view subtle quantitative conclusions based on quenched films with appropriate skepticism until they are confirmed by more direct experiments.

Chain Length Effects

The literature is full of dramatically conflicting reports regarding the effects of chain length on thiol SAM growth kinetics. Regarding the initial fast stage of growth, Bain et al[81] found that C18 grew faster than C10 from ethanolic solution, Xu and coworkers[92] reported that C22 formed more quickly than C18 from 2-butanol solution, and Jung and Campbell[93] performed a systematic SPR study and found that the growth rate increased with chain lengths in the range C2-C18 from ethanolic solution. Thus, these studies consistently found that adsorption rate increased with chain length. Other studies reported exactly the opposite trend, however. Peterlinz and Georgiadis[94] reported growth rates for the initial step in the order C8>C12>C16>C18 from ethanolic solution, and Dannenberger et al[95] found that growth rates obeyed the trend C4>C12>C22 for both ethanolic and hexane solution. Complicating the matter even further, two additional reports were inconsistent with all of these results. DeBono and co-workers[96] found that the initial stages of growth for C16 thiol occurred at about the same rate as C6 and that both were faster than C12 from ethanolic solution. Karpovich and Blanchard found that the early stages of growth for C8 and C18 thiols (from hexane solution) were approximately equal in overall rate. Analyzing the concentration dependence of the growth kinetics, they reported that

the adsorption rate for C18 was greater than that for C8, but that the desorption rates had the opposite behavior. There is also some confusion regarding the chain length dependence of the later slow-growth regime. Peterlinz and Georgiadis[94] reported that the rate of this process increased with chain length from C12 to C16 to C18. DeBono et al[96] also found that C16 was faster than C12, but they observed that the trend was reversed for C6, which was equally as fast as C16. There is, unfortunately, little basis on which to critically analyze these results. The discrepancies do not divide along the lines of experimental technique, solvent, concentration range, or any other obvious parameter. In addition, it is not intuitively clear which trend should be correct for a given regime. In considering a hypothetical activated process for adsorption, one might think that the enhanced interactions between a longer chain and the surface would lower the energy barrier and increase the adsorption rate.[93] On the other hand, if mobility is an issue, longer chains might move more slowly. It is clear that none of the results summarized above are dominated by bulk solution-phase molecular diffusion because of the absolute rates, the details of the time dependence, and the concentration dependence of the rate constants. However, one cannot rule out the importance of molecular mobility in moving through a hypothetical phys-isorbed layer,[94-95] etc.

Adsorption Energy

Several approaches have been used to get at the energetics of thiol SAMs. Bain et al[81] determined desorption rates of alkanethiol SAMs into hexadecane at 83 °C. Assuming an Arrhenius-type expression, they found that the activation energy for desorption increased by ~0.2 kcal/mol for each methylene group. Their estimate for the absolute activation energy for C22 thiol was 28 kcal/mol. Jung and Campbell[93] determined the "sticking probabilities" of various-chain-length thiols by analyzing the observed SAM growth kinetics with a model incorporating molecular diffusion in solution and adsorption from the subsurface layer. Again assuming an activated energy process for adsorption, they reported that the activation free energy for adsorption decreased by ~0.16 kcal/mol per methylene group and that the absolute activation extrapolated to ~11 kcal/mol for zero chain length. The Blanchard group[97] determined the free energy of adsorption, ΔG_{ads}, of C8 and C18 thiols by analyzing the concentration dependence of the observed growth rate constant. They found that ΔG_{ads} = -5.5 kcal/mol for C18 and -4.4

kcal/mol for C8 thiol SAMs. By measuring the temperature dependence of ΔG_{ads} for C18, they found the molar enthalpy of adsorption, ΔH_{ads} = 48 kcal/mol, and the entropy of adsorption, ΔS_{ads} = -48 cal $mol^{-1} K^{-1}$. It should be noted that these measurements are not completely consistent. For example, one would expect that ΔG_{ads} should be approximately the difference between the activation energies for desorption and adsorption. Using the values from the above references, this would give approximately $\Delta G_{ads} \approx 8 \div 27 = -19$ kcal/mol for C18 thiol compared with the -5.5 kcal/mol quoted by Karpovich et al.[97] However, these absolute free energies involve an approximate value of the pre-exponential frequency factor in the Arrhenius expression and are, therefore, somewhat arbitrary. Considering the change with chain length, one finds that the activation energy measurements predict that longer chains will be stabilized by approximately 0.2 + 0.16 = 0.36 kcal/mol per methylene group. This predicts that ΔG_{ads} for C18 should be 3.5 kcal/mol lower than that for C8, whereas the value quoted is only 1.1 kcal/mol lower. Of course, there were numerous simplifications in the analyses, not least of which was the assumption of Arrhenius-like behavior in experiments performed at only one temperature.[81,93] SAM energetics should be a fruitful area for future work.

Defects in SAMs

Because they form by self-assembly, that is, because they adopt adsorbed structures that are directed by the thermodynamics of a reasonably complex chemisorption process, SAMs provide, in theory, convenient access to highly ordered organic interfaces whose molecular and aggregate structures can be varied by principles of rational design. The structures of SAMs are generally regarded as if they contained few defects. A point of fact, they are substantially more complex than the highly ordered arrangements that are commonly assumed (Figure 2.5).

The causes of defects in SAMs are both intrinsic and extrinsic: external factors, such as cleanliness of the substrate, methods for preparing the substrates, and purity of the solution of adsorbates, are responsible for some defects in SAMs, but some result simply because SAMs are, in fact, *dynamic* systems with complex phase behaviors.

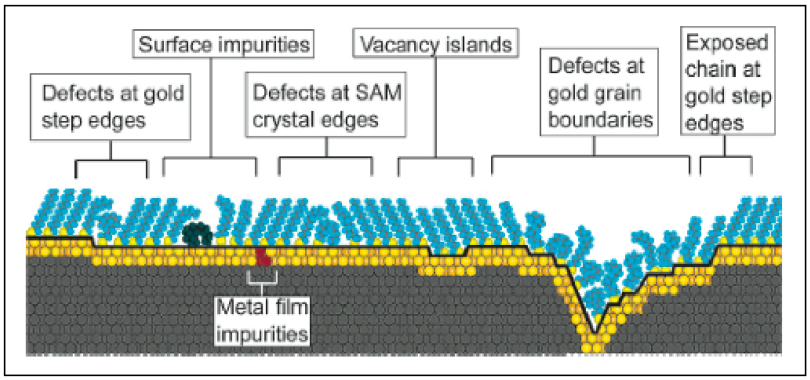

Figure 2.5. Schematic illustration of some of the intrinsic and extrinsic defects found in SAMs formed on poly-crystalline substrates. The dark line at the metal-sulfur interface is a visual guide for the reader and indicates the changing topography of the substrate itself.

Defects Caused by Variations in the Surface of the Substrate

The substrates on which SAMs form are replete with many structural defects. Polycrystalline gold substratessa system that has been a benchmark choice for much of the published work in the fields present a grain structure characterized by dense arrangements of intergrain boundaries, faceting, occlusions, twins, and other gross structural irregularities. Even for samples that present a strong (111) texture misalignments are common as are other low-index crystallographic textures. All metal substrates also have a varying density of atomic steps, and these in turn impact the structures and defect content of SAMs as judged by numerous STM studies.[84-85,88]

Reconstruction of the Surface During Assembly

One type of defect inherent to the formation of SAMs on gold is monatomic vacancies, that is, regions of the SAM offset in height by one (gold) atomic diameter from the surrounding regions. The probable origins of these pit-like defect structures are easily understood by considering the structure of the gold surface prior to adsorption of the SAM. A clean Au(111) surface normally exhibits a $(23\times\sqrt{3})$ reconstruction; the surface density of gold atoms in this reconstruction is greater than that on the ideal (111) plane.[98] The adsorption of thiols onto the bare gold surface lifts the reconstruction and induces a change in the atom density at the surface. The relaxation of the surface is achieved via the formation of single-atom vacancies; these defects subsequently nucleate and grow into large vacancy "islands" that are seen in STM studies.[84,98] The topography of SAMs faithfully replicate the topography of these defects and, for interfacial properties that are sensitive to them, cannot fully obviate their impacts. Such effects, for example, are strongly evident in electrochemical studies and probably complicate the structures used in studies of molecular electronics as well.

Composition of the SAMs

In simple terms, the formation of a SAM is a form of chemical selection. The assembly process involves a thermodynamic equilibrium between adsorbates on the surface and their precursors free in solution. The composition of a SAM must reflect, therefore, a concentration-dependent binding of the most strongly interacting adsorbate species present in the solution (or gas vapor) used to prepare it. Impurities in solvents and reagents can thus complicate both the kinetics of formation and the final structure of a SAM. These defects are extrinsic, and careful control of experimental methods can minimize them.

SAMs present other types of defects that are less well appreciated than are those related to the characteristics of the substrates or the purity of the adsorbates used to prepare them. These are the defects that are intrinsic to the dynamic nature of the SAM itself.[99-100] In this regard, one must consider both the intrinsic structural (i.e., phase) dynamics of the SAM and the thermodynamically imposed constraints to its stability. The latter issue is one that is easily understood. SAMs form via a thermodynamically driven assembly of an adsorbate at a surface/interface. Where the adsorbate-substrate interaction is sufficiently strong (as for the case of the prototypi-

cal layers formed by alkanethiols on gold), the SAM may be safely removed from the solution used to prepare it and studied or used further. Although these SAMs may be kinetically stable in the absence of a flux of adsorbate, the high coverage of the adsorbate present in the SAM is, in fact, thermodynamically unstable. Only in a case where the rate of desorption is rigorously zero would the SAM be expected to exist for an indeterminate period outside the solution used to prepare it.

The unique aspects of the systems that have attracted wide attention in studies of SAMs are the essential abilities of the best adsorbate-substrate pairings to resist the competitive binding of impurities at the interface and their substantial stabilities with respect to thermal desorption or displacement by other chemical species. This stability is, however, one that is limited by the finite strength of the metal-sulfur bond and by the susceptibility of the simplest thiolate systems toward decomposition (whether via oxidative degradation or other dissociative pathways) reactions that are sensitive to the ambients in which the SAMs are used. Still, the main concern for stability remains desorption. For simple SAMs of thiolates on gold, the limit of thermal stability due to desorption is modest but quite useful (especially at room temperature).[101] One also encounters classes of defects that are related to intrinsic dynamics of the organic component of the SAM. The chain dynamics of alkanethiolate SAMs on gold provide an instructive example. First, because the chains of these SAMs are canted (reflecting the gold-sulfur spacings), the chains are subject to a variety of complex phase transitionss thermally driven population of gauche conformers and tilt-order phase transitions are among some of the phase dynamics that have been investigated and used to rationalize aspects of their interfacial properties.[99-100] Order-order phase transitions (such as those involving a posited thermal coexistence of the c(4× 2) and ($\sqrt{3}\times\sqrt{3}$)R30° phases) constitute another example. In yet another example, Grunze interpreted the relative protein-binding affinities of oligo(ethylene glycol) (OEG)-modified SAMs on gold as arising from a coverage-dependent rod-helix ordering transition of the OEG chain end segments.[102] This last example illustrates the subtle interplay of physical features that might serve to modulate the properties of SAMs in a specific application.

Liquid Phase Deposited Thiol Films

Preparation of Thin Metal Films as Substrates for SAMs

Sulfur compounds have a strong affinity to transition metal surfaces. This is probably because of the possibility to form multiple bonds with surface metal clusters. Organosulfur compounds coordinate very strongly to silver, copper, platinum, mercury, iron, colloidal gold particles, GaAs and InP surfaces. However, the most investigated, even not jet completely understood thiolated SAMs are that on Au(111) and in particular thin films of gold supported on silicon wafers, glass, mica, or plastic substrates. These substrates are easy to prepare by physical vapor deposition (PVD) methods (thermal or electron beam evaporation),[103] electrodeposition,[104] or electroless deposition.[105] Anyway, PVD and electrodeposition can generate thin films of a wide range of metals (including gold, silver, copper, palladium, platinum, and nickel) and alloys.

Why is Gold the standard?

The answer to this question has two parts: (1) on gold good (but not uniquely good) SAMs form and (2) it is historically the most studied. In fact, for many applications gold may not be the best substrate. There are at least five characteristics of gold that make it a good choice as a substrate for SAMs. *First*, gold is easy to obtain, both as a thin film and as a colloid. It is straightforward to prepare thin films of gold by physical vapor deposition, sputtering, or electrodeposition. Although expensive and not essential to most studies of SAMs, single crystals are available commercially. *Second*, gold is exceptionally easy to pattern by a combination of lithographic tools (photolithography, micromachining, others) and chemical etchants. *Third*, gold is a reasonably inert metal: it does not oxidize at temperatures below its melting point; it does not react with atmospheric O_2; it does not react with most chemicals. These properties make it possible to handle and manipulate samples under atmospheric conditions instead of under UHV a great practical convenience for conducting experiments that require "dirty" conditions, e.g., microfabrication (outside of a clean room environment) and cell biology. Gold binds thiols with a high affinity,[13] and it does not undergo any unwanted reactions with them, e.g., the formation of a substitutional sulfide interphase. (Because thiols have a high affinity for gold, they also displace adventitious materials from the surface readily.) *Fourth*, thin films of gold are common substrates used for a number of existing spectroscopies and analytical techniques, including SPR spectroscopy, quartz crystal microbalances (QCM), RAIRS, and ellipsometry. This characteristic is particularly useful for applications of SAMs as interfaces for studies in biology. *Fifth*, gold is compatible with cells, that is, cells can adhere and function on gold surfaces without evidence of toxicity. SAMs formed from thiols on gold are stable for periods of days to weeks when in contact with the complex liquid media required for cell studies (see Outlooks).

Thin Films on Mica

Freshly cleaved mica supporting a thin film of metal is a common substrate used as a pseudo-"single crystal" for microscopic studies of SAMs by scanning tunneling microscopy (STM) or atomic force microscopy (AFM).[22,106] Gold films grow epitaxially with a strongly oriented (111) texture on the (100) surface of mica. The films usually are prepared by thermal evaporation of gold at a rate of ~0.1÷0.2 nm/s onto a heated (250÷650 °C) sample of mica. The grain sizes of these films, strongly dependent on rate and temperature values, may be larger than ~1000 nm with flat (111) terraces of more than ~100 nm in width.

A method called template stripping can be easily employed to generate surfaces with roughness <1 nm. [107] In this technique a glass slide or other solid support is glued to the exposed surface of a gold film deposited on mica, and then the gold film is peeled from the mica to expose the surface that had been in direct contact with the mica. Knarr et al. showed that the mechanical shear required to separate these surfaces is large (~1800 mN/m) and induces roughening of the gold surface[108]. Gooding et al. demonstrated that immersion of the mica-gold-support structure into liquid nitrogen cleaved the mica from the surface and produced films with roughness on the order of ~1 nm over areas of ~200×200 nm^2 (measured by STM).[109] Ulman et al. reported another method for reducing the mechanical stress imparted on the gold film during separation. [110] They removed the mica film in an ethanolic solution containing thiol (200 μM), and a SAM formed at the gold/mica interface. The roughness of these surfaces was ~0.3÷0.7 nm (rms), and the advancing and receding contact angles of water on the SAMs were essentially indistinguishable, that is, there was almost no hysteresis (~1÷5°). (The hysteresis measured for SAMs of alkanethiolates prepared on polycrystalline substrates with no additional treatments is 10°÷ 20°).

SAMs Preparation

Adsorption of Alkanethiols from Solution

The most common protocol for preparing SAMs on metals is immersion of a freshly prepared or cleaned substrate into a diluite (~10÷1000 μM) ethanolic solution of thiols for 12÷24 hours at room temperature. This procedure is widely used and originates from early studies of SAMs; the experimental details resulted from a combination of studies designed to optimize the reproducibility of the SAMs.[81] Dense coverage of adsorbates are obtained quickly from millimolar solutions (seconds to minutes), but a slow reorganization process requires times of the order of hours to maximize the density of molecules and minimize the defects in the SAM. There are, however, a number of experimental factors that can affect the structure of the resulting SAM and the rate of formation: type of solvent, temperature, concentration of adsorbate, immersion time, purity of the adsorbate, concentration of oxygen in solution, cleanliness of the substrate, and chain length (or more generally, structure of the adsorbate).

In practice, most experimental conditions for the preparation of SAMs yield organic interfaces with reproducible and desired functional behaviors. These characteristics are acceptable for some applications of SAMs, but fundamental studies of certain materials properties such as wettability, corrosion, tribology, and charge-transfer processes (among others) require an understanding of how to minimize defects in SAMs and maximize order in these systems. The effects that some parameters, such as immersion time, concentration of adsorbate, and chain length, have on the structure and properties of SAMs are known to a small degree, but less is known about others (choice of solvent, temperature). We summarize below the present knowledge determined by specific experiments or empirical evidence about several of these factors.

Factors Effecting SAM Quality

Solvents: Ethanol is the solvent that is most widely used for preparing SAMs however, SAMs formed from solutions of alkanethiols comprising solvents other than ethanol (tetrahydrofuran, dimethylformamide, acetonitrile, cyclooctane, toluene) do not vary significantly from those formed from ethanolic solutions.[81] At least four other factors also contributed to the widespread use of ethanol: it solvates a variety of alkanethiols with varying degrees of polar character and chain length; it is inexpensive; it is available with high purity; and it has low toxicity.

The effects of the choice of a solvent on the kinetics of formation and the mechanism of assembly are complex and poorly understood. Studies on this topic have led to some qualitative understanding of how solvent can affect the assembly process. The presence of a solvent adds additional parameters to the dynamic equilibrium governing the adsorption of thiols: solvent-substrate and solvent-adsorbate interactions complicate the thermodynamics and kinetics of assembly. Solvent-substrate interactions can hinder the rate of adsorption of thiols from solution because the solvent molecules must be displaced from the surface prior to the adsorption of thiols, which are less prevalent in solution than the solvating molecules.

Studies suggest that the rate of formation of SAMs of alkanethiolates is faster in certain non polar solvents (heptane, hexanes) than ethanol.[111] The use of long hydrocarbons, such as dodecane and hexadecane, as solvents reduces the rates of formation to values comparable to those for SAMs from ethanolic solutions.[111] Hydrocarbon solvents may improve the kinetics of formation in some cases, but the strong solvent-adsorbate interactions in these solutions impede the organization of alkanethiols SAMs. Contact angle measurements and electrochemistry suggest that SAMs formed from solutions of thiols in non polar organic solvents are less organized than SAMs formed in ethanol.[81,112] Polar liquids-poor solvents for n-alkanethiols seem to reduce the quantity of some types of defects found in SAMs (conformational arrangements, regions of missing adsorbates) and promote densely packed monolayers.[113] The low solubility of thiols in such solvents and the low segmental heats of adsorption for these solvents (that is, the heat associated with each additional interaction of the solvent molecules with the surface, for example, the heat of adsorption per methylene or alcohol group) probably serve to segregate the thiols at the metal surface and thus more efficiently drive the assembly processes

involving them. SAMs with few conformational and pinhole defects also can form from aqueous solutions containing micelles of ionic or nonionic surfactants.[112] To summarize, the studies of the effects of solvent on the prototypical example of SAMs of alkanethiolates on gold indicate that the choice of solvent clearly is an important parameter for determining the resulting quality of a SAM deposited from solution, but there remains significant challenges in developing a detailed understanding of the complex and dynamic interactions that occur between the solvent, surface, and adsorbates during the formation process.

Temperature: Temperatures above 25 °C can improve the kinetics of SAM formation and reduce the number of defects in them. Elevated temperatures increase the rate of desorption for adventitious materials and solvent molecules physisorbed on the surface and make it possible for the system to cross activation barriers for processes such as chain reorganization and lateral rearrangements of the adsorbates more easily than at room temperature. Uosaki and co-workers suggest that the effect of temperature is particularly relevant during the first few minutes of the formation of a SAM when most of the adsorption and reorganization of the SAM is taking place.[112]

Concentration and Immersion Time: These two parameters are inversely related: low concentrations of thiols in solution require long immersion times.[81] For SAMs formed from alkanethiols on gold, the typical surface density of molecules (when maximum coverage is obtained) is ~4.5×10^{14} molecules/cm^2; thus, the minimum concentration for forming a dense SAM is ~1 μM, or ~6×10^{14} molecules/cm^3. In practice, SAMs formed by immersion for a week in solutions with concentrations at or below 1 μM do not exhibit the same physical properties as those formed from more concentrated solutions.[81] The amount of impurities or other sulfur-containing compounds also can complicate the use of extremely dilute solutions to form SAMs. Most spectroscopic and experimental evidence suggests that the average properties of SAMs formed from n-alkanethiols (wettability, mass coverage, and, to a large extent, the structure deduced by RAIRS) do not change significantly when exposed to ~1 mM solutions of thiols for more than 12÷18 hours. Electrochemistry,[18] STM,[21] and RAIRS[13] indicate, however, that the structure of the SAM can continue to evolve over immersion times of ~7÷10 days. These results imply that the coverage of the surface increases with extended immersion times and suggest that there are two consequences: (1) the number of pinhole defects in the SAMs decreases and (2) the

conformational defects in the alkane chains decrease. The typical time allowed for formation (12÷18 h) is convenient experimentally, but for some applications, formation over many days can improve the reproducibility of subsequent experiments that use the SAM, for example, studies of electron transfer through SAMs.[41,45-46,53,72]

Purity of Solvents and Thiols: Common impurities derived from thiols are disulfides: an oxidation product. Experiments suggest that small amounts of these materials (<5%) do not necessarily impede the formation or alter the structure of the SAM.[81] The disulfides usually are, however, less soluble than their thiol precursors; the reduced solubility can result in physisorption of these materials and alteration of the physical properties of the SAM. Oxidized, polar contaminants (sulfonates, etc.) can be removed by percolating the thiols over activated, neutral alumina prior to use.[81]

Concerning the oxygen content of the solution, there is little, if any, quantitative knowledge about the effects that oxygen can have on the rate of formation and the structure of SAMs formed when it is present in solution. Empirical evidence suggests that degassing the solvent with an inert gas, such as argon, prior to preparing the solution of thiols and maintaining an inert atmosphere over the solution during formation improve the reproducibility of the SAMs.[81] Reducing the concentration of oxygen in the solution limits the oxidation of the thiols to sulfonates and other oxygenated species. This precaution is more important for SAMs prepared on palladium, silver, copper, and (perhaps) platinum than on gold.

Cleanliness of Substrate: The formation of SAMs on substrates that are handled in a laboratory atmosphere is essentially an exchange process: the thiols must displace whatever adventitious materialhas adsorbed onto the substrate prior to immersion in the thiol solution. The assumption supporting this statement is that the thiols are, in fact, able to displace the miscellaneous adsorbates already present. Displacement by thiols first requires desorption of the contaminants and impurities; the rate of desorption of the contaminants must, therefore, affect the kinetics of formation. SAMs have reproducible materials properties when formed on substrates that are immersed into solutions of thiols within ~1 h of preparation or cleaned with strongly oxidizing chemicals (“piranha” solution-H_2SO_4:H_2O_2) or oxygen plasmas. Exposure to ambient condi-

tions for prolonged times seems to allow adsorption of materials that are not easily displaced in the typical time allowed for the formation of SAMs.

3

Electrical Characterization of Molecular Junctions Using AFM-based Techniques

Many techniques have been used in past years to study and characterize transport in molecular junctions. Strategies for fabricating Metal-molecule-Metal junctions (M-m-M) include assembling molecules inside metal-capped nanopores[35-36] and mechanical break junctions[39-41,47] or between mercury drops,[37-38] nanofabricated electrodes,[42] and cross wires.[43] Metallic nanoparticles have also been used as electrical contacts to molecular monolayers supported on metal surfaces.[44,114] In this thesis work we chose an approach where scanning probe microscopy based techniques were used. We used an alternative approach to Metal-molecule-Metal junction formation and study using the nanolithographic and current detection capabilities of atomic force microscopy (AFM). The AFM, in fact, offers the uncommon chance to join together high-resolution surface topography imaging (contact mode AFM),[106] high-accuracy molecular lithography (nanografting)[62,115] and moreover, current detection using a

conductive tip and an opportune amplification circuit (CT-AFM).[116] A key advantage of scanning probe microscopy for junction formation is that no micro- or nano-fabrication processes are necessary. Also in our case, the nanolithography was used only to immobilize more than a single molecule below the tip in order to extend the number of molecules simultaneously studied and was not a real junction fabrication process. This means that, in terms of time, screening of junction behavior is limited by synthesis of molecules and their self or assisted assembly on conducting substrates, and not by the measurement methodology itself. Junction fabrication by CT-AFM is also a "soft" process in that there are no high-temperature contact-forming or high pressure stamping steps. Molecules may be contacted by any conducting film that can be coated onto an AFM tip, offering flexibility for examining the role of contacts on the junction *I/V* behavior.

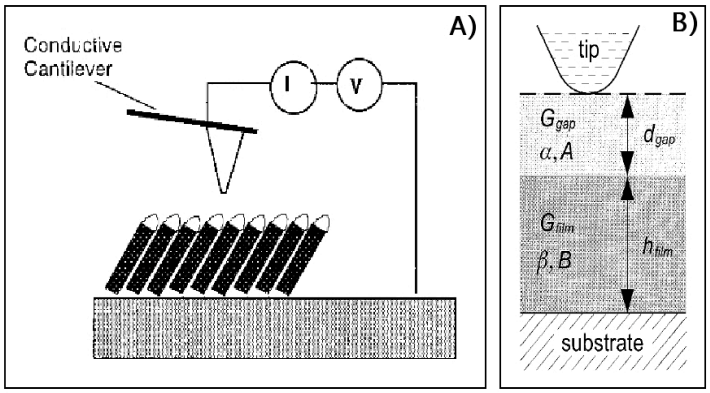

Figure 3.1. (A) Schematic of a CT-AFM set-up. Above a SAM of the molecules of interest grown on a gold substrate is placed a conductive AFM tip. A closed amplification circuit connecting substrate and cantilever provide bias and current detection. Scanning feedback stays in force during surface CT-AFM characterization. (B) Two-layer tunnel junction model. The STM tunnel junction is composed of two distinct layers: the vacuum gap and the film. Each region is characterized by a transconductance, G, which is dependent on the physical thickness of the layer. The film thickness is an intrinsic property, while the vacuum gap thickness is controlled by the STM to maintain a constant overall transconductance. Working at constant current on differently conductive molecules implicates a variation of the vacuum gap.

It is important to note the difference between this CT-AFM method and scanning tunneling microscopy (STM) for characterizing molecular junctions (refer to Figure 3.1). In STM, current, not force, is used to control tip-positioning. Because the conductance properties of molecules are generally unknown, the position of the probe with respect to the molecules can be ambiguous. If the STM tip is not in contact with the monolayer, the junction transport properties are determined by the molecules and the vacuum (or air) gap between the molecules and the tip. If the tip

penetrates the monolayer, it is difficult to know how far it has penetrated and thus what portion of the molecules contribute to the current. CT-AFM does not have this difficulty because an independent feedback signal, namely normal force, allow the probe to be controllably positioned just in contact with the monolayer as is shown in Figure 3.1A. At low contact forces, there is much less ambiguity in CT-AFM about where the tip is with respect to the endgroups of the SAM. Some attempt in the direction of a systematic understanding of the vacuum (or air) gap contribution in STM characterization of molecular layers was done by Weiss and coworkers.[45] Their work focuses in particular on the behavior of the STM tip during the motion over different molecules in a mixed SAM. The usually unknown changing in the tip-surface distance when moving over molecules (or in general over surface areas) of different conductibility is a problem that has to be addressed when STM is used to perform transport studies (see Figure 3.1B).

There is another important point in favor of the use of CT-AFM instead of STM to perform current measurements on low conductive SAMs, as for example, long alkanethiol ones. In STM operations, the feedback signal is the same quantity that we are measuring, the current. That means that the acquisition speed of the amplifier has to be fast enough to assure a good feedback response in order to regulate the tip-surface distance. However it is well known that for amplifiers an inverse relationship between gain and bandwidth exists. The implication of that statement is a limitation of the maximum gain and so, directly, to the minimum current detectable, due to the impossibility to reduce below a certain value the bandwidth of the feedback circuit. STM usually works with currents starting from 1 pA rather, the CT-AFM, easily succeeds in handling fA range ones.

1. The Atomic Force Microscopy

The atomic force microscope (AFM), or scanning force microscope (SFM) was invented in 1986 by Binnig, Quate and Gerber.[106] Like all other scanning probe microscopes, the AFM utilizes a sharp probe moving over the surface of a sample in a raster scan. In the case of the AFM, the probe is a tip on the end of a cantilever, which reacts changing some dynamic (resonant frequency) or static (bending shape) property in response to the force that acts between the tip and the sample. The capability to detect these changes may give us the possibility to reconstruct the surface morphology. The first AFM used a scanning tunneling microscope at the end of the cantilever to detect the bending of the lever, but now the great majority of commercially available AFMs employ an optical lever technique.

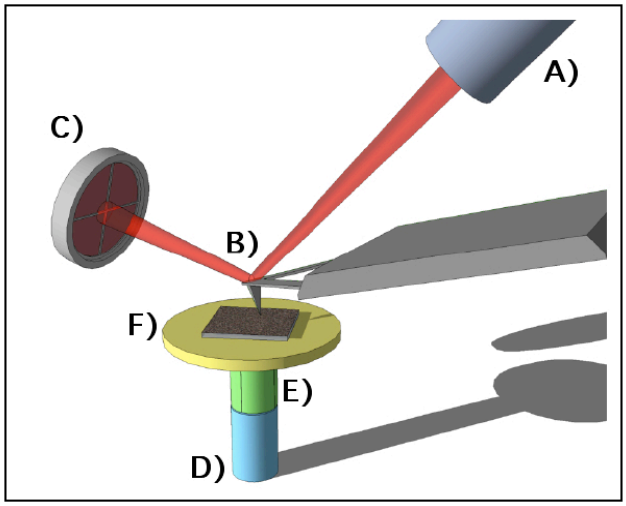

Figure 3.2. An explicative cartoon of AFM working principle. It is possible to recognize the laser (A) focusing a laser beam at the top end of a cantilever (B) from where it is reflected at the center of a 4 quadrants photodiode (C). Every cantilever deformation (bending or torsion) will be easily detected as spot movements on the photodiode. At the end of cantilever there is a very sharp tip in close proximity with the sample surface (F). Surface is moved below the tip using an x and y piezoscanner (E). During the rastering process tip bends (or changes its resonant frequency) as function of surface morphology. A z piezoscanner (D) approaches or moves away the surface from the tip in order to maintain constant bending or resonant frequency. Voltages needed to do this corrections are used to reconstruct surface topography.

Briefly, a laser beam is focused on the back end of the cantilever and subsequently reflected on a position sensitive photo diode (PSPD) as a four quadrant light detector upon which it is centered. The diode is able to track every spatial movement of the laser spot so a deviation due to a

cantilever deformation (bending or torsion) is easily detachable with high precision thanks also to the optical level magnification. Since the cantilever obeys Hooke's Law for small displacements (in fact it may be imaged as a beam spring), the interaction force between the tip and the sample can be found. From geometric calculations the displacement of the laser spot on the PSPD can give the value of the vertical tip displacement that, in combination with the intrinsic elastic constant of the cantilever furnish the force applied by the tip to the surface. The movement of the tip or sample is performed by an extremely precise positioning device made from piezoelectric ceramics, most often in the form of a tube scanner but more complex solutions are available. The scanner is capable of sub-ångstrom resolution in x, y and in z directions. The z-axis is conventionally perpendicular to the sample.

The reconstruction of the surface morphology is possible directly recording for example the tip bending, but in this case the applied force is out of control or even impossible for very corrugate surfaces. A different approach uses a feedback circuit to maintain constant the force (working in static mode) or tip oscillation amplitude (dynamic mode) while the tip is scanning the surface.

Static Mode AFM

Working in static mode, also referred to as contact mode, the AFM can so operate in two principal modes: with feedback control and without feedback control. If the electronic feedback is switched on, then the positioning piezo that is moving the sample (or tip) up and down can respond to any changes in force (or, to be more precise, cantilever deflection), which are detected, and alter the tip-sample separation to restore the force to a predetermined value (imposed by the operator). This mode of operation is known as constant force, and usually enables a fairly faithful topographical image to be obtained reducing, at the same time, tip crash risk. If the feedback electronics are switched off, then the microscope is said to be operating in constant height or deflection mode. This is particularly useful for imaging very flat samples at high resolution and high speed. Often it is best to have a small amount of feedback loop gain, to avoid problems with thermal drift or the possibility of a rough sample damaging the tip and/or cantilever. Strictly, this should then be called error signal mode.

Contact mode is the most common method of operation of the AFM. As the name suggests, tip and sample remain in close contact as the scanning proceeds. By “contact” we mean in the

repulsive regime of the inter-molecular force curve as shown in Figure 3.3A. The repulsive region of the curve lies above the x-axis and extends for some fraction of nanometer depending mainly on the tip and surface composition. From here on we refer to tip/surface contact when the tip is, somehow, feeling this repulsive interaction, both in static or dynamic mode.

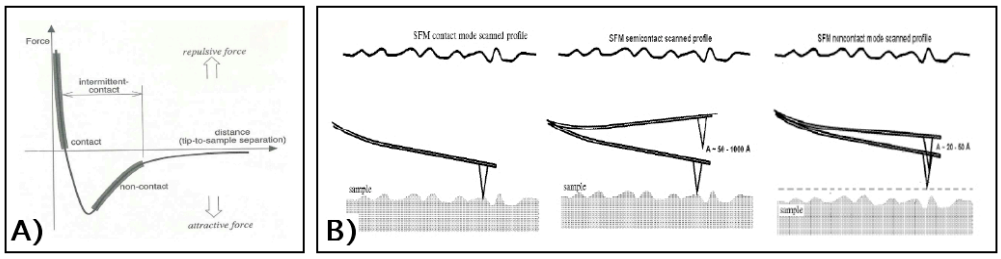

Figure 3.3. (A) Force versus tip to surface plot. The tip, approaching to the surface, starts to feel attractive, long range forces (non-contact AFM region) until tip and surface electron orbitals are so close to start exerting repulsive forces (contact mode AFM region). Between these two regimes lies the intermittent-contact (or tapping mode) region. (B) Cartoons of the three AFM operation modes. From left to right, contact, non-contact (large tip oscillations), and intermittent contact (small tip oscillations) modes.

One of the characteristics of remaining in contact with the sample is that there exist large lateral forces on the sample as the tip is "dragged" over the specimen. These transversal interactions induce torsion in the cantilever proportional to the tip/surface friction. The operation mode in which this interaction is recorded is usually called lateral force (LF-AFM) and is a commonly used technique for studying rheological properties or surface forces (an example of this application is presented in Chapter 7 of this thesis). A drawback of these lateral interactions is the surface damaging that occurs during scanning of very soft materials as polymers or organic layers especially if working at high forces. To overcome this problem a dynamic approach was developed.

Dynamic Mode AFM

Basically, in the dynamic mode, the cantilever is oscillated close to its resonant frequency (and also characterized by a resonant oscillation amplitude) and positioned above the surface. Now, once the tip starts to approach to the sample and feeling the surface forces, a changing in the cantilever resonance frequency is induced. This change may be detected as a frequency shift (frequency modulation AFM) or as an amplitude change (amplitude modulation AFM). In both cases the information is usable to reconstruct the surface topography directly or using, as previously described for the contact mode case, some feedback correction in order to maintain constant a certain value of the frequency shift or of the amplitude. Regarding the forces sensed by the tip we can stay in the attractive regime of the surface potential, and in this case we relate to non-contact mode (NC-AFM), or sensing also the repulsive branch of the potential intermittently (tapping or semicontact AFM). Factors inducing one or the other behavior are, for example, cantilever stiffness, choose set-point value, tip/surface chemistry, working environment, etc.

Although it is a very gentle technique, non-contact operation is a very difficult mode to operate in ambient conditions with the AFM. The thin layer of water that exists on the surface on the sample will invariably form a small capillary bridge between the tip and the sample and cause the tip to “jump-to-contact” inducing undesirable instability during scanning (even under liquids and in vacuum, jump-to-contact is extremely likely due, for example, to electrostatic interactions). Moreover, a not accurate choice of the scanning variables, induce usually poorer lateral resolution than contact mode AFM. To overcome the problem a technique that may be positioned exactly between contact and non-contact mode was developed. We refer to it as semicontact mode. It is the next most common mode used in AFM after contact mode. When operated in air or other gases, the cantilever is oscillated at its resonant frequency (often hundreds of kilohertz) and positioned above the surface so that it only taps the surface for a very small fraction of its oscillation period. This is still contact with the sample in the sense defined earlier, but the very short time over which this contact occurs means that lateral forces are dramatically reduced as the tip scans over the surface reducing so damaging and, at the same time, offering easily better spatial resolution than non-contact. When imaging poorly immobilized or soft samples, tapping mode may be a far better choice than contact mode for imaging.

More recently, there has been much interest in phase imaging. This works by measuring the phase difference between the oscillations of the cantilever driving piezo and the detected oscillations. In general phase is more sensitive to changes in attractive and repulsive tip-surface interaction, especially to electrostatic or magnetic long range ones.

Working in Liquid Environment: the Liquid Cell

The main aspect of atomic force microscopy is the remarkable adaptability. Many different geometries and techniques were developed in order to extend the instrument capabilities to a wide range of environments, and to performing specialized task. AFMs able to work in ultra high vacuum (UHV), liquid (e.g. water, alcohols, physiologic solutions), air and controlled atmosphere (as, for example, a nitrogen box with humidity, temperature and pressure control) are present in research laboratories.

In addition to the standard sample topography determination, AFM may be used to study more complex surface properties. Studies of long range electrostatic and magnetic forces exerted by the surface,[23] short-range adhesive forces,[24] elasticity and plasticity,[25] charge transport, [26] polarizability[27] and thermal characterization and stimulation[28] are only some of the possible branch of application of AFM on surfaces. In this thesis work we took advantage in particular of the AFM capability to work easily in a liquid environment. Such ambient will be necessary to perform all the nanolithographic tasks necessary to build surface nanostructure of different molecules (into an hosting molecular matrix) in order to perform simultaneous molecular characterization as described in the following chapter. Moreover, there is a large debate in the scientific community about the role of different solvents to mediate electrical transport in single molecules or through (or across) SAMs. Answer to this question may be addressed only performing a molecular electrical characterization in liquid. Passing momentarily over the argument of this thesis, liquid environment may be absolutely necessary handling organic or biological material in order to avoid molecular degradation or to perform studies in “real” ambient (e.g. proteins in physiological saline solution).

AFM measurements may be done in liquid using a liquid cell. Two basic designs are usable: an open liquid cell and a closed one. In the first case the cell is a very small tub (some mL usually)

and the AFM is inserted into the liquid mounted on a crystal or below a small glass window in order to assure a perfect optical view through the liquid interface.

The closed liquid cell is similar to the open one but present a silicon membrane able to seal it and usually has a smaller volume. The advantage of this solution is the ability to reduce evaporation of the liquid. The concentration of molecules in an alcohol solution or the amount of salts in a buffer may be maintained constant into the closed liquid cell. Inlet and outlet tubes are present for refilling or liquid exchanging. One of the drawbacks of this solution is the mechanical coupling of the inferior part of the instrument, where usually the sample and the piezo-scanners are located, and the above part, where there are the tip and all the laser detection parts. As a consequence of this there is the possibility to introduce mechanical noise in the measurement caused by liquid evaporation instabilities or spurious cantilever vibrational modes. In fact induced liquid oscillations into the cell may create interference problems determining the resonance frequency when working in dynamic mode.

Summarizing, the most difficult design targets to achieve are to avoid air bubbles formation along the laser path, reduce the unwonted oscillation modes of the cell during dynamic operation in liquid and assure, in case of close liquid cells, absence of stresses due to the membrane sealing. For our purposes we chose to modify a commercial open liquid cell to overcome all the above-mentioned difficulties and to fit all of our requirements.

2. Nanografting

Nano and microfabrication of self-assembled monolayers (SAMs) has attracted tremendous attention because it opens to the unprecedented capability to control surface properties at the nanometric scale. For example, tailoring the exposed functional group of the nanopatterned molecules and of the surrounding SAM ones, hybrid hydrophobic-hydrophilic surfaces may be prepared.[71] Moreover patterned SAMs can be used as resist for pattern transfer and as templates to pattern proteins and other biosystems.[117-120] Micrometer-sized patterns have been fabricated within SAMs using microlithographic techniques such as photolithography,[121] microcontact printing,[6,118] microwriting,[6,118] and micromachining.[6] Argon ion or electron beam lithography can produce smaller patterns (down to tens of nanometers) but require a high-vacuum (HV) environment.[122] Another approach to produce nanometer-sized domains of SAMs is the coadsorption of two or more adsorbate.[123] However, with this approach, it is difficult to precisely control the size and distribution of these nanodomains because the structure is determined by the interplay of the kinetics and thermodynamics of the self-assembly process.[124]

Creating nanopatterns of SAMs of different molecules with molecular precision and in short time requires new fabrication strategies. Atomic force microscopy (AFM) is well-known for its ability to visualize surfaces of materials with high spatial resolution[125] in many physical environments. Taking advantage of the sharpness of the tip and the strong and localized tip-surface interactions, AFM has also been used to manipulate molecules on surfaces and to fabricate nanopatterns of metal and semiconductor surfaces via electro-oxidative processes. Despite the structural complexity of SAMs, molecular resolution images have been obtained using AFM.[61,126] The fact that molecules within SAMs can be resolved indicates that tip-SAM interaction in AFM imaging is localized to molecular dimensions. Therefore, in principle, by enhancing the local tip/surface interaction (the applied force in AFM case) one is able to break chemical bonds selectively. Various approaches for controlling the local interactions have been reported. These methods include AFM-based lithography such as tip-catalyzed surface reactions and dip-pen nanolithography,[115]

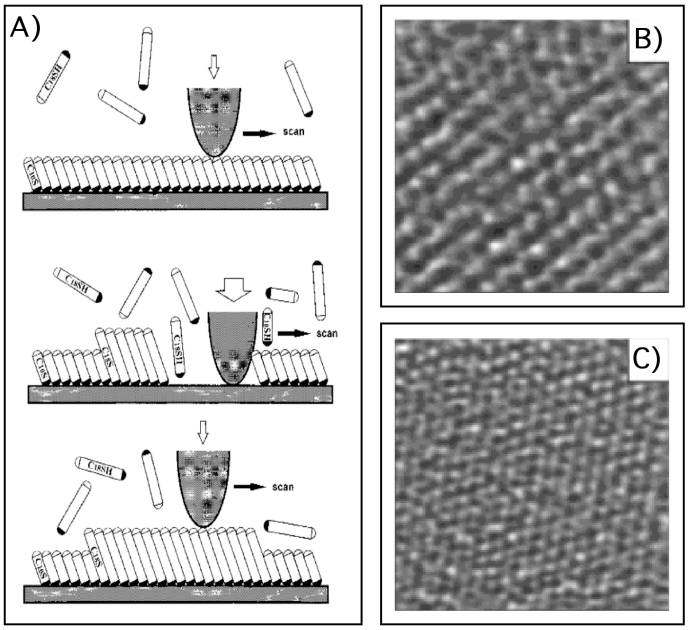

Figure 3.4. (A) Procedure for nanografting. The schematic diagram provides an example of the fabrication of a C18 nanostructure inlaid in a C10 monolayer. The drawings are not to scale. Initially a well-ordered C10 on gold is imaged via AFM with a low imaging force of 0.5 nN in ethanol solution containing C18. At the image force of about 50 nN (depending on the tip sharpness), C10 molecules can be displaced during the scan, and C18 molecules (0.5 mM in concentration) self-assemble on the exposed gold surface. The resulting nanopatch of C18 can be imaged by AFM at a low imaging force. The typical time to complete all the nanofabrication procedure is ~5 min. The threshold force for nanografting is determined

looking at the atomic periodicity of the surface. At low force C18 SAM lattice is imaged (B), increasing the force, at a certain point, lattice changes into the periodicity of the Au(111) (C).

For our purposes we chose to take advantage of the nanografting technique, introduced for the first time by Song Xu and Gang-yu Liu in 1997.[62] The technique is performed in its entirety in a liquid medium using a common AFM tip in a liquid cell set-up. The highest resolution AFM images of thiol SAMs were acquired in liquid under very low imaging loads (e.g., 0.5 nN).[61,126] The pressure exerted by the tip was about 0.1 GPa (assuming a tip radius of about 10 nm and using Hertzian contact theory). The van der Waals energy per CH_2 group is ~2 kcal/mol.[127] Therefore, under such imaging pressure, the AFM tip was in contact with the alkane chains, causing small local deformation.[25,127] Increasing the local pressure would increase the deformation, disrupt the packing, and eventually displace thiol molecules from their adsorption sites because the Au-S interface bond is the weakest one (the binding energies for S-Au, C-C, C-H, and C-S are 40, 145, 81, and 171 kcal/mol, respectively). In addition, the lateral movement of thiols on gold requires less activation energy than desorption. Increasing the load further would cause the underlying gold substrate to deform.

Basic Nanografting Procedure

The process of nanografting includes three steps as illustrated in Figure 3.4. All of those are performed with the tip immersed in a liquid solution of, usually, a different thiolated molecule. The first step is to characterize the matrix SAM and select areas for the nanofabrication. During this process, the surface structure of the SAM (matrix) is imaged by AFM under a low force, normally below 1 nN. The second step is to fabricate desired patterns within the SAM. In this step, SAM molecules in selected regions of the surface are removed by scanning these areas with an AFM tip at a force greater than the threshold displacement force. As the matrix molecules are removed, new thiol molecules from the surrounding solution immediately adsorb onto these areas following the scanning track of the AFM tip.[62] The final step is to characterize the patterned SAMs using the same AFM tip at a reduced imaging force. The geometry of the resulting patterns is defined by the scanning trajectrory, and the spatial precision of the fabrication depends on the sharpness of the AFM tip and the thermal and mechanical stability of the AFM. The best spatial precision achievable is of about 1 nm.[62]

Factor Influencing Nanografting

Omitting the kind of thiolated molecule used, three are the main factors influencing the nanografting procedure: the fabrication force, the scanning speed, and the concentration of thiols in solution. Since the geometry and the chemical nature of AFM tips vary, the corresponding threshold force must be determined for each tip before initiation of a fabrication process. Typically, a small area of 5×5 nm^2 was scanned under a gradually increasing load until the periodicity changed from that for a thiol monolayer to that for Au(111), i.e., from an hexagonal lattice (a=0.50 nm) to a smaller hexagonal lattice (a=0.29 nm).[128] This change indicates the displacement of the matrix molecules from their adsorption sites. To ensure complete removal of the matrix molecules without causing plastic deformation of the underlying gold surface, the nanografting force was set 10÷50% higher than the threshold force. The concentration of thiol in solution was not a critical parameter as we have successfully achieved nanografting with concentrations ranging from 2 μM to 2 mM. The results of nanografting were sensitive to scan rate as slow scans often produced pattern distortion due to thermal drifts while fast scans did not produce patterns with high coverage. We found that scan rates ranging from 100 to 2000 nm/s resulted in the rapid and reproducible formation of patterns with well-defined geometry and sharp edges. Thiol molecules within these patterns were well ordered and densely packed as demonstrated also by some recent current measurements performed on alkanethiol molecules (Chapter 6 of this thesis).

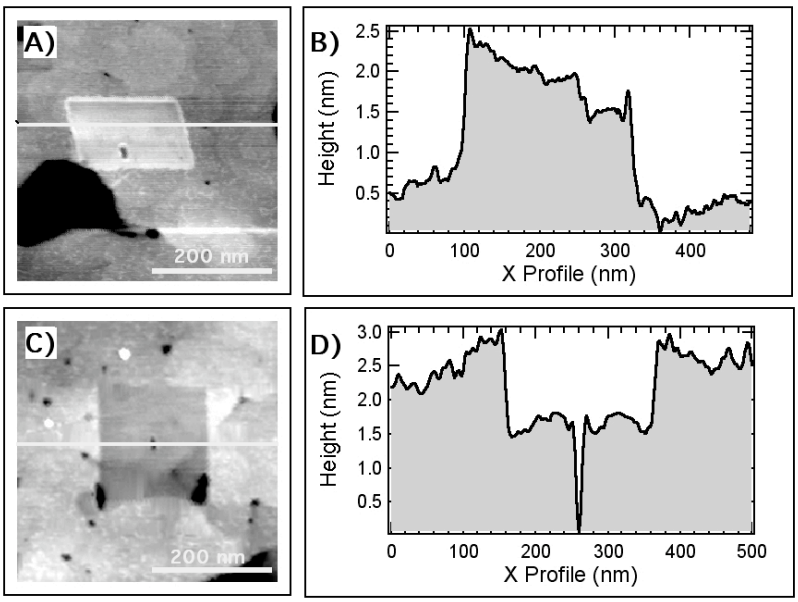

Figure 3.5. (A) Nanopatch of C18 fabricated using nanografting into a C10 matrix. Difference in height from line profile (B) is close to the theoretical difference in thickness between C18/C10 SAMs. (C) Topographic image of a nanografted C10 patch into a C18 SAM with the relative line profile (D).

Nanografting offers many advantages compared with others AFM based nanolithographic techniques as, for example, dip-pen nanolithography.[115] Due to the fact that the technique is performed entirely in the liquid environment of an AFM liquid cell, the sample never sees the air and moreover, it is very easy to graft different molecules simply changing the solution filling the cell (the tip used for the fabrication is always the same). Another benefit of the technique is the fact that concentration of molecules in solution is perfectly known; in opposition in dip-pen the amount of molecules soaked by the tip is unknown. Also from the point of view of pattern resolution the nanografting may be considered superior in performance compared to dip-pen. In nanografting patterns are created into a hosting SAM of molecules that serves as diffusion confinement for them. That means higher spatial resolution and time stability of the fabricated nanostructures than in dip-pen nanolithography.

3. CT-AFM

AFM based electrical characterization of many different organic layers has been carried out by panoply of groups in the past years.[34,53,114,129] The common procedure was to fabricate M-m-M junctions placing a conductive AFM tip in contact with a metal-supported molecular film, such as a self-assembled monolayer on gold. While the normal force feedback circuit of the AFM controls the mechanical load on the microcontact, a voltage swap is done recording so the *I*/*V* characteristic of the junction. We will refer to that approach as punctual measurements or punctual CT-AFM.

In our experiments we didn't perform punctual measurements but, instead, a complete bi-dimensional mapping of the currents flowing through the area below AFM tip during scanning. [46] As usual the junction is formed placing the conductive AFM tip in contact with the molecules of interest assembled on a gold surface. Has to be considered that now, thanks to the nanografting technique,[62] the molecular layer is not formed by a unique type of molecule but, instead, by two or more ones, auto-assembled in highly ordered nanostructures in well localized areas of the surface. The electrical characterization is performed simultaneously with a topographic imaging of the surface with the feedback working at constant force (contact mode) as is possible to see sketched out in Figure 6.2. The use of a conductive tip connected with a high gain amplification chain let us to collect current values for every point forming the 2D image when a potential is applied between tip and surface. Usually we allude to this technique in terms of surface measurement or scanning CT-AFM.

The electrical characteristic of junction, usually called *I*/*V* characteristic, is now obtained for every molecular junction acquiring a set of current images at different applied voltages (usually swapping from -250 mV to + 250 mV). A set of twenty images is sufficient to assure a good junction analysis. An example of an *I*/*V* plot obtained from the analysis of current images at different biases is reported in Figure 4.3A. The voltage increasing steps range from 1 to 20 mV, clearly more dense points were acquired close to the zero voltage origin. Starting from current images, an average value for the current was extrapolated for every molecular patch present in

the image (usually this was done also for the hosting SAM). The procedure was repeated for all the images acquired at different applied biases. *I/V* curve of current values plotted as function of applied voltage may be then easily obtained.

Benefits of Scanning CT-AFM

Scanning CT-AFM takes on many of punctual measurements capabilities. In particular has to be recalled the ability to analyze very low currents through quasi-insulating materials (e.g. alkanethiol SAMs longer than 16 carbons) with a well-known tip/surface position (especially comparing with STM junction characterization, as previously mentioned). Additionally, in both techniques the feedback controlling the tip surface interaction is the force that is specified by the AFM operator. This opens the possibility to perform electrical measurements where transport is in strong correlation with the mechanical pulling of the junction. An example of this methodology will be discussed in the next section.

The main difference between the two techniques is the fact that, in punctual analysis with CT-AFM, a statistical approach is needed. This is due to the large variance in the obtained current-voltage characteristics. The reason of those deviations is primary attributable to the presence of SAM defects that false the punctual scans (see Chapter 2 and Chapter 7 of this thesis). To go over the problem a large quantity of numerical data has to be obtained in order to increase the amount of measurements done on good portions of the SAM and carrying useful information. Usually tens to hundred of thousand punctual measurements are done to assure a representative statistical analysis of a certain molecular property. Although automatic tasks are usually used to perform this kind of experiments, it can be defined as a time consuming procedure. In addition has to be considered the fact that the procedure has to be repeated many times as is the number of molecules involved in the study. The scanning approach overcomes these two troubles.

First of all, the technique consists of the simultaneous acquisition of a “normal” topographic image of the surface and a second image carrying the information under investigation (current values, energy dissipation, friction, etc.). This gives the possibility to associate the information coming from the second image to the surface morphological attributes. Defects are now detectable, and so the possibility to a better interpretation (or to the discharge) of the results is open. A

second important point that has to be considered is the intrinsic statistical information that is held by a current image. For example, usual image resolution, during a standard scanning CT-AFM characterization of a surface, is about 512×512 pixels, meaning more than 250.000 punctual sampling at a certain applied voltage. Even though the molecules of interest may cover only a portion of the surface, an impressive amount of data is recorded.

Unfortunately, the scanning procedure, although assuring all the previously mentioned improvement on the punctual approach, is causing other major troubles. Try to picture in your mind a gold tip moving in narrow contact with an alkanethiol SAM. The tip acts as a "vacuum cleaner" for all residual molecules which are physisorbed on the top of the SAM, or picks up SAM molecules in correspondence of SAM defects or gold irregularities (if the SAM was grown on a polycrystalline gold surface). As result of this action the state of the tip will change after few scans offering more resistance to the current flow. This, at a glance, insurmountable problem may be effectively overcome only with a differential approach as thoroughly described in Chapter 4 for alkanethiol SAMs. Briefly, we take advantage from the capability that we have to immobilize many different molecules in nanopatches on a surface using the nanografting technique. The nanopatches may be so closed one to the other to be imaged all together in a single scan of some microns. If we now suppose, reasonably, that the tip, although contaminated by physisorbed molecules, doesn't change its state during a scan, a normalization, or better, a relative comparison, will allow us to overcome the problem of the tip contamination. More precisely, as described in the experimental chapter, all boundary conditions affecting the measurement can be neglected when looking for properties coming from the ratio between experimental values.

The Force Variable

As in the case of punctual measurements the tip is constantly in contact with the end-group of the molecules forming the SAMs. Although current measurements were performed at very low force in order to avoid SAM damaging and/or tip contamination (due to molecular adsorption), the possibility to change the applied force with high accuracy introduce a new analysis variable. It is well known that single component films of alkanethiols react to an increasing load exerted, for example, by an AFM tip following a stepwise behavior. In fact, under applied load, the thiol island undergo a stepwise decrease in height.[25,130] At the smallest applied loads the island height corresponds to the one expected for molecules tilt around 30° from the vertical. When increasing the load, a first step of approximately 0.4 nm is observed, compatible with a 48° chain tilting. Increasing further the load a third step at a tilting of about 55° can be distinguished. After each of these compressions, the initial height of the island was recovered when lowest load was used. The process is thus reversible, meaning that it is an elastic behavior. The discrete film height observed in these experiments indicates the existence of particularly favorable molecular configurations.

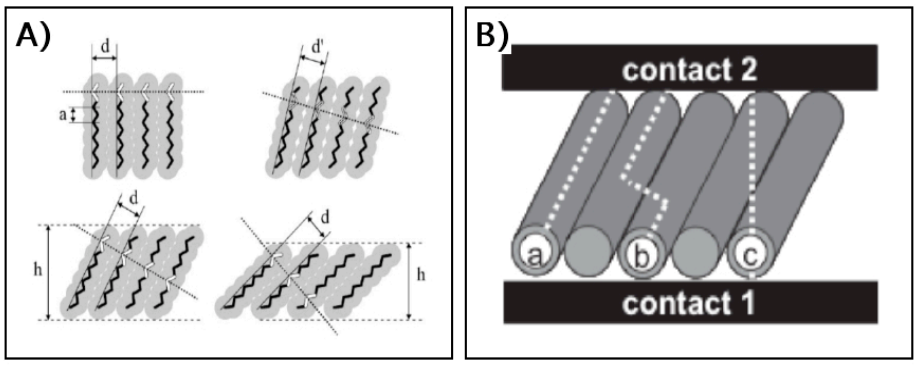

Figure 3.6. (A) Schematic model of all-trans alkyl chains that illustrates tilt configurations which fulfill the condition of maximum packing density. Only certain angles are allowed due to the zig-zag arrangement of the methylene groups. At top left the uncompressed, upright configuration. At top right opposed zig-zag, causing an increased separation of the molecules. This unfavorable energy state has to be overcome to reach the first (bottom left) and second (bottom right) tilted configuration.(B) Schematic illustration of possible mechanism for (elastic) electronic charge carrier tunneling across molecules. Through bond (a), across bond (b), and through dielectric (c).

A similar behavior may be explained by a simple 1D geometrical model that takes into account the zig-zag structure of alkanethiol chains (see Figure 3.6A). The model assumes chain interlock-

ing at specific angles to achieve optimum packing.[131] The implication of this structure change in transport measurements is the possibility to address one of the more debated questions about transport in alkane chains: is the charge transported through the molecules forming the film or across adjacent molecules (see Figure 3.6B)?

A density functional theory study of electronic properties of n-alkanedithiols sandwiched between two Au(111) infinite slab electrodes[132] claims that while the length of the hydrocarbon chain is a determining factor in charge flow, the tilt angle of the packed molecules with respect to the electrode surface, and therefore the distance between the electrodes, has a small influence on the local density of states (LDOS) at the center of the molecules. The picture, which emerges from these calculations, is totally consistent with a through bond tunneling mechanism. From the other side, punctual CT-AFM experimental evidences of molecular-tilt dependent chain-to-chain tunneling are also present in literature.[50] The strong influence that SAM order and substrate and tip morphology have on this measurements leave anyway the question open.

4. Theoretical Basis of Electron Tunneling in Self-Assembled Monolayers

Possible Conduction Mechanisms

In Table 3.1, possible conduction mechanisms are listed with their characteristic current, temperature, and voltage dependencies[133] On the basis of whether thermal activation is involved, the conduction mechanisms fall into two distinct categories: (i) thermionic or hopping conduction, which has temperature-dependent I(V) behavior and (ii) direct tunneling or Fowler-Nordheim tunneling, which does not have temperature-dependent I(V) behavior. For example, both thermionic and hopping conduction have been observed for 4-Thioacetyl-Biphenyl SAMs[35] and 1,4-Phenelyene-Diisocyanide SAMs.[134] However, the conduction mechanism is expected to be tunneling when the Fermi levels of contacts lie within the large HOMO-LUMO gap for short molecules, as for the case of an alkanethiol molecular system.[135-136] Previous work on Langmuir-Blodgett alkane monolayers exhibited a significant impurity-dominated transport component, complicating the analysis. I(V) measurements on self-assembled alkanethiol monolayers have also been reported;[26,38,41,137] however, all of these measurements were performed at a fixed temperature (300 K) that is insufficient for proving tunneling to be the dominant mechanism.

Table 3.1. Possible Conduction Mechanisms

conduction mechanism	*characteristic behavior*	*temperature dependence*	*voltage dependence*
direct tunneling	$I \approx V\, e^{\left(-\frac{2d}{\hbar}\sqrt{2m\Phi}\right)}$	none	I≈V
Fowler-Nordheim tunneling	$I \approx V^2\, e^{\left(-\frac{4d\sqrt{2m\Phi^{3/2}}}{3q\hbar V}\right)}$	none	$\ln(\frac{I}{V^2}) \approx \frac{1}{V}$
thermoionic emission	$I \approx T^2\, e^{\left(-\frac{\Phi - q\sqrt{\frac{qV}{4\pi\epsilon d}}}{K_B T}\right)}$	$\ln(\frac{I}{T^2}) \approx \frac{1}{T}$	$\ln(I) \approx V^{1/2}$
hopping conduction	$I \approx V\, e^{\left(-\frac{\Phi}{K_B T}\right)}$	$\ln(\frac{I}{T}) \approx \frac{1}{T}$	Data

For direct tunneling we focus only in the low voltage regime.

Tunneling Models

To describe the transport through a molecular system having HOMO and LUMO energy levels, one of the applicable models is the Franz two-band model.[138-140] This model provides a nonparabolic energy-momentum E(k) dispersion relationship by considering the contributions of both the HOMO and LUMO energy levels:[138]

$$k^2 = \frac{2m^*}{\hbar^2} E\left(1 + \frac{E}{E_g}\right)$$

where k is the imaginary part of the wave vector of electrons, m* is the electron effective mass, h(=$2\pi\hbar$) is the Planck's constant, E is the electron energy, and E_g is the HOMO-LUMO energy gap. From this nonparabolic E(k) relationship, the effective mass of the electron tunneling through the SAM can be deduced by knowing the barrier height of the metal-SAM-metal junction. When the Fermi level of the metal is aligned closely enough to one energy level (either HOMO or LUMO), the effect of the other distant energy level on the tunneling transport is negligible, and the widely used Simmons model[141] is an excellent approximation.[142] The Simmons model expresses the tunneling current density through a barrier in the tunneling regime of $V < \Phi_B/e$ as:

$$I = \left(\frac{e}{4\pi^2 \hbar d^2}\right)\left(\left(\Phi_B - \frac{eV}{2}\right) e^{\left(-\frac{2(2m)^{1/2}}{\hbar}\alpha\left(\Phi_B - \frac{eV}{2}\right)^{1/2} d\right)} - \left(\Phi_B + \frac{eV}{2}\right) e^{\left(-\frac{2(2m)^{1/2}}{\hbar}\alpha\left(\Phi_B + \frac{eV}{2}\right)^{1/2} d\right)}\right)$$

where m is the electron mass, d is the barrier width, Φ_B is the barrier height, and V is the applied bias. For molecular systems, the Simmons model has been modified with a parameter α.[143-144] α is a unitless adjustable parameter that is introduced to provide either a way of applying the tunneling model of a rectangular barrier to tunneling through a non rectangular barrier[143] or an adjustment to account for the effective mass (m*) of the tunneling electrons through a rectangular barrier[140,143-145] or both. $\alpha = 1$ corresponds to the case for a rectangular barrier and bare electron mass. By fitting individual I(V) data using the above equation, Φ_B and α values can be obtained. The above equation can be approximated in two limits: low bias and high bias as compared with the barrier height Φ_B. For the low bias range, the equation can be approximated as[141]

$$I \approx \left(\frac{(2\,m\,\Phi_B)^{1/2}\ e^2\ \alpha}{\hbar^2\ d} \right) V\ e^{\left(-\frac{2\,(2\,m)^{1/2}}{\hbar}\ \alpha(\Phi_B)^{1/2}\ d\right)}$$

of the applicable models is the Franz two-band model.[138-140] This model provides a nonparabolic energy-momentum E(k) dispersion relationship by considering the contributions of both the To determine the high-bias limit, we compare the relative magnitudes of the first and second exponential terms in eq 2. At high bias, the first term is dominant, and thus the current density can be approximated as

$$I \approx \left(\frac{e}{4\,\pi^2\ \hbar\,d^2} \right) \left(\Phi_B - \frac{\mathrm{eV}}{2} \right) e^{\left(-\frac{2\,(2\,m)^{1/2}}{\hbar}\ \alpha\left(\Phi_B - \frac{\mathrm{eV}}{2}\right)^{1/2}\ d\right)}$$

The tunneling currents in both bias regimes are exponentially dependent on the barrier width *d*. In the low-bias regime, the tunneling current density is

$$I \propto \frac{1}{d}\ e^{(-\beta_0\ d)}$$

where β_0 is a bias-independent decay coefficient

$$\beta_0 = \frac{2\,(2\,m)^{1/2}}{\hbar}\ \alpha(\Phi_B)^{1/2}$$

whereas in the high-bias regime

$$I \propto \frac{1}{d^2}\ e^{(-\beta_V\ d)}$$

where β_V is a bias-dependent decay coefficient

$$\beta_V = \frac{2\,(2\,m)^{1/2}}{\hbar}\ \alpha\left(\Phi_B - \frac{\mathrm{eV}}{2\,\Phi_B}\right)^{1/2}$$

At high bias, β_V decreases as bias increases, which results from a barrier lowering effect due to the applied bias.

4

Electron Transfer Mediating Properties of Hyrocarbons as a Function of Chain Length: a Differential Scanning CT-AFM Investigation

Understanding charge transport at the molecular level is of crucial importance for developing molecular assemblies with uncommon properties for novel applications, such as molecular electronic devices and sensors.[146-150] Precise measurements of the charge transport and tunneling at the contacts and through the molecules are likely to provide crucial insight into the electronic couplings within and between molecules and with the interface.[151] From a more

general point of view such studies aim at expanding our fundamental understanding of molecular electronics: a central issue in biophysics and biochemistry.

Metal-molecule-Metal junctions (M-m-M) have been extensively studied in the past years in order to understand the factors influencing the transport of charges through or across different molecules. Systems ranging from single molecule contacted by two metal electrodes to Self-Assembled Monolayers (SAMs) sandwiched between two contacts have been investigated by using a panoply of different techniques. Unfortunately there is a wide spectrum of factors influencing the electron transfer behavior in these systems which is responsible for the presence of large inconsistencies in the literature. Values spreading over 3 orders of magnitude are easily found for the same molecule.[34]

Strategies for fabricating M-m-M junctions include assembling of molecules into metal-capped nanopores[35-36] or between a semiconductor surface and a mercury drop.[37-38] Also, mechanically controlled break junctions[39-41] and nanofabricated electrodes[42] or crossed wires[43] have been used. Of particular interest is the use of the metallic tip of a scanning probe microscope to form and characterize M-m-M junctions.[26,44-46] Scanning Tunneling Microscopy (STM) and Conductive Tip Atomic Force Microscopy (CT-AFM) are ideally suited to make local measurements of electron transfer through organic thin films. In both cases, in fact, it is possible to record simultaneously electron transport details (in both instruments the tip interacts with the sample via electron tunneling) and the spatial characterization of the molecules. The major distinction between the two techniques concerns the feedback signal used. In the STM case the current itself is used as feedback signal while, in CT-AFM, the optical feedback is enforced even during current measurements. The advantage of this second solution is the possibility to use high gain, low noise and therefore slow amplifiers even with highly corrugated samples. This is more difficult with STM because the amplifier has to be fast enough to allow for the feedback to follow the sample morphology. This limits the current to about 10 pA or higher for routine measurements. Another point to remember when using an STM, is the change in tip-surface distance (or in electrical parameters) that happens when the probe moves above differently conductive molecules.[45]

A common characteristic of the almost totality of approaches evolved so far, is the fact that they rely on *absolute* transport measurements with the consequence that the values obtained are strongly affected by the experimental boundary conditions. Molecular dimensions (and so, indirectly, the distance between the two electrodes), molecular HOMO-LUMO energy gaps, molecular ionization potentials, metal work functions, molecule-substrate bonding and functional group architectures, contact properties (i.e., the number of molecules involved), all have a strong impact on the transport characteristics.[56-59] Moreover, to these factors, other factors that influence the measurements have to be added, such as substrate roughness, tip chemistry, the possible presence of solvent or water meniscus, extended tip usage, and contact dimension, which is related to the radius of the tip in the case of AFM studies. It follows, that it is next to impossible, not only to compare current values coming from different techniques, but frequently also values coming from the same experimental run. In fact, for example, it is hard to verify whether, from the beginning to the end of an experiment, the tip stays always in the same conditions.

To overcome these problems a differential approach has to be considered. In fact, measuring simultaneously at least two different monolayers, self-assembled *side-by-side* on the same surface, eliminates most of the above mentioned difficulties. By considering the ratio between the values of the current through the different molecules the effects of the boundary conditions that affect the transport measurements can be minimized.

An attempt to carry out relative measurements has been done by Liang et al. who proved the feasibility of the differential approach to electrically characterize isomeric aromatic molecules using a combination of CT-AFM and Density Functional Theory based Tersoff-Hamann calculations.[46] The authors used an AFM based nanolithographic technique performed in a liquid environment, referred to as nanografting,[89] to build a nanopatch of one molecule inside the SAM made of its isomer and then electrically characterized the bi-molecular system using CT-AFM. The contribution of the different functional groups and of the gold-thiol link to electron tunneling through two distinct monolayers was pointed out. The authors conclude highlighting the large spread in absolute current values obtained in different experiments but focusing on the fact that the ratios between different molecules are reasonably constant.

The drawback of this differential approach is the impossibility to obtain an absolute measure of the electron transport through a specific type of molecules unless comparing it with one well characterized by absolute measurements. However, if the molecules considered in the same experiment belong to the same family, e.g. alkanethiols, we can obtain quantitative information about specific physical properties that are function, for instance, of the molecular length or of the arrangement of chemical groups along the chain. An effort to characterize mixed SAMs of alkanethiols of different length using an STM has been reported by Weiss and co-workers[45] introducing a bilayer model to explain their results.

The present chapter of the thesis pushes the differential philosophy to its limit by fabricating at least two patches of different thiols in a simple reference monolayer. The simultaneous presence of these molecules on the surface let us evaluate directly the ratio between currents. As a test case we apply the technique to the chain length dependence of electron transport in alkanethiol molecules obtaining a value of the electron tunnel decay constant β with unprecedented precision.

Results and Discussion

Nanofabrication and Measurements

Using nanografting we fabricate *several* monolayer-thick nano-assemblies of alkanethiols of different chain length, side by side, into a reference alkanethiol SAM on a gold film. M-m-M junctions are then created by placing a clean conducting AFM tip in contact with the top part of the molecules and scanning the surface while a fixed tip-surface bias voltage is applied. The current flowing through the nanografted patches and through the reference monolayer (the carpet) can be recorded in a single image, where differences in contrast are representative of the variation of current levels. Current data coming from all images are then used to determine the average current values for a specific applied bias looking over the current histogram of the image. The force feedback circuit of the AFM controls the mechanical load on the nanocontact keeping it constant while the current image is collected. The current image, together with the topographic image acquired by reading out the AFM laser-deflection feedback, is simultaneously registered. This provides the capability to obtain information about order in the monolayer packing by measuring the patch-to-carpet height difference, and comparing this number with the one evaluated by assuming that the alkanethiol molecules are inclined by about 30° with respect to the surface normal[84,137] (see Table 4.1 in Methods). To go one step further, the tip load can be increased to induce controlled changes in the molecular configuration of the SAMs to be correlated with changes in the transport through the M-m-M junction.[25,50] The feasibility of this approach for order evaluation has been proven several times for different applications.[46,62-63,65,71,89] The well defined physical structures resulting from nanografting are ideal for measuring in a comparative way properties such as mechanical stability and electron transfer. In the following we will show that, because of ubiquitous problems with the AFM tip cleanliness, a bi-layer junction is needed to model the transport through the M-m-M junction created by using the AFM metal tip as one of the two electrodes, and that *relative* measurements between molecules that are not too different are the only ones in which the results can be fully trusted.

We have chosen here a set of alkanethiol molecules with slightly different alkyl chain length, namely 1-octanethiol ($CH_3(CH_2)_7SH$, briefly C8), 1-nonanethiol ($CH_3(CH_2)_8SH$, briefly C9), 1-decanethiol ($CH_3(CH_2)_9SH$, briefly C10), 1-undecanethiol ($CH_3(CH_2)_{10}SH$, briefly C11), and 1-dodecanethiol ($CH_3(CH_2)_{11}SH$, briefly C12). The calculated difference in film thickness between SAMs of two consecutive chains (e.g. the 10-carbon 1-decanethiol and the 11-carbon 1-undecanethiol) is always about 1.1 Å for an alkyl chain tilt angle of 30°.[137] Within these ordered domains, molecules adopt identical conformations and film structure.

Compared with STM, CT-AFM provides the electrical characterization of a SAM with the simultaneous control of the effective tip-surface distance.[45] In CT-AFM the feedback signal is the cantilever deflection and, even at low load, the tip is in contact with the molecules. In principle, the size of the contact area can be varied by changing the applied load. Loads smaller than 0.5 nN are required to prevent any tip penetration into the SAM. However, it is not possible, even at low load, to prevent the tip from gathering up contaminants adsorbed at the top of the SAM. Such contaminants could be, for example, alkanethiol molecules physisorbed on top of the SAM, that will stick to the metallized tip during the scanning. We think that such contaminant molecules are responsible for the large fluctuations over the current values observed in previous works[46]. This contamination process is likely to be proportional to the size of the scanning area and to be affected by the surface morphology. In particular we have seen that a small-size scanning over a very smooth and even area induces very small contamination, while large scan areas on irregular and bumpy regions and, in general, large travels of the tip over the sample, easily change the tip state. In the less perturbative case, i.e. small scanning size and/or smooth surfaces, it is at least reasonable to make the assumption that if a contamination layer covers the tip, such a layer does not change composition and conformation during the entire measurement. Our system will be therefore represented not as a single molecular layer embedded between two electrodes, but rather as a more complex double-layer junction.

A tunneling M-m-M junction having two *side-by-side* SAMs, the nanopatch SAM and the carpet SAM, on the same metal surface is sketched in Figure 4.1. At the lower level are the molecular assemblies, with a thickness and a conductance determined by the specific molecule; at the upper level is the tip with its contamination layer, which is considered here remaining the same over

the whole scanning area. Obviously, each boundary variable influencing electron tunneling through the junction should also be added to the contamination layer.

For testing our differential approach we have chosen molecules belonging to the alkanethiol family. This enables us to refer to the large volume of experimental and theoretical work that has addressed the chain length dependence of the electron transfer through alkane σ-bonded bridges. In particular, in the case of alkanethiol SAMs junctions, it has been demonstrated that the electron transport is dominated by coherent non-resonant tunneling and that, therefore, the junction resistance depends exponentially on the molecular length[53] and that, for small voltages, the *I*/*V* characteristic is consequently linear.[141] Different kinds of experimental techniques, such as scanning probes, metal-molecule-metal junction devices and electrochemical techniques, have shown that the electron current through the junction is proportional to $\exp(-\beta l)$, where β is the tunneling decay constant of the molecules and l is the length of the formed junction. However, the obtained values of β for alkanethiols present in literature widely range from 0.8 to 1.4 Å^{-1} (1.0 to 1.8 per methylene group).

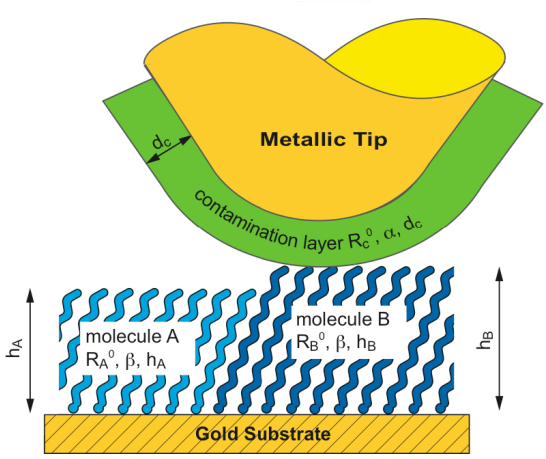

Figure 4.1. Two-layer tunnel junction model sketching, for example, a nanopatch of short molecules A into a SAM of long ones B. The tip moving from left to right engages two distinct double layers: the contamination layer C and the SAM A, the contamination layer and the SAM B. The two molecular assemblies are characterized by the same contact resistance R^0 and tunnel decay constant β if they fit to the same molecular family (e.g. alkanethiols) but different thickness. Contamination layer properties are usually unknown but we can make the hypothesis that stay constant during an image scan on both molecular films. The contact area does not change from A to B since the feedback signal is given by the interaction force.

The resistance of an alkanethiol SAM in a Metal-molecule-Metal junction as a function of the molecular length is given, under non-resonant conditions, by:

$$R = R_0\, e^{(\beta h)}$$

Where the prefactor R^0 is the contacts resistance of the SAM, h is the thickness of the SAM and β is the molecule tunneling decay constant.

In our set-up, schematized in Figure 4.1, we study the transport through two adjacent SAMs of different alkanethiol molecules (referred to as molecule A and B) sandwiched between two metallic contacts. Further, to complete the model description of the junctions, we introduce a third layer that takes into account the presence of contaminants adsorbed on the tip during scanning. The layer is obviously located between the metal AFM tip and the top of the SAM under investigation. Transport through these double junctions is affected by the transmission coefficient of the layers involved (the well know alkanethiol monolayer and the unknown contamination layer), by the layer-by-layer electron hopping and, clearly, by the contact resistances located at the interface between the metal tip and the contamination layer and between the alkanethiol SAMs and the gold substrate.

Since our resistance depends on an electron tunneling probability, the total resistance of each of the two composite two-layer junctions contains contributions from the SAM and the contamination layer. The system may be described by the relations:

$$\begin{cases} R^A_{\text{tot}} = R^0_{\text{tot}}\, V_{\text{CA}}\, e^{(\beta h_A + \alpha d_C)} \\ R^B_{\text{tot}} = R^0_{\text{tot}}\, V_{\text{CB}}\, e^{(\beta h_B + \alpha d_C)} \end{cases}$$

Where the prefactor $R^0{}_{tot}$ is the total contact resistance of all the double junction, the second term is the electron hopping factor linking transport through the two layers, β and α are respectively the tunneling decay constants of the alkanethiol SAMs and of the contamination layer, h indicates the thickness of the SAMs and d the thickness of the contamination layer. A and B indicate the alkanethiol molecules involved while C identifies the contamination layer.

Our model can be further simplified assuming that the alkanethiol molecules, the ones in the surrounding SAM and the ones in the patches, are in the same, unperturbed, standing-up configuration and, as a consequence, that β is the same for both SAMs. Furthermore since all the molecules belong to the same family, it is reasonable to make the hypothesis that the contact resistance at the sulfur-gold interface is the same and that the composition of the contamination layer does not change during repeated tip scans over the two adjacent junctions. As a conse-

quence both α and d_C will stay constant together with the tip/layer contact resistance. Finally, since the two molecules in the SAMs have the same functional end-group, we assume that the density of states is the same for both the double junctions.

From all the previous considerations we can easily evaluate the ratio between the total resistances of the two faced double-layers, which simplifies to:

$$\frac{R^A_{\text{tot}}}{R^B_{\text{tot}}} = e^{[\beta\,(h_A - h_B)]}$$

From the last equation, we can extrapolate the value of the decay constant β for the molecules involved:

$$\beta = \frac{\ln\left(\frac{R^A_{\text{tot}}}{R^B_{\text{tot}}}\right)}{(h_A - h_B)}$$

Therefore, by measuring point by point in a current image the electron transport through two SAMs of molecules of the same homologous series, placed *side-by-side* on the same surface, and measuring at the same time their height difference from simultaneously recorded topographic images, as in our approach, we can determine the decay factor β ruling out the effect of the, usually unknown, contact resistance at the tip side of the measurement, as we will demonstrate in the following section.

Direct Differential Comparison of Molecular Systems

We refer hereafter to "differential comparison" between different molecular systems when such comparison is made without the need of any normalization. This is usually possible when all our molecular systems can be imaged, and so characterized, in a single measurement frame, so that we can reasonably assume that the tip does not change during the entire measurement. The ultra-flat Ulman gold film, described later on in the methods section, allows for the fabrication of nanopatches of different molecules close one to the other (e.g. in a matrix arrangement). We can therefore acquire the transport information through all the molecules simultaneously in the same image, keeping the size of the same reasonably small.

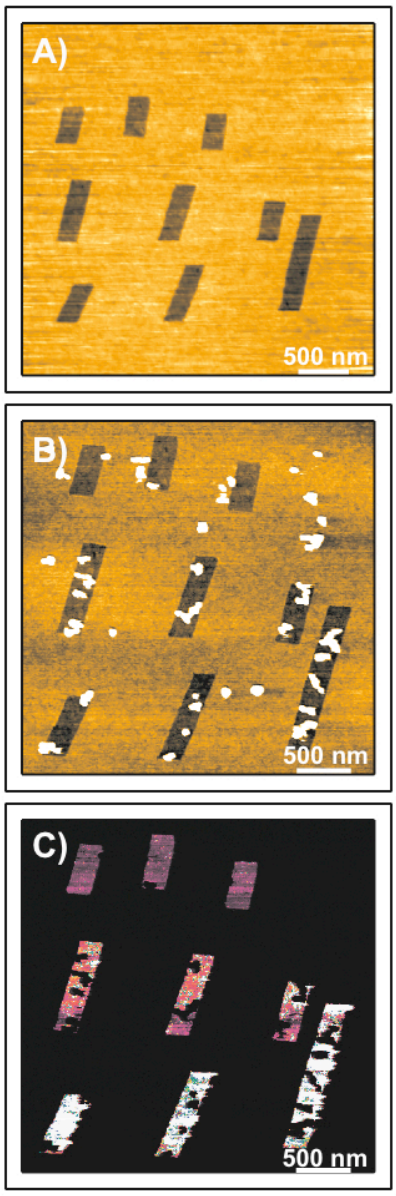

Figure 4.2. (A) Topographic AFM image acquired with a silicon tip immediately after nanografting of a matrix of 3×3 patches containing C10 (first row), C9 (second row) and C8 (third row) molecules embedded in a C18 SAM matrix. Differences in height between the patches and the surrounding C18 SAM are 8.69 Å, 9.81 Å and 10.85 Å respectively. (B) Topographic AFM image of the same area acquired with a Pt coated silicon tip. (C) Current image acquired simultaneously to (B) with the Pt coated tip at +5.5 mV bias. Distortions in the shape of patches are related to the drift of the x-y piezo-scanner.

Figure 4.2A shows the topographic image of a three by three matrix of nanopatches, made of three different alkanethiol molecules nanografted into the same C18 SAM background as seen immediately after the nanografting process by a conventional silicon AFM tip. The first row is

formed by C10 patches, the second by C9 patches and the last consists of C8 structures. In this image it is possible to appreciate the flatness of the gold surface, that allows for good height resolution although the scan size is about 3.5 μm by 3.5 μm. Figures 4.2B and 4.2C represent the simultaneously acquired topographic and current images recorded after the exchanging of the previous silicon tip with a conductive, Pt covered, one. The current image (Figure 4.2C) was taken at +5.5 mV bias voltage applied from the surface to the tip. Larger currents flow through the shorter molecule (1-octanethiol), as seen from the color contrast in the figure. Physisorption of dust particles occurs during sample drying as can be seen from the comparison of the two topographic images in Figure 4.2A and 4.2B. Such dust particles generate the no-conduction areas visible inside the patches in Figure 4.2C. These areas were not taken into account for estimating the current values in the patches. Successively, images of the same area were taken at different applied voltages. Figure 4.3A shows the average current-voltage (I-V) trace extrapolated from such images for each kind of molecule. Every point in the curve is the average from the current values of each patch. The load applied to the tip during scanning was less than 1 nN and the same Pt-coated tip was used for the whole experimental session. All the traces are linear over the voltage sweeps and are used to define a junction resistance equal to 1/slope. Resistances of about 726±15 MΩ, 219±3 MΩ and 67±1 MΩ were determined for C10, C9 and C8 respectively, with an error of about 2%. The flattening of the current through the C8 patch outside the ±7 mV voltage region is due to the current cut-off due to the saturation of the amplifier.

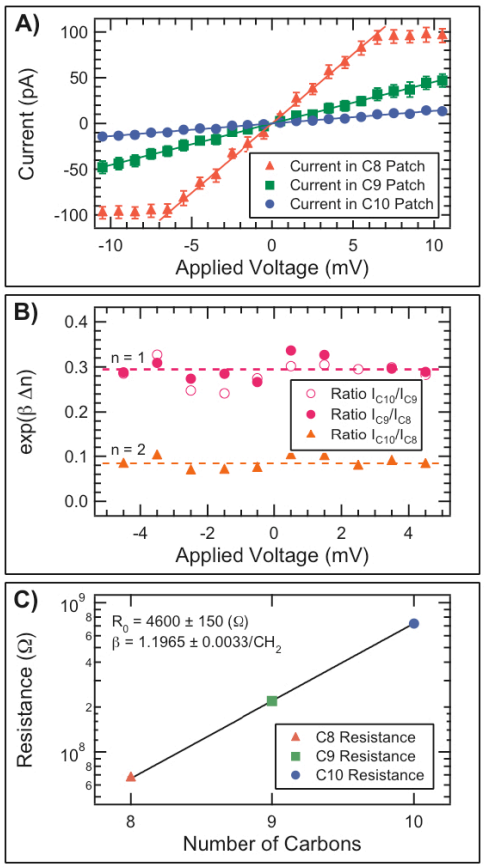

Figure 4.3. (A) I-V characteristic of C8, C9 and C10, patches nanografted into a C18 SAM. Flat parts in the C8 plot are due to the saturation of the current amplifier. (B) Current ratios between one-carbon variation chains (C10/C9 and C9/C8) and between two-carbon variation chains (C10/C8). The ratio gives the exponential of the product between the current decay constant and the difference in the number of carbon of the two alkanethiol chains involved. A good overlap of the C10/C9 and C9/C8 ratios is observable. For Δn of 1 and 2 experimental values are very close to the calculated values of 0.301 and 0.091 respectively ($\beta = 1.2/CH_2$). (C) Semilog plot of average resistance vs. SAM thickness. Fit line is an exponential with β fixed to $1.2/CH_2$).

The ratios between C10/C9, C9/C8 and C10/C8 data are plotted in Figure 4.3B. These ratios are similar in the case of C10/C9 and C9/C8, since both differ by one methylene group, and are close to the theoretical value of 0.30. A value of about 0.09 is derived for the ratio between C10 and C8 ($n = 2$). Figure 4.3C shows a semilog plot of the average junction resistance vs. alkanethiol chain length for the three molecules involved in the experiment. It is clear that the resistance increases exponentially with the number of methylene groups in the chain, as expected for non-resonant electron tunneling. The slope of the plot gives a tunneling decay constant β = 1.1965±0.0033 per methylene group or, ~0.94 $Å^{-1}$, at a contact resistance of about 4600±150 Ω

. The C–C length that we used is 1.27 Å[152]. The uncertainty of about 0.3% in the fitting of β leads to an error in the resistance values extrapolated from the plot of about 3.3%.

Normalized Differential Comparison of Molecular Systems

When a direct comparison between SAMs of different alkanethiol molecules is not possible, it becomes crucial to establish a way to compare data coming from different experiments or different frames. In fact, when the tip has to travel longer distances to image all the desired molecular patches, the probability that the tip changes during the measurement increases. What we need then is a correct normalization protocol. In particular, if the hosting SAM is always the same, every molecular patch embedded in it can be referred to that SAM. We refer to this procedure as "normalized differential comparison".

We tested the method using as a substrate a gold film produced by thermal evaporation on hot mica as described in the monolayer preparation section. The final surface was composed of monoatomically flat islands of about 500 nm in diameter. We fabricated nanopatches of C9, C10 and C11 in a matrix of C12 SAM. No more than one patch can be located on the same gold island. Distances between patches of different molecules were about 1μm. The islands were separated by boundaries that looked as deep canyons that made impossible to acquire large images with sufficient height resolution or without current artifacts, for these reasons every patch was imaged separately.

Filled dots in the three plots of Figure 4.4 represent the *I/V* curves for the three measured molecular patches of C9, C10 and C11 respectively, as extrapolated from the set of current images taken at different voltages. Each *I/V* curve for each patch is compared, in the same plot, with the *I/V* curve determined for the C12 SAM carpet from the same set of images (empty dots in the three plots). Not surprisingly, the three values obtained from the three set of images for the resistance of the C12 SAM are different, in particular we obtained a resistance of 1372±18 GΩ from the C9 patch image, 5315±95 GΩ in the case of the C10 image and 5775±204 GΩ for the C11 image. It is important to notice here that the resistance is progressively increasing with the number of repeated scans, but also that from the first to the last set of images the length of the molecules in the nanopatches increased, both phenomena concurring to the increasing of the contact resistance

at the tip. This has an impact also on the measured resistance of the alkanethiol patches, that are two or three orders of magnitude higher with respect to the values expected from the previous section of experiments.

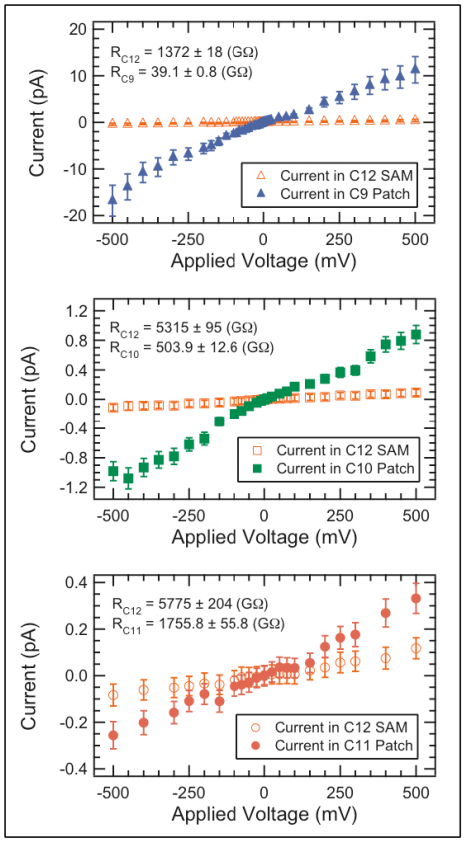

Figure 4.4. I-V Characteristics of a C9 patch, a C10 patch and a C11 patch nanografted into a C12 SAM matrix. All the patches were imaged in current independently; that explains the difference in C12 resistance measured in the three cases. Resistance was taken to be the reciprocal of the slope of each straight-line fit. Values for C12 were 1372±18 GΩ, 5315±95 GΩ , and 5775±204 GΩ in the presence of C9, C10 and C11 respectively.

This problem can be overcome by operating a weighted normalization of C9, C10 and C11 resistances. To this end we fix a value for the C12 SAM resistance that is, for simplicity, the value extrapolated from Figure 4.3C for a twelve carbon chain. Data normalized in this way can be directly compared.

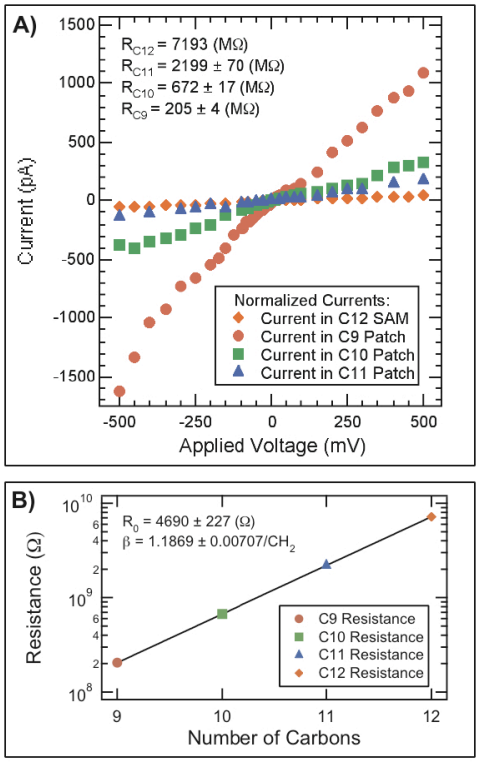

Figure 4.5. (A) I-V plot of the normalized C9, C10 and C11 currents. C12 SAM resistance was fixed to the value of about 7193 MΩ, extrapolated extending the plot in Figure 4.3C to a 12 carbon chain. Ratios between the experimental C12 resistance values and this "theoretical" one were used to normalize all the patches resistances. (B) Semilog plot of normalized resistance vs. number of carbons constituting the alkanethiol chains. Straight line is an exponential fit done using a contact resistance of about 5 KΩ and decay constant close to 1.187/CH_2. Values are in good agreement with the previous experiment: a difference of 0.8% in the extrapolated values of β for the two experiments gives a difference in calculated resistance values of about 9%.

Figure 4.5A shows the normalized *I/V* plots for the four alkanethiol molecules. Filled markers describe the behavior of the molecules in the nanopatches, whereas the empty ones correspond to the 7193 MΩ resistance for C12 SAM extrapolated from the curve in Figure 4.3C. The normalized data are used to evaluate the resistance of the alkanethiols in term of 1/slope of the *I/V* curves. The logarithm of impedance values is then plotted versus the number of carbons in the

chains (Figure 4.5B) in order to extrapolate the tunneling current decay constant from the slant of the fitting exponential function. The slope of the plot gives a tunneling decay constant β = 1.1869±0.0071/carbon or ~0.93 $Å^{-1}$ at a contact resistance of about 4690±227 Ω. The validity of this differential approach is corroborated by the fact that the β values of the two experiments are very close one to the other (less than 1%) meaning that we are not distorting the true physical meaning of the data.

Conclusions and Outlook

We demonstrated here that, by combining nanografting with a differential measurement approach, we can determine the resistance of alkanethiol molecules with an higher precision than it was possible so far. Our approach has the considerable advantage of circumventing the problem of the contribution of the junction properties to the molecular transport measurements. By accepting the unavoidable presence of a tip-contamination layer on top of the SAM molecules, and by considering relative, instead of absolute, measurements, we have demonstrated that the contribution of such layer can be cancelled out, provided that experimental data are correctly normalized. In particular, it is necessary that all the nano-patches of the different molecules involved in the study are imaged simultaneously in the same frame or, alternatively, that the patches are imaged separately while each one is embedded in a reference SAM of the same molecule. The tunneling current decay constant β, obtained from our data is in good agreement with the values reported in the literature. Moreover, the determination of *I*/*V* characteristics in our approach is faster and has a much lower experimental error when compared with other point-by-point *I*/*V* methods, due to the high number of data points obtained from a single image.

As shown in Figure 4.4, the errors affecting current measurements increase as the length of the molecules under investigation increases. An explanation of this trend can be found in the higher resistance of such molecules and, therefore, the low detected currents that force the amplifier to work closely to its sensing limit. Differential comparison between longer molecules is actually under investigation using an improved amplification chain.

Concerning the set-up presented in this work, and in particular the experimental environment, there are other kinds of complication that have to be addressed. When working in air, in fact, the adhesion effect of atmospheric water has to be taken into account. A perfect knowledge of the force applied by the tip is impossible in air. Measured tip-SAM pull-off forces can reach tens of nN, depending on tip radius, meaning that even at nominal zero applied force, there is an effective load of up to 15 nN load on the junction. This effect may be controlled moving to a vacuum or a liquid environment. The latter route, even if more challenging, looks like the most promising one, especially when the aim, as in our case, is to extend this kind of study to more complex, biological systems in their physiological environment.

Methods

Materials and Instrumentation

Gold wire (99.99% pure) was purchased from Metalli Preziosi S.p.a., Milan, Italy, Muscovite mica from Goodfellow Cambridge Limited, Huntingdon, England. Ethanol (99.8% purity) and all alkane thiols were used as received from Fluka and Sigma Aldrich respectively. All the measurements were carried out using a commercial NT-MDT Solver PRO AFM endowed with a low noise, high gain amplifier (AU020-NTF, NT-MDT Co.) characterized by a 3 fA/√Hz noise level, and able to measure currents up to 100 pA, where the amplifier saturates. Nanografting was performed in an open liquid cell using silicon rectangular cantilevers (μMash NSC36/noAl, spring constant 0.6 nN/nm) while all the current measurements were carried out with conductive Pt covered silicon V-shaped cantilevers (μMash CSC21/TiPt, spring constant 0.12 nN/nm). The loads applied during imaging and current measurements were set to about 0.5 nN in order to assure good tip-film contact avoiding at the same time penetration of the monolayer. In case of nanografting, the load was as large as 50 nN. Current measurements were carried out under atmospheric conditions.

Monolayer Preparation

Two different kinds of gold substrates were used in the described experiments: a cold deposited gold surface obtained by slightly revising the procedure described by the Ulman group[110] (refered to as Ulman gold) and a hot deposited gold on mica.

Briefly, a thin gold film was first thermally deposited onto a freshly cleaved mica surface that afterwards was cut into 8 x 8 mm2 pieces. Epoxy SU8-100 glue was then distributed in drops on the gold side of the slides. The samples were backed at 95° C for 5 hours in order to remove the solvent from the glue drops. Successively the SU8 was cured by exposure under a 462 nm wavelength UV lamp at a power of about 70 μW/cm^2 for 15 minutes. All samples were then annealed at 95° C for at least 3 hours. The SU8 drop, now looking as a flat hard surface strongly attached to the gold layer, can in this way be mechanically detached in air from the mica substrate, keeping the gold film attached to it. The surface of gold originally buried at the interface with the mica is now available. Such a Au film surface has the advantage of reproducing the flatness of mica, giving an extremely reduced roughness, of about 4 Å. Gold island boundaries look very light and almost indistinguishable from large-scale topographic images. Samples are, immediately after stripping, soaked in a freshly prepared 100 μM solution of thiols in ethanol.

The second kind of substrate used in the present work is a more conventional gold film deposited onto heated mica substrates using a thermal evaporator at a background pressure of 5 x 10^{-8} Torr. Freshly cleaved mica was inserted into the vacuum chamber and subsequently backed at 400° C for 24 h. Typically, 800 Å of gold was deposited at 0.2 Å/s with the substrate heated at a temperature of about 340° C. Immediately after metallization and cooling down to room temperature, the gold was placed into freshly prepared 100 μM thiol solution in ethanol for at least 48 h. [2]

Before use, each sample was rinsed with several mL of absolute ethanol and gently blown dry with nitrogen.

Junction Formation and Characterization

Our junctions are formed by nanopatches of the molecules of interest inlaid in a reference SAM matrix. The molecular patches or the surrounding SAM are than "sandwiched" between the supporting gold surface and a platinum covered AFM tip that acts as the second metallic contact of the junction.

For the nanofabrication we start from a gold surface with a well packed SAM on top of it. The whole procedure is performed in a sealed liquid cell filled with an ethanol solution (100 μM) of a different thiolated molecule. SAM molecules are easily imaged by AFM by using a low imaging force of about 0.5 nN. If we increase the force above a certain threshold, that depends on the molecule's chain length, the molecules of the SAM are displaced during the scan and replaced by the ones in solution which self-assemble on the freshly exposed gold surface. In the case of alkanethiol molecules, using a tip with a radius smaller than 10 nm, the threshold is around 50 nN. The resulting nanofeatures, of about 200 x 200 nm^2, can be imaged by AFM at low imaging force, e.g. 0.5 nN. The molecules in the patch rapidly self-assemble, due to the nanometer-confined environment and to the tip local effect31. Completion of the molecular substitution can be proved by resolving the $(\sqrt{3}\times\sqrt{3})R30°$ structure of alkanethiols on Au(111) film inside the patch,[62] or from the height distribution analysis. Table 4.1 reports the measured height differences between C8, C9 and C10 nanopatches and a surrounding C18 reference SAM. Each value has been obtained by measuring the distance between the Gaussians describing the height distribution of the patch and of the SAM molecules in a sufficiently large area holding the patch of interest. Theoretical values are also reported as comparison. The height difference between C8 and C9, and between C9 and C10 (corresponding of a single methylene group height contribution) are about 0.104 nm and 0.112 nm respectively, both very closed to the theoretical value of about 0.11 nm.[45]

After nanografting the silicon tip is removed, and replaced with a Pt covered conductive one. Tip replacement is always necessary after nanografting, because this process degrades the tip reducing its sharpness and generally contaminating it. To find the nanostructured area after tip-exchanging, we produce on the surface, before nanografting, micron-sized markers, easily

visible with an optical microscope. The shape of the markers was chosen in order to optimize the repositioning of the AFM tip: with the new tip optically aligned over the markers, the patches are found within a radius of 3 μm or less.

Table 4.1. Patches height differences realtive to a C18 reference SAM

	C18 - C8	*C18 - C9*	*C18 - C10*
Experimental	1.085±0.027 nm	0.981±0.036 nm	0.869±0.027 nm
Theoretical	1.083±0.001 nm	0.974±0.001 nm	0.866±0.001 nm
Deviation	0.2%	0.7%	0.3%

The experimental differences are defined as the distance between the centers of the Gaussians describing the height distribution in the topographic images taken around the patch of interest. The theoretical differences are obtained by multiplication of a methylene height contribution (1.082 Å) times the difference in carbon units between the C18 reference SAM and the molecule composing the patch.

Voltages are then applied between the tip and the substrate monitoring the current flowing through the molecular assembly. The force applied by the tip was, at all times, less than 0.5 nN in order to assure good electrical coupling, avoiding at the same time tip penetration into the SAM. In fact, above 1 nN, a lower value for the height difference between the patch and the SAM was measured.[71] The range of voltage sweep during current measurements was indirectly limited by the maximum value of current readable by the amplifier, that is ±100 pA. In any case, in order to avoid damaging of the layers, voltages larger than ±500 mV were never used in the experiments. Scanning speed during current imaging was always below 200 nm/s.

From current images, collected at different applied voltages, we have extrapolated the values of current flowing through each type of molecule present on the surface. Currents are defined as the mean value of the Gaussians describing the current distribution over the patches and, eventually, over the surrounding reference SAM. This procedure is repeated for each patch and obtained values are successively used to draw the *I/V* characteristic for every molecule as shown in Figure 4.3. We would like to point out here that a single current image contains a large amount of data (usually 512×512 sampled pixels) and therefore statistical information on the molecular conductance. As a result the electrical characterization of a group of molecules can be obtained from the analysis of few tens of current images, one for each voltage value, instead of the thousands *I/V* curves needed in the case of single-point measurements.

5

Factors Affecting the Measured Current Values

In Chapter 4 the importance of a differential approach to study molecular transport with CT-AFM was demonstrated. There have been many reports in the literature on current-voltage characteristics of thiol SAMs on gold surfaces. However, as already discussed in the previous chapters, the published results from different groups are often inconsistent with one another and the underlying causes are not clear. Many factors, including the substrate/tip roughness, degree of order of the SAMs, presence of solvent, contaminants on the tip, applied load, contact area and environmental humidity, may all play important roles in the electrical measurements. [153-154]

The differential measurement by CT-AFM combined with nanografting, which has been introduced in Chapter 3 and in the previous chapter, minimizes the contribution of boundary conditions during the determination of molecular properties obtained from ratios between homologous molecules. In this chapter, some interesting phenomena that would affect the measured current

values will be discussed providing some valuable insights into the problem of current fluctuations.

The work reported in this chapter was made possible thanks to the collaboration with colleagues from the Chemistry Department of Princeton University and, in particular, thanks to the investigations done by Dr. J. Liang.

The Initial Layer and the Grafted Molecules

To compare the conductance of two or more SAMs of different molecules we can carry out differential measurements. Interestingly, we found that different measured current values have been obtained when more conductive molecules are nanografted into a layer composed of less conductive molecules, or vice versa. Usually, when the more insulated molecules are the nanografted ones, the measured current intensities, both in the patch and in the matrix layers are lower than in the reversed case (i.e. more conductive molecules forming the nanografted patch). Hereafter an example will be given to clarify the statement. Attempts to nanograft isomeric aromatic molecules were done not to long ago at Princeton University. Nanopatches of 2-Ethylbenzenethiol (CH_3CH_2PhSH, briefly EBT) were fabricated into a 2-Benzenethanethiol ($PhCH_2CH_2SH$, briefly BET) reference SAM. The measured current intensities for both SAMs were in the nA range. However, when halogenated long alkanethiol, as the case of Perfluoropentadecanethiol ($CF_3(CH_2)15_SH$, FC16 in short) molecules, were grafted in the same BET reference SAM, the measured current intensity in BET was only in the pA as shown in Figure 5.1.

To explain this result we may imagine that when performing nanografting working in a liquid-cell filled with the solution of long, insulating, molecules, some of them will be left in a physisorbed state on top of the SAM and remain also after sample removing and washing with pure ethanol. This physisorbtion will involve more energy if the number of methylene groups composing the chain, increases. In the current measurements, because the conductive tip is covered with a thin film of noble metal (usually Au or Pt), which has good affinity to the thiols, some of the residual molecules can adsorb from the top of the SAM onto the tip as contaminants. If the molecule being nanografted is a rather conductive one, the resulting contaminant layer gives a

low screening contribution. The current detected in this case (the EBT case) is higher than when an insulating molecule being nanografted (the FC16 case). Obviously, EBT is supposed to be more conductive than FC16 because of the shorter alkyl chain, the presence of the conjugated phenyl ring (with many delocalized electrons accessible to conduction) and the absence of the polar halogenated terminal head group (CF_3–).

Usually the longer the CT-AFM tip scans across the sample, the more likely the tip cleanliness is compromised. In Chapter 4 was demonstrated as long tip travels on corrugated surfaces induce a continuous increasing in the current-reducing effect due to the growth in the number of molecules forming the contamination layer. Interestingly, removing the sample from the AFM after nanografting and carefully rinsing it with pure ethanol cannot improve the situation, indicating that the amount of molecules is extremely small and agreeing well with the results in Chapter 4. A stationary tip that does not scan may adsorb fewer molecules but still can not at all guarantee the entire cleanness of it. In particular, a punctual CT-AFM characterization encounters other kinds of problems that force to a statistical approach as will be described in Chapter 6.

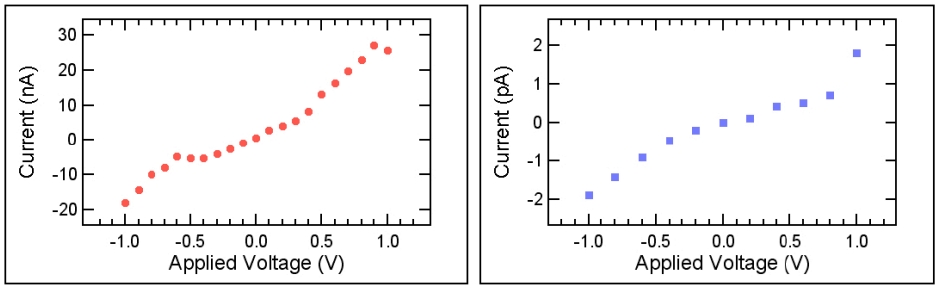

Figure 5.1. Measured current through a BET reference layer when an EBT patch (red dots plot at the left) or a FC16 patch (blue squares plot at the right) is nanografted into it. Each data point is averaged from three measurements and the standard deviation is shown.

Contamination of the tip, which has been shown to be able to change the measured current by several orders of magnitude, is the most important factor we have found that is responsible for the inconsistency of the results in the literature. This can be justified by the high sensitivity of the current to even tiny change of the tunneling distance. According to the tunneling mechanism, exposed in Chapter 3 and Chapter 4, the current I should decay exponentially with the increment of distance d, as

$$I = I_0 \, e^{(-\beta d)}$$

Where β is the decay constant. Assuming for β a value of about 1.0 $Å^{-1}$, consistent with the value found in Chapter 4 and literature,[34] the current can decay by 3 orders of magnitude if the contaminant layer is ~7 Å thick ($\Delta I = exp(\beta \Delta d)$). Has to be noticed that this thickness is comparable to half the length of a C10 alkanethiol molecule.

Because of the small radius of curvature (less than 20 nm) and surface roughness of the end of the metal-covered tip, the captured thiols are unlikely to form a compact and ordered layer on it. Thus, the double-layer model,[53] which assumes another perfectly formed and ordered layer on the probe in contact with the layer on the substrate during the measurement, may not be appropriate for describing the nature of the contact. Although the nanografting history will affect the absolute value of the current, it does not change the conductivity ratios of the SAMs in our differential measurement (the tip condition may be leveled using this method), as extensively described in Chapter 4.

Figure 5.2 shows some other experimental results that support the above conclusion. In Fig. 5.2A, we show the current image of a FC16 patch nanografted into a Benzyl Mercaptan (Ph-CH_2SH, shortly BM) reference layer. The resulting current through BM matrix, which is one methylene group shorter than the BET molecule, is only ~5 pA at a bias of 1 V, much smaller than the current value for BET reported in the plot of Figure 5.1A, but in agreement with what measured in Fig. 5.1B. In Figure 5.2C, FC16 molecules are nanografted into a C10 reference layer followed by current measurements. The current through the C10 layer is also very small (~1 pA), less than that reported before in Chapter 4 (see for example Figure 4.3A), but different also from literature values coming from STM characterization.[84,155] Meanwhile, similar to Figure 5.2A, the current flowing through the FC16 patch is zero because it composes of a long, well insulating saturated molecule.

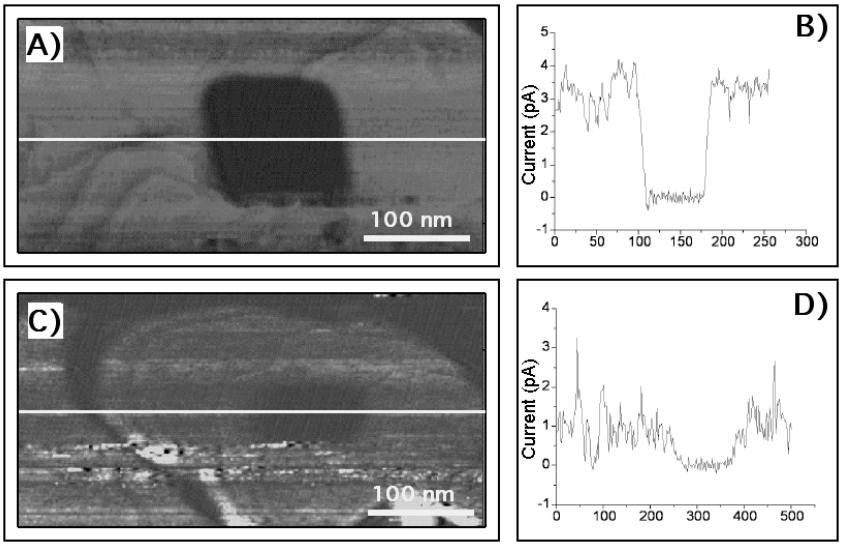

Figure 5.2. (A) The current image (bias = -1 V) of a FC16 patch in a BM reference layer and (B) the corresponding current line profile; (C) the current image (bias = -2 V) of a FC16 patch in a C10 matrix and (D) the corresponding current line profile.

In general has been seen that nanografting technique, compared with dip-pen nanolithography, [115] leaves a smaller amount of residual molecules on the surface. Explanation of that is the fact that the relative concentration of "dried" molecules onto AFM tip during nanofabrication is higher (or better, unknowing higher) compared with the molecules in the nanografting solution. Consequently, during the nanofabrication, a large number of molecules will diffuse not only inside the area of interest but also on the top of the surrounding SAM matrix.

A fundamental point to focus on is the difficulty to obtain consistent values from the differential approach also in the case when the nanografted molecules are very good insulators. This is somewhat unexpected because, in principle, differential analysis of currents has the ability, as demonstrated, to remove the contribution of the contamination layer. Unfortunately if the junction becomes too insulating, and the currents flowing through it very small, the amplifier may be not able to detect them or, if it can, the instrumental error afflicting the measurements will be very high. In conclusion, nanografting of long molecules in short ones is to be avoided if at all possible, preferring instead the inverse nanofabrication order.

Humidity and Temperature

The atomic force microscope used in our laboratory for the electrical characterization of molecular junctions is equipped with a metallic cap covering all the instrument head. This protective lid is electrically grounded assuring electromagnetic and acoustic insulation during measurements. The hermetic ambient so created gives us the possibility to have temperature and humidity control. A small heather coupled with a PID feedback controller and a inlet pipe for nitrogen flow may be used for environmental control.

The usual relative humidity inside the box is 20-30% while the temperature is held approximately to 20÷25 ºC. When the AFM is operated for more than 1 hour, the heat produced by the instrument can increase the temperature by 1÷2 ºC. In principle, the measured current should not depend on the slight temperature variance if the electron transport follows the elastic tunneling mechanism as reported in Chapter 3 and in literature.[32,133,144] Humidity reduction can be achieved by placing desiccant in the box or flowing in a gentle flow of nitrogen. The purging method usually can reach lower humidity (<10%) than the desiccating one. To increase the humidity, a beaker containing water is inserted in the box until the humidity reaches equilibrium. A high sensibility thermo-hygrometer is used to monitor local and ambient temperature and humidity. Current through a C10 layer was measured at two different humidities (10% and 40%, respectively), at the same temperature (~24 ºC) and using the same AFM tip. The conductive probe was immersed in the piranha solution (3:1 ratio between sulfuric acid and hydrogen

peroxide) for 15 minutes and then rinsed with deionized water and dried with a gentle flow of nitrogen before being used. After engagement, the tip scans a small region (10x10 nm^2) on the flat top of a gold sample. The current intensities are recorded as randomly picked scan lines (each scan line has 512 data points) and then averaged along the lines. The first 15 recorded scan lines are further averaged and the results are reported in Table 5.1. The results indicate that the averaged current does not show strong dependence on the humidity. The measured currents, regardless of the polarity of the bias, are all at the same order of magnitude at the humidity of 10% or 40%.

Table 5.1. Humidity dependence of measured current on a C10 SAM.

	Low relative humidity (10%)		*High relative humidity (40%)*	
	Bias = +1V	Bias = -1V	Bias = +1V	Bias = -1V
Averaged current (pA)	0.82	2.72	2.11	1.49
Standard deviation (pA)	0.36	0.62	0.39	0.18

The plus and minus sign applies when the potential of the tip is more positive or negative than the sample, respectively.

Normal Force

Force in AFM is determined by the detection of the cantilever deflection and the knowledge of cantilever elastic constant and many factors may affect the load felt by the surface. First of all has to be mentioned the fact that commercial AFM tips are sold with a large imprecision in the declared force constant value *K*. Usually *K* variance is in the order of 25% to 250% of asserted value. To this the variance in the load, in terms of pressure, due to variations in the radius of curvature of the AFM tip plays an important role. Larger is the radius greater is the tip/surface contact area and so, minor is the exerted pressure at parity of applied force. To conclude, an environmental factor is also present. Due to the ambient humidity, a more or less uniform layer of water of some hundreds of nanometers thick, covers every surfaces. The meniscus forming when the tip is in contact with these surfaces exerts an extra force on it (also called capillary force) that, in case of hydrophilic surfaces and tips, is in the order of some nN. All these factors are responsible for a not perfectly know applied load.

Depending on the applied load, going from low to high force regime, three different scenarios may be considered. At small loads, in ambient conditions, the tip is in "apparent" contact with the top of the SAM. The term "apparent" is used because between tip and surface may be present a very thin layer of environmental water. Increasing the force may induce displacement of this water until none, or only some, molecular layers are present. At intermediate loads the tip starts to deform, usually bending or tilting, the molecular SAM. Some molecular water layer may remain depending of the entity of SAM terminal head to water interaction (e.g. hydrophobicity or hydrophilicity). At high forces the tip punches the SAM undergoing, for example, to gold substrate contact. The last two regimes have not a clear distinction due to the fact that, depending on the tip apex size and SAM imperfections, penetration may appear at very low forces. It is easy to understand that every of the three listed regimes present different transport behavior. The main reasons of that are the reduction of the distance between tip and the top of the SAM, depending if the transport is through or across molecule also the reduction of the molecular junction thickness influence the current intensity and, finally, force induced SAM defects may induce fluctuations and spikes in detected currents.

Figure 5.3 shows how the current changes for a FC16 patch nanografted into a BET matrix as the applied tip load is increased. The long alkyl chain in FC16H generates relatively strong intermolecular van der Waals force that stabilizes the SAM and consequently, up to 50 nN, the current recorded for the patch is always zero. However, for BET surrounding layer, the current increases very slowly at force below 30 nN but is very fast after that.

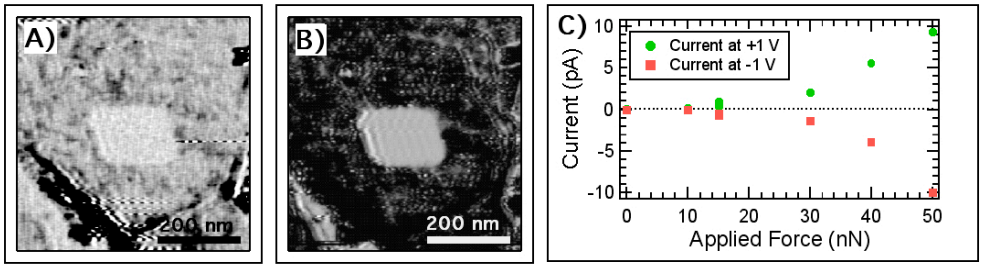

Figure 5.3. Current images of a FC16 patch nanografted into a BET matrix. (A) Normal load exerted is 10 nN; (B) normal load is 50 nN; (C) the current versus normal load relationship of the BET layer for positive and negative applied voltages (green and red markers respectively).

These results suggest the tip probably penetrates (especially for very sharp tips) or deforms the layer (this is the case when using blunt tips) at force larger than 30 nN[25,50,130-131] and shorten the tunneling distance. Although the force can effectively affect the current, as demonstrate in Figure 5.3C, the intensity change is no more than one order of magnitude when the normal load is raised from 1 nN to 50 nN. Although the sensitivity of the AFM cantilevers has been proved to be able to detect differences in force in the pN range in controlled enviroment, [156-157] we have already listed reasons that make difficult an absolute estimation of the real applied force. These factors, anyway, have a contribution of some nN in the force indetermination. Consequently, the normal force is not the major concern for the huge discrepancies of the measured current reported in the literature.

Different Probes

In CT-AFM the (cantilever) tip is the probe detecting currents so the strong influence it has is expected. We had already occasion in previous sections of the thesis to point out the fact that even the same type of AFM tips are different (also tips coming from the same box are slightly different). In particular, in our work we focused on the large spread in the factory declared geometrical, and indirectly elastic, cantilever properties. Regarding the cantilever tip, its radius of curvature is provided as lower than some value (e.g. less than 10 nm), meaning that smaller radii are possible. Various experimental techniques and calculation methods have been developed and applied for measuring and/or estimating this value.[158-160] However, even if the starting radius would be known precisely, the effective tip radius of curvature can change dynamically because of the wearing of the tip or adsorbing of contaminants during operation. Thus the contact area under the AFM tip and the number of molecules actually measured are very case-specific. To add further complication, material forming or covering the tip to make it conductive may have strong contribution due to different contact potential or affinity with molecular layers under investigation. Tips made using highly doped silicon or covered with a layer of a metallic (Au, Pt, Pt/Ir, etc.) or ceramic (W_2C, TiN, etc.) conductor are commercially available.

To prove the consistency of current values coming from the same type of conductive AFM tip some electrical measurement on Biphenyl 4, 4'-dithiol (BPDT, in short) patches nanografted in a C10 matrix have been successfully performed in different experimental setups using the same type of Pt/Ir coated silicon nitride tips (SCM-PIC, Veeco instruments). The current values at a positive applied voltage of 1 volt were: (85.7 pA, 66.4 pA, and 82.6 pA); 90.1 pA; (71.0 pA, 85.1 pA, 92.1 pA, and 95.6 pA); 56.6 pA; 79.8 pA (values in each pair of parentheses are different patches measured using the same tip). Surprisingly, the maximum and minimal current values obtained using 5 tips on 10 BPDT patches just differ from each other by a factor of ~2, indicating that the contact properties of the same type of tips probably are very similar to each other when following the same experimental procedures in the same experimental shot. This explains the fact that the current values reported from the same group for a certain molecule are usually self-consistent, but not with those from others group obtained following different or the same experimental protocol.[34]

Summary

We have discussed several factors that influence the measured current values in our differential characterization of the electron transport properties of SAMs by CT-AFM combined with the nanografting technique. These factors, including the nanografting process, the compactness of the SAM, normal load, contact area of a specific tip and environmental factors as humidity and temperature, can all affect the experimental results to different extent. The contaminants on the tip, which can shift the current value by several orders of magnitude, are probably the most crucial reason for the discrepancies of the data obtained from different experiments. Other factors affect the current value to a less degree (around one order of magnitude or less) and are easier to control. Further investigations are necessary in the direction of a better understanding of tunneling junction components. In particular role of water has to be addressed. To do that two possible routes may be followed: ultra high vacuum (UHV) differential CT-AFM experiments may help to increase the cleanness of the system, while liquid current measurements, performed in a liquid cell, may extend our knowledge about solvent contribution in molecular transport.

Both cases eliminate the water meniscus force contribution from the surface reducing so the applied load indetermination.

6

CT-AFM Investigations with Aromatic Thiol SAMs

In Chapter 4 we focused on the development of a new, *differential*, approach to electrical characterization of molecular junctions. Motivation for this strategy was to bypass all the uncontrollable factors influencing the Metal-molecule-Metal junction such as tip/molecules contact quality and composition (see Chapter 5). To do that we used CT-AFM as main investigation tool showing how it is possible to determine easily, and with low experimental errors, properties that depend on the ratio between the "resistance" of molecules belonging to the same family. The tunneling current decay constant (*vs*. chain length) was measured for molecules that belong to the alkane-thiol family (see Chapter 4).

Aim of this chapter is the extension of the technique to molecules that don't belong to the same family (non-homologous molecules) such as comparing aliphatic and aromatic thiols in the same experiment. Using a reference SAM layer of a well-characterized molecular family (as the case of alkanethiols) a normalization of electrical properties for all the molecule under investigation is possible. Doing that a value for the resistance of a short aromatic thiol (2-Benzene Ethanethiol) is determined. An indirect comparison of this value with values coming from literature shows that the order of magnitude for resistance is correct.

1. Comparison Between Heterogeneous Molecules

In recent years, molecular electronics research has generated considerable interest.[161] To create molecular devices, new "conductive" organic molecules, e.g., conjugated molecular wires have been synthesized. Self-assembled monolayers (SAMs) of such conjugated molecules have also been reported.[162-165] Furthermore, many interesting studies on the transport of electrons through molecules have appeared concerning the electron transfer along the molecular axis using scanning probe microscopy (SPM),[26,44-46] mechanical break junction,[39] and nanogap electrode techniques.[35,166]

The transport of charge through adsorbed molecules using STM is quite complicated compared to other techniques such as break junctions or nanogap electrodes, where the electrode is directly attached to the molecules. While it is possible to estimate molecular "conductivity" using scanning tunneling spectroscopy (STS), it is not so easy to minimize the effect on the measurements of the tunneling gap between the STM tip and the molecules. Atomic force microscopy (AFM) using a conductive cantilever (usually referred as CT-AFM, see Chapter 3) in contact with the molecules under investigation, is a good candidate for direct measurement of electrical conduction of organic monolayers such as SAMs.[53,167]

The detailed electron transport mechanism through organic monolayers is still unclear, although great progress has recently been made. Further systematic experimental studies are necessary, because reliable nanoscale electron transport measurements through organic molecules have just begun.

In the study presented in this section of the thesis we are going to discuss the transport of electrons through a nanoscale patch of a short aromatic molecule (2-Benzenethanethiol) confined into a short alkanethiol SAM matrix (1-Hexanethiol) making use of a nanolithographic technique (nanografting, see Chapter 3). Our objective is to explore the possibility of applying the *differential* scanning CT-AFM technique, studies presented in Chapter 4, to molecules that are not homologous with the saturated hydrocarbon series measured before. In particular, keeping in mind the difficulty of an absolute approach to a measurement, we are trying to understand if, at

least, an indicative absolute value for the "molecular resistance" is obtainable starting from our differential approach.

Nanofabrication and Measurements

Using nanografting we fabricate four, one monolayer-thick, nano-assemblies of 2-Benzenethanethiol ($Ph(CH_2)_2SH$, briefly BET), side by side, into a reference 1-Hexanethiol ($CH_3(CH_2)_5SH$, briefly C6) SAM on a gold film (Figure 6.1). Metal-molecule-Metal junctions are then created, as extensively described in Chapters 3 and Chapter 4, by placing a clean conducting AFM tip in contact with the top part of the molecules and scanning the surface while a fixed tip-surface bias voltage is applied. The current flowing through the nanografted patches of BET and through the reference C6 monolayer (the carpet) can be recorded in a single image, where differences in contrast are representative of the variation of current levels. Current data coming from all images are then used to determine the average current values for a specific applied bias looking over the current histogram of the image.

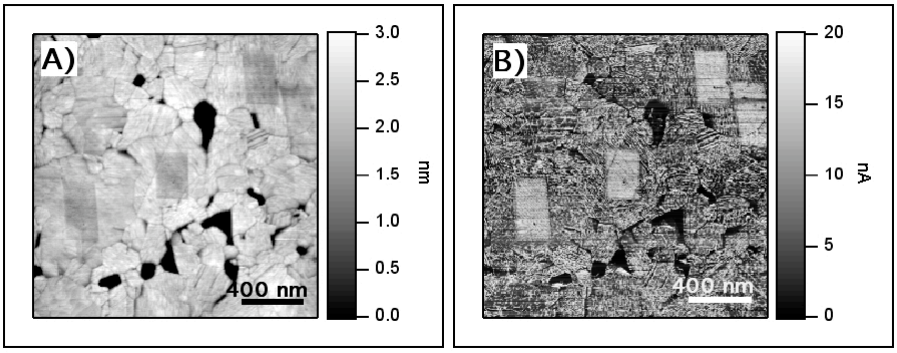

Figure 6.1. (A) Topographic AFM image acquired with a Pt coated silicon tip immediately after nanografting of four BET patches into a C6 SAM matrix. Difference in height between the patches and the surrounding C6 SAM is about 1.2 Å. (B) Current image acquired simultaneously to (A) at +500 mV bias. Distortions in the shape of patches are related to the drift of the x-y piezo-scanner.

The force feedback circuit of the AFM controls the mechanical load on the nanocontact keeping it constant while the current image is collected. The current image, together with the topographic image acquired by reading out the AFM laser-deflection feedback, is simultaneously registered. This provides the capability to obtain information about order in the monolayer packing by measuring the patch-to-carpet height difference, and comparing this number with the one

evaluated by assuming that the alkanethiol molecules are inclined by about 30° with respect to the surface normal[84,137] and, in spite of the presence of the phenyl ring, assuming a molecular tilting of BET of about 20° adopting in a $(\sqrt{3}\times\sqrt{3})R30°$ structure.[49,129,162,168] The calculated difference in film thickness between these two SAMs is about 1.4±0.05 Å, considering that the normal to surface carbon-carbon distance in tilted alkanethiol chains is always about 1.1 Å for a chain tilt angle of 30°[137] and 1.19 Å for a 20° tilt angle. Carbon-carbon distance in the phenyl ring was considered of about 1.4 Å. This theoretical value is close to the BET/C6 difference in height experimentally determined from height profile analysis on the topographic image (1.2±0.5 Å).

A tunneling M-m-M junction having a BET nanopatch placed into a C6 SAM carpet, on the same metal surface, is sketched in Figure 6.2. At the lower level are the molecular assemblies, with thickness and conductance determined by the specific molecule; at the upper level there is the metalized CT-AFM tip with its circuit scheme.

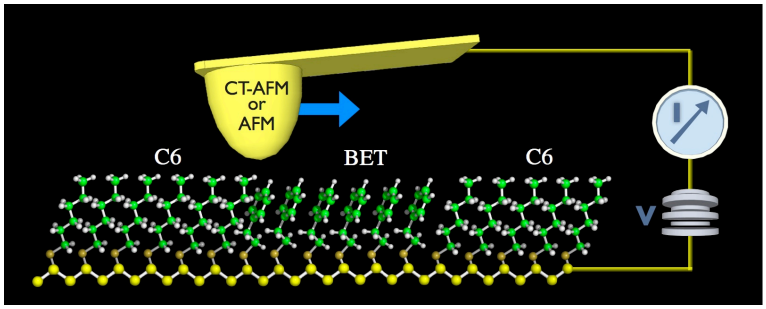

Figure 6.2. Two-layer tunnel junction model sketching a nanopatch of shorter (by ~1.2 Å) 2-benzenethanethiol molecules into a SAM made of 1-exanethiol molecules. The tip moving from left to right engage the two distinct molecules. When a difference in potential is applied between tip and gold substrate a current flow is recorded using a high gain current meter. The tip records, for every applied potential, a topographic and a current image simultaneously. The contact area does not change from A to B because of the feedback on the interaction force of the AFM. Concerning current sampling, we acquire current images rastering lines of 1000 nm of surface at 1 Hz. If we consider molecules spaced of about 0.5 nm, 2000 molecules are scanned in one second (2 kHz). The amplifier used (NT-MDT AU006) has a bandwidth of about 10 kHz meaning that one molecule is sampled 5 times before tip moves to the adjacent one.

In Chapter 4 we demonstrated, by measuring point by point in a current image the electron transport through two SAMs of molecules of the same homologous series, placed *side-by-side* on the same surface, that it is possible to determine the decay factor β ruling out the effect of the, usually unknown, boundary conditions. The strong influence of the contact resistance on the tip side of the measurement was also highlighted.

For testing the possibility to compare molecules belonging to different families with the already explained differential approach (see Chapter 4), we have chosen to use saturated and conjugated molecules. Behind that choice, is the possibility to refer to the large volume of experimental and theoretical work that has addressed the chain length dependence of the electron transfer through σ and π systems.[57] In particular, it has been demonstrated that the electron transport is dominated by coherent non-resonant tunneling and that, therefore, the junction resistance depends exponentially on the molecular length[53] and that, for small voltages, the *I*/*V* characteristic is consequently linear.[141] Different kinds of experimental techniques, have shown that the electron current through the junction is proportional to $\exp(-\beta l)$, where β is the tunneling decay constant of the molecules and l is the length of the formed junction. As in the case of homologous studies, the two adjacent SAMs of different molecules sandwiched between two metallic contacts may be imaged as part of a two double junctions system, in which a third layer (the contamination layer) is present (refer to Figure 4.1 for details about the junction). Transport through these double junctions is affected by the transmission coefficient of the layers involved (the well know SAMs and the unknown contamination layer), by the layer-by-layer electron hopping and, clearly, by the contact resistances located at the interface between the metal tip and the contamination layer and between the thiol SAMs and the gold substrate.

Absolute Resistance Values for Molecules Non-Homologous whit the Alkanes

In previous discussions the concept of the difficulty to obtain absolute values from a measurement was presented. To extrapolate a reasonable absolute value for the molecular “resistance” the normalization protocol introduced in Chapter 4 is used. The determined resistance value of 2-Benzenethanethiol will be normalized using the value obtained for 1-Hexanethiol and the current tunneling decay constant β coming from Plot 4.3C. The ultra-flat Ulman gold film[110] allows for the fabrication of many BET nanopatches close one to the other in order to increase the number of current samplings.

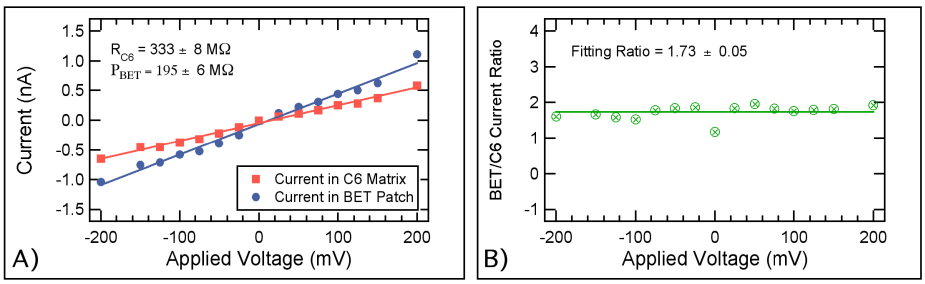

Figure 6.3. (A) *I/V* characteristic of C6 (red squares) and BET (blue dots). Aromatic thiols were nanografted into the aliphatic reference matrix. (B) Current ratios between BET and C6. The ratio gives an idea about the evolution of the tip contamination during succeeding scans. The good alignment of the ratios around a value of about 1.73 is a good indication of the tip state and assures that currents stay for both molecules in the linear regime of tunneling. The value at zero voltage was not taken into account.

Figure 6.3A shows the average current-voltage (I-V) trace extrapolated from current images for BET and C6 molecule. Every point in the red curve is the average from the current values of each of the four patches, whereas the blue line is the fitting of the average values of all the surrounding C6 matrix. The load applied to the tip during scanning was less than 1 nN and the same Pt-coated tip was used for the whole experimental session. All the traces are linear over the voltage sweeps as indicated also by the good alignment of the BET/C6 current ratios represented in Figure 6.3B. The fitting lines of molecular resistance are used to define a junction resistance equal to 1/slope. Resistances of about 333±8 MΩ and 195±6 MΩ were determined for C6 and BET respectively, with an error of about 2%.

The obtained resistance, in order to be comparable with absolute values coming from literature, has to be normalized. To do that we can take advantage of the knowledge of the experimental resistance ratio between BET and C6 and of the possibility to calculate a theoretical value of C6 resistance using the results of Chapter 4. The calculated resistance of a C6 SAM using the relation $R=R_0\exp(\beta n)$ where, R_0 and β are respectively the contact resistance and the tunneling current decay constant for every carbon forming an alkanethiol chain, is of about 6.2 MΩ. The term n is the number of carbon constituting the alkane molecule. The tunneling decay constant β (1.1965±0.0033 per methylene group or, ~0.94 $Å^{-1}$) is given by the slope of Plot 4.3C, while the contact resistance is of about 4600±150 Ω. Using the determined fitting ratio of 1.73 (Plot 6.3B) a resistance of 3.6±0.1 MΩ is given for BET.

The values determined are not values per molecule but represent the global values of the molecules touched by the tip. Taking into account that both C6 and BET present a $(\sqrt{3}\times\sqrt{3})R30°$ structure on gold, the best molecular density achievable is ~5 molecule/nm^2.[2] If we suppose now for the tip a contact area of about 20 nm^2, the currents detected by the conductive tip are an average on the ~100 molecules forming the junction. From that, a resistance of about hundred times larger for a single molecule may be calculated supposing our system as a classical parallel of resistors (~360 MΩ for a single BET molecule). Anyhow, the uncertainness in tip size and applied force (see Sections 5.3 and Section 5.4) induce uncertainness in the tip/SAM contact area that may induce large errors in the estimation of molecules forming the junction. Moreover, simply considering an across molecules transport contribution in tunneling, the simple model of parallel resistors may be not adequate to describe the collegial molecular behavior to charge transport.[151,169-170] For these reasons more work as to be done in order to be able to extrapolate single molecule information from massive measurements.

Conclusions

We demonstrated here that, by combining nanografting with a differential measurement approach, we could determine the absolute resistance of an aromatic thiolated molecule (2-Benzenethanethiol, BET in short). The approach has the advantage of circumventing in part the problem of the contribution of the junction properties to the molecular transport measurements. The fact that the nanopatches of BET and the 1-Hexanethiol matrix are imaged simultaneously in the same frame allow for a normalization of the obtained resistance values. In fact, using the tunneling current decay constant β, obtained from previous experiments for alkanethiols, and assuming a contact resistance of about 4600 Ω, a theoretical value of resistance for C6 was calculated and used to extrapolate BET resistance after normalization. The obtained value of 3.6±0.1 MΩ for BET may be compared with the results presented by Ishima et al. about electrical conduction of conjugated molecular SAMs studied by punctual CT-AFM. In this work a resistance value of about 0.5 MΩ is obtained for 2-Benzenemethylenthiol (BMT) that, instead of two methylene groups as BET, presents only one. Anyway, considering that two carbons in alkanethiols contribute to a current reduction of about 1 order of magnitude (see Plot 4.3C, where β = 1.1965±0.0033 per methylene group or, ~0.94 $Å^{-1}$) an indirect evaluation for BET

resistance may be obtained using the relation $R_{BET} = R_{BMT} \exp(\beta)$. The calculus gives a value of about 1.65 MΩ for the 2-Benzenethanethiol's resistance. This is evidently more than two times smaller than the obtained one, remarking the difficulty to obtain absolute values from measurements but, anyway, they are of the same order of magnitude. The presented approach represents so a valid and quick procedure to obtain values that can give a first idea of the resistance of a molecular film.

Materials and methods

Gold wire (99.99% pure) was purchased from Metalli Preziosi S.p.a., Milan, Italy, Muscovite mica from Goodfellow Cambridge Limited, Huntingdon, England. Ethanol (99.8% purity) and all molecules were used as received from Fluka and Sigma Aldrich respectively. All the measurements were carried out using the same equipment of Chapter 4 apart from the amplifier. The commercial NT-MDT Solver PRO AFM was in this case endowed with a high gain amplifier modified to measure current through conductive cantilever from 50pA to 20nA. Nanografting was performed in an open liquid cell using silicon rectangular cantilevers (μMash NSC19/noAl, spring constant 0.6 nN/nm) while all the current measurements were carried out with conductive Pt covered silicon V-shaped cantilevers (μMash CSC21/TiPt, spring constant 0.12 nN/nm). The loads applied during imaging and current measurements were set to about 0.5 nN in order to assure good tip-film contact avoiding at the same time penetration of the monolayer. In case of nanografting, the load was as large as 50 nN. Current measurements were carried out under atmospheric conditions.

Regarding gold substrates for monolayer grown and nanolithography, Ulman gold was used as described in detail in Chapter 4.

Our junctions are formed by nanopatches of the molecules of interest inlaid in a reference SAM matrix. The molecular patches or the surrounding SAM are than "sandwiched" between the supporting gold surface and a platinum covered AFM tip that acts as the second metallic contact of the junction. To build these molecular nanostructures we take advantage of the nanografting technique extensively described in Chapter 3. For all the experiment details and procedure followed the information's present in Chapter 4. Concerning the measured height difference

between BET patches and C6 SAM, that is a good indicator of molecular packing, a value of about 0.2±0.1 nm was obtained. The value has been obtained by measuring the distance between the Gaussians describing the height distribution of the patch and of the SAM molecules in an area covering all the scan image of 2x2 μm^2. The obtained value is very closed to the theoretical value of about 0.14 nm.

After nanografting the silicon tip is removed, and replaced with a Pt covered conductive one. To find the nanostructured area after tip-exchanging micron-sized markers, easily visible with an optical microscope, were engraved on the surface.

Voltages are then applied between the tip and the substrate monitoring the current flowing through the molecular assembly. The force applied by the tip was, at all times, less than 0.5 nN in order to assure good electrical coupling, avoiding at the same time tip penetration into the SAM. Many information about surface characterization using CT-AFM are present in Chapter 3. In any case, in order to avoid damaging of the layers, voltages larger than ±500 mV were never used in the experiments. Scanning speed during current imaging was always below 200 nm/s. From current images, collected at different applied voltages, we have extrapolated the values of current flowing through each type of molecule present on the surface. Currents are defined as the mean value of the Gaussians describing the current distribution over the patches and over the surrounding reference SAM. This procedure is repeated for each patch and obtained values are successively used to draw the *I/V* characteristic for every molecule as shown in Figure 6.3A.

7 Qualitative Analysis Using CT-AFM: Molecular Order in Nanografted Patches

Nanografting, an AFM based nanolithographic technique, extensively described in Chapter 3 has several advantages over *standard* lithography and other microfabrication techniques. First, edge resolutions of 2 nm are routinely obtained and molecular precision is likely to be achieved with a sharp tip. Second, the fabricated nanostructures can be characterized in situ and with molecular resolution using the same AFM tip. Third, once set up, one can quickly change and/or modify the fabricated patterns in situ without changing the mask or repeating the entire fabrication procedure. Due to its compatibility with operating in solution, this method may, ultimately, prove to be extremely useful in forming novel nano-bioelectronic devices for research or diagnostic purposes. Nanografting has been already proven many times to have the capability to immobilize specific molecules into a surface covered by a reference self-assembled monolayer (SAM) taking advantage to the well known lateral mobility of the sulfur-gold interaction (see Chapter 2 for details). Bi-dimensional structures characterized by spatial dimensions ranging from tens of nanometers to couple of microns were successfully fabricated. Molecules composing these nanostructure ranged from aliphatic and aromatic thiols[46,70,89] to complex bio-molecules, such as proteins[69,171] and thiolated single strand and double strand DNA (ssDNA and dsDNA).[30] The ability to fabricate nanostructures, one close to the other, of such different

molecules opens to the possibility of differential studies of many molecular properties. Compressibility and friction analisis of alkanethiols,[71,171] surface-liquid interactions in membrane like systems[71] and compressibility studies on DNA are only some of a multitude of investigations performed on these nanostructured systems.

A very critical role in this scenario is played by molecular order. Mechanical properties of self-assembled molecules, such as the compressibility of the chains or the friction exerted by the terminal head group, depend strongly by the molecular packing and flatness of the surface. Regarding the immobilization of DNA probes on surfaces, one of the most appealing applications is the production of new biosensors able to detect with unprecedented sensibility genetic material present in a test solution. To do that, an explored route by our group was the fabrication of nanostructure of ssDNA of different sequences *side-by-side* in a high-density matrix.[30] The nanopatches, usually embedded in a DNA-repellent matrix of polyethylene glycol terminated thiols (PEG-thiols), are detected in height by means of AFM topographic imaging. Detection of surface immobilized complementary ssDNA molecules present in a solution spilled on the nanostructured surface will be possible detecting the patches height changes due to DNA hybridization. In fact, dsDNA is much stiffer than ssDNA (persistence length 50 times longer) [172] inducing the nanopatch to stand up taller giving, in addition, an increased rigidity to the lay.

In order to produce a device able to provide reliable results, every factor inducing changes in nanopatches rigidity not directly correlated to the hybridization process have to be eliminated. Molecular packing variations due to defects are responsible for that undesired behavior and, moreover, may make the device characterization and calibration much more difficult.[30,69,171]

Concluding with an example closer to the subject of this thesis we would like to point out that changes in molecular order or the presence of defects in a bi-dimensional Metal-molecule-Metal junction induce large fluctuations in the revealed currents due to the change in the density of molecules forming the junction and to the penetration of the tip into the SAM when using conductive tip AFM characterization (see Chapter 4).[173] In summary, concerning the degree of crystalline perfection of thiol SAMs on gold, the presence of disorder or pinholes could compromise the physical and electron-transfer blocking ability of the monolayers.[21,174-175]

SAMs prepared from liquid or gas phase on gold are characterized by a characteristic molecular structure broken by the presence of defects as domain boundaries, gold vacancy islands and molecular vacancies.[84] The question that will be addressed in this section of the thesis is if the molecular order in a nanografted structure is comparable with that present in a spontaneously formed SAM.

Resulted Order in Nanografted Alkanethiols Nanostructures Revealed with High Resolution Topographic Measurements

As described in Chapter 3, in nanografting an AFM tip is used to stimulate the exchange of molecules that belong to a matrix monolayer immersed in a solution containing molecules that are different from those of the matrix. As the AFM tip plows through the matrix monolayer, the matrix molecules are removed and replaced by these reactive molecules in solution. An example of fabricated patterns is shown in Figure 7.1A where two $CH_3(CH_2)_{17}SH$ (C18) islands inlaid in the $CH_3(CH_2)_9SH$ (C10) matrix monolayer formed on Au(111). The dimensions of the two islands are 3×5 nm^2 and 50×60 nm^2, respectively, with an edge resolution of 1 nm. By zooming into the C18 and surrounding C10 areas, molecular resolution AFM images have been acquired. The results, shown in Figure 7.1B and C, reveal a two-dimensional close-packed structure with a lattice constant of 5.0 Å.

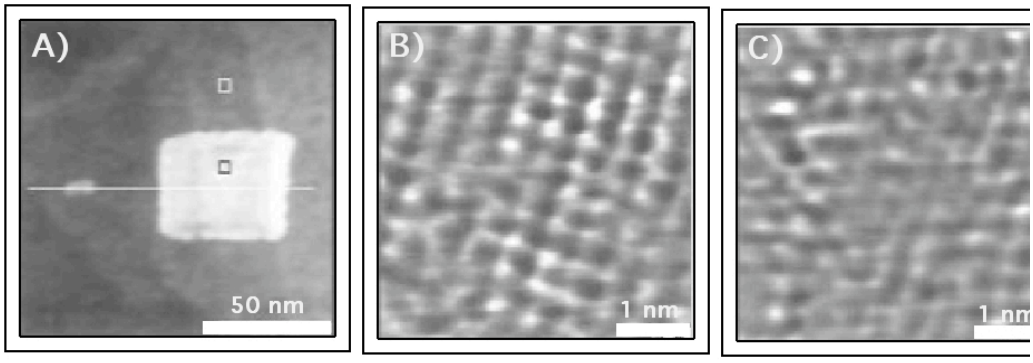

Figure 7.1. (A) Topographic image of two fabricated C18 nanoislands (brighter areas) inlaid in the matrix C10 monolayer. The steps present on the surface are due to the single atomic step of Au(111). Profile analysis, not included in the picture, shows

that C18 islands are 8.8 Å higher than the surrounding C10 monolayer, wich is in excellent agreement with the theoretical value for crystalline phase SAMs. Molecular resolution images (50×50 $Å^2$) acquired from C10 (white square in part A) and C18 (black square in part A) covered areas are shown in parts (B) and (C) respectively.

Such periodicity is consistent with the well known $(\sqrt{3}\times\sqrt{3})R30°$ based structure, in which hydrocarbon chains are close-packed and tilted ~30° with respect to the surface normal.[85-86,176-177] No C18-C10 exchange reaction was observed in the non-fabricated area during the entire course of the experiment as well no residual C10 areas are distinguishable inside the C18 nanopatches, which assures the high spatial selectivity and precision of nanografting. Only in case of substitution of very short alkanethiols into a matrix of long chain molecules some residual molecule were found to be present inside the fabricated nanopatches. This possible problem may be easily solved reducing the scan speed during nanografting and/or repeating two or three times the scan above the same area. The AFM molecular resolution image obtained above the nanografted C18 patch (Figure 7.1C) demonstrate that nanografting offers the capability to build structures with packing, and so density, comparable with SAMs formed by normal liquid or gas phase procedure.

Increased Film Homogeneity in Nanografted Alkanethiol Structures Revealed with Friction and CT-AFM Measurements

In previous experiments performed in our laboratory on nanografting of alkanethiols we conducted AFM friction analysis on several alkanethiols of different length. In friction analysis the AFM tip is moved in contact with the sample surface at fixed load while the cantilever torsion due to the tip/surface interaction is recorded. The cantilever twisting, constant during scanning on a perfectly homogeneous surface, increase or decrease because of changes either the gold surface morphology (boundary edges, surface steps or holes, but also gold surface roughness) or in the molecular film properties. Belong to this second group variations in the terminal head group of thiolated molecules, as the case when hydrophobic molecules are nanografted into a matrix of hydrophilic ones, changes in the orientation of the terminal head group, as for alkanethiols with odd or even number of carbons that present a different orientation of the terminal methyl group, and molecular disorder (vacancies, etch-pits, etc.).

To isolate the influence of molecular order in the friction deformation felt by the tip we introduced the concept of autografting. In autografting nanopatches of the same molecule forming the reference SAM carpet are fabricated. The advantage of this approach is that, if the nanostructures are enough small and the surface sufficiently flat, all the geometric contribution of the gold surface may be neglected. All the remaining contribution is the one due to the molecular order. In fact using the same molecules for the nanopatches and for the matrix SAM allows neglecting all the head contributions. Figure 7.2 shows the topographic image and the simultaneously acquired friction image of a 1-octadecanethiol (C18) patch enclosed into a C18 SAM. SAM matrix was prepared from a 100 μM ethanol solution of alkanethiol and 24 h incubation time for the thermal evaporated gold on mica (see Chapter 2 and Chapter 4 for details about gold and film preparation). Nanografting was performed in ethanol solution of the same molecules (250 μM) scanning the surface only one time at ~65 nN load. Images displayed in Figure 7.2 were acquired at an applied load of 15 nN at 1000 nm/s scan speed using a silicon tip (NSC36/NoAl from μ Masch, 0.6 N/m) with an apex radius of about 10 nm.

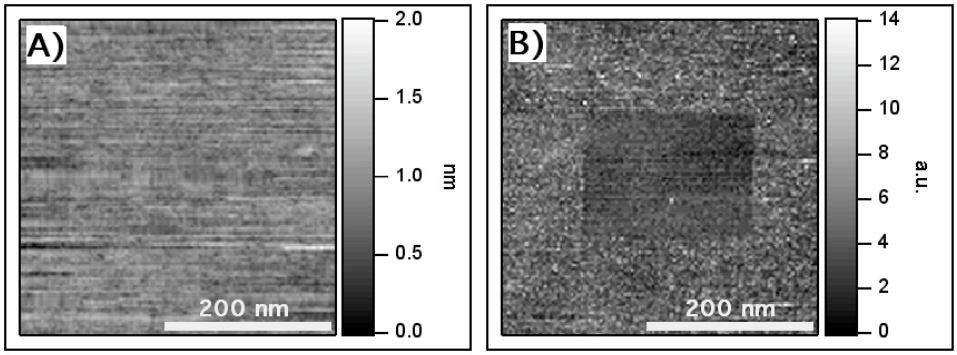

Figure 7.2. (A) Topographic image of an autografted C18 patch enclosed into a C18 matrix SAM and (B) the simultaneously acquired friction image. It is almost impossible to detect the patch in topography but there is an evident contrast reduction in the friction image. Darker areas mean lower cantilever torsion, so lower tip/surface lateral interaction.

In the topographic image (Figure 7.2A) edges of the autografted nanopatch are very hard to recognize while, in the lateral force image (endowing part of the tip/surface friction information) the patch is clearly visible as a decreasing in contrast meaning that the tip moves more freely on the patched area. This is, in our opinion, a proof of the better molecular stacking into nanostructures fabricated by nanografting.

To obtain confirmation of this speculation we attempt to use CT-AFM to have a similar characterization of molecular order. Current flow is, in fact, more sensitive to order variations inside SAM than AFM torsional analysis giving, at the same time, better spatial resolution. Irregularities in the order of few nanometers may be easily detected using conductive tip AFM. Figure 7.3 reports topographic and current images, simultaneously acquired, of a 1-decanethiol (C10) nanopatch autografted into an homologues C10 carper on gold. For details about CT-AFM refer to Chapter 3 and Chapter 4 of the thesis. Force load during scanning was less than 1 nN at a scan speed of about 500 nm/s. The AFM tip was a conductive one (gold coverd silicon tip) produced by μMasch (CSC17/Cr-Au, 0.15 N/m). Applied voltage during the scan was -0.2 volts. Regarding SAM preparation and autografting procedure, the C10 carpet was prepared following the same procedure described previously for C18/C18 autografting. The nanolithography was done at a force of only 50 nN.

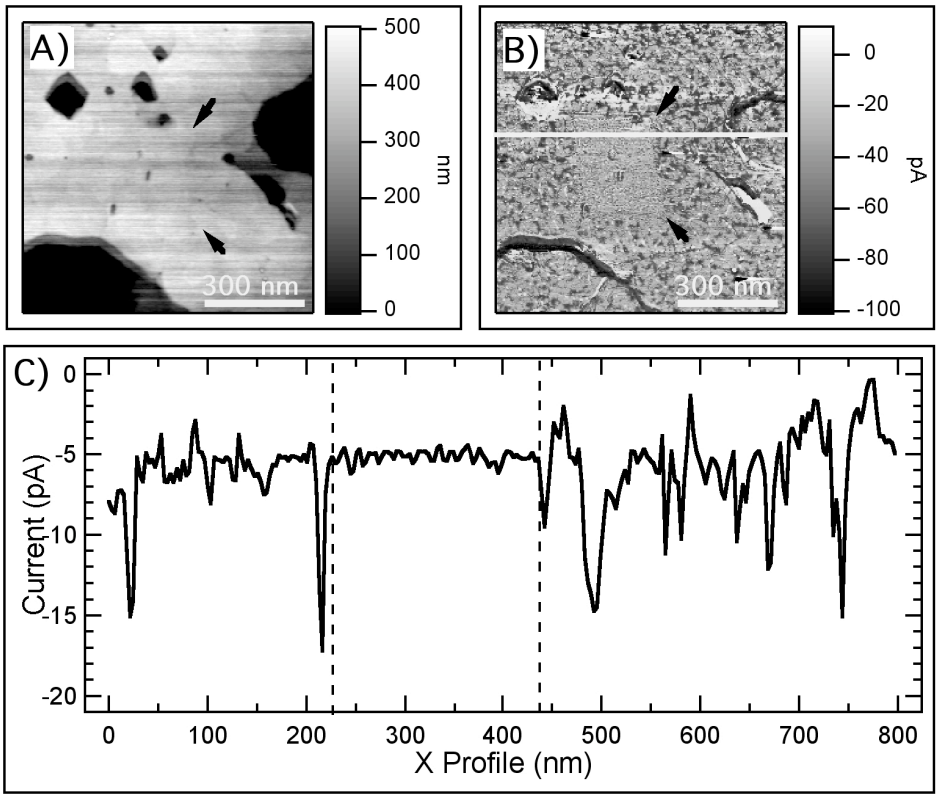

Figure 7.3. (A) Topographic image of an autografted C10 patch enclosed into a C10 matrix SAM and (B) the simultaneously acquired current image. As in the previous friction case it is almost impossible to detect the patch in topography but it is evident in the current image. Current was acquired at negative bias that means currents are negatives and flow entering the

patch plane. Consequently, darker areas mean larger negative currents. (C) Current profile of the evidenced white line in the current image. Increased current homogeneity of the patch is evident and, moreover, a drastic reduction in current spikes (dark spots) is evident in the nanopatch that looks more uniform. Gold grain boundaries induce large currents probably due to tip/gold surface short contacting.

As happened in the previous friction experiment (C18 into a C18 SAM), also in this case the patch is hardly seen in the topographic images (Figure 7.3A), while it is clearly visible in current images (Figure 7.3B). The markers laid upon the pictures help to recognize the inlaid C10 nanopatch. Analysis of the current image highlights the presence of current spikes (dark regions) in correspondence to the gold islands boundaries. Analogously, defective areas are clearly identified by current spikes outside the nanopatch. This defects, practically absent inside the autografted patch, are characterized by a size of about 50÷100 nm in diameter. These size are comparable with the dimensions of gold etch pits formed by SAM prepared from the liquid phase at room temperature and not post annealed. Anyway, profile analysis on the current image (Figure 7.3C) proves that the main value of the flowing current inside and outside the nanopatch is exactly the same but more uniform inside the C10 patch rather in the C10 carpet SAM.

Conclusions

Friction (LF-AFM) and current (CT-AFM) investigations made with atomic force microscopy demonstrate the reliability of obtaining well packed and with a low density of defects nanostructures fabricated using an AFM assisted nanolithographic technique called nanografting. Furthermore, a substantial reduction of defects inside nanografted patch is demonstrated by electrical conductivity measurements. The high sensitivity of SAM defects by CT-AFM may be understood thinking about the fact that they are defective areas easily penetrable by the AFM tip due to the local SAM weakness[84,155]. Tip penetration leads easily to formation of conducting tip/surface (Au/Au or Pt/Au depending on the metalized AFM tip used) metal filaments responsible of the current spikes.[173]

The reason of this nanografting induced defects reduction is still unclear and under investigation. However a rough thermo-mechanical model may work as a first approach to the phenomenon. First, the AFM tip, scanning at relatively high forces during nanografting procedure, may act as a nano-slice smoothing the underneath gold surface from out-plane irregularities. Second, the high

friction exerted by the tip at the gold surface interface, may induce a significant surface heating localized at the tip/surface contact area. Estimation of the contact area using Hertzian contact theory gives a contact surface of about 20 nm^2 that induces a local pressure in the order of some GPa at 50 nN tip applied load. This pressure, especially if goes with high scan speeds, is more than sufficient to induce a gold surface annealing localized below the AFM tip. The furnished thermal energy induces two main effects: an increasing in gold mobility that induce a local surface reorganization (and maybe reduction of gold defects as vacancy islands) and an increasing in alkanethiol surface mobility that arrange in closed packing molecules (explaining so the obtained molecular resolution on nanografted patch despite the ultra-fast formation kinetic). So, if it is true the thermal annealing mechanism, has to be true also a better molecular reorganization due to an increased sulfur/gold mobility.

Concluding, nanografting can produce nanostructures of SAMs with specific shape, dimension, and composition with molecular order higher than in the usual SAMs prepared from liquid or gas phase. In addition, SAM defects reduction is observable in the nanostructured area. These characteristics support the enhanced lithographic and analytical capabilities of the technique. The ability to fabricate multiple patterns regionspecifically from desired components opens the possibility for new routes in surface analysis. These patterned SAMs produced by nanografting should provide new opportunities for pursuing systematic studies of such size-dependent properties as conductivity, nanotribology, and spatially confined surface reactions in a differential way as described, for transport properties, in Chapter 4 of this thesis. Furthermore, production of selective recognition sites for sensors with orthogonal detection capabilities opens to a new generation of biosensors with unprecedented molecular recognition sensibility.[30]

8 Conclusions and Outlook

Conclusions

In this thesis we exploited and studied the AFM capability to work easily in a liquid environment to perform all the nanolithographic tasks necessary to build surface nanostructures of different molecules into a common hosting molecular SAM matrix and to carry out simultaneous characterizations of molecular properties. Nanografting, an AFM based nanolithographic technique which was first introduced by Liu and co-workers in 1997,[61] was extensively described. The three main factors influencing the nanografting procedure (fabrication force, scanning speed, and concentration of thiols in solution) were studied and discussed.

The use of CT-AFM, for Metal-molecule-Metal junction characterizations was discussed focusing in particular on the advantage offered by this technique if compared with STM. Instead of the common procedure to fabricate and characterize M-m-M junctions by statically positioning a conductive AFM tip in contact with a metal-supported molecular film while a voltage swap is performed (recording so the *I/V* characteristic of the junction), we chose a scanning approach for CT-AFM junction characterization. In our experiments we didn't perform punctual measurements but, instead, a complete bi-dimensional mapping of the currents flowing through the area below the AFM tip, at fixed voltages. The electrical characterization was performed simultaneously with a topographic imaging of the surface with the feedback working at constant force

(contact mode). The use of a conductive tip connected with a high gain amplification chain let us to collect current values for every point scanned by the AFM tip when a potential is applied between it and the surface. Benefits of this approach were discussed at the end of the chapter, together with the possibility to use the force applied by the tip to modify the structure of the SAM (e.g. tilting) in order to study the structural dependence of the passage of electrical current through SAMs.

In Chapter 4 we demonstrated that, by combining nanografting with a differential measurement approach, we can determine the resistance of alkanethiol molecules with higher precision than it was possible so far. Our approach has the considerable advantage of circumventing the problem of the contribution of the junction properties to the molecular transport measurements. By accepting the unavoidable presence of a tip-contamination layer on top of the SAM molecules, and by considering relative, instead of absolute, measurements, we demonstrated that the contribution of such layer can be neglected, provided that the experimental data are correctly normalized. In particular, it is necessary that all the nano-patches of the different molecules involved in the study are imaged simultaneously in the same frame or, alternatively, that the patches are imaged separately while each one is embedded in a reference SAM of the same molecule. The tunneling current decay (with the chain length) constant β, obtained from our data is more precise than, and in good agreement with, the values reported in the literature. Moreover, the determination of *I*/*V* characteristics in our approach is faster when compared with other point-by-point *I*/*V* methods, due to the high number of data points obtained from a single image. During our experiments we also realized that errors affecting current measurements increase as the length of the molecules under investigation (the nanografted one) increases. An explanation of this trend can be found in the higher resistance of such molecules and, therefore, the low detected currents that force the amplifier to work closely to its sensing limit. Differential comparison between longer molecules is actually under investigation using an improved amplification chain.

In Chapter 5 we focused on several factors that influence the measured current values in our differential characterization of the electron transport properties of SAMs by CT-AFM combined with the nanografting technique. These factors, including the nanografting process, the compact-

ness of the SAM, normal load, contact area of a specific tip and environmental factors as humidity and temperature, can all affect the experimental results to different extent. Contaminants on the tip, which can shift the current value by several orders of magnitude, are probably the most crucial reason for the discrepancies of the data obtained in different experiments. Other factors affect the current value to a less degree (around one order of magnitude or less) and are easier to control. Further investigations are necessary in the direction of a better understanding of tunneling junction components. In particular the role of water has to be addressed. To do that two possible routes may be followed: ultra high vacuum (UHV) differential CT-AFM experiments may help to increase the cleanness of the system, while current measurements, performed in a liquid cell, may extend our knowledge about solvent contribution in molecular transport. Both cases eliminate the water meniscus force contribution from the surface reducing in this way the uncertainties due to the applied load indetermination.

In Chapter 6 we demonstrated, studing an aromatic thiolated molecule (2-Benzenethanethiol, BET in short), that an information about the magnitude of the absolute resistance is achievable. The approach has the advantage of circumventing in part the problem of the contribution of the junction properties to the molecular transport measurements. The fact that the nanopatches of BET and the 1-Hexanethiol matrix are imaged simultaneously in the same frame allow for a normalization of the obtained resistance values. In fact, using the tunneling current decay constant and contact resistance from previous experiments for alkanethiols, a theoretical value of resistance for C6 was calculated and used to extrapolate BET resistance after normalization. The obtained value of 3.6±0.1 MΩ per 100±50 BET molecules may be compared with results present in literature about electrical conduction of conjugated molecular SAMs studied by punctual CT-AFM.[129] A resistance value of about 0.5 MΩ was obtained for 2-Benzenemethylenthiol that, instead of two methylene groups as BET, presents only one. Anyway, considering the current reduction produced by the extra methylene, an indirect evaluation for BET resistance was obtained. This calculation gives a value of about 1.65 MΩ per 100 molecules for the 2-Benzenethanethiol's SAM resistance which is two times smaller than the value obtained above, underlining the difficulty to obtain absolute values from this type of measurements, even though a factor of two between measured and calculated values is to be considered, in this field, if not

satisfactory , at least not too bad. The presented approach represents, therefore, a fast but valid procedure to obtain values that can give a first idea of the resistance of a molecular film.

Aim of Chapter 7 was to demonstrate through a combination of friction and current investigations made with the atomic force microscope that a nanostructured monolayer fabricated using nanografting is better packed and with a lower density of defects than a spontaneously assembled monolayer. A substantial reduction of defects inside nanografted patches was demonstrated by electrical conductivity measurements. The reason of this nanografting-induced defects reduction is still unclear and under investigation. However a rough thermo-mechanical model may work as a first approach to the phenomenon. Indeed, high friction exerted by the tip at the gold surface interface, may induce a significant surface heating localized at the tip/surface contact area. Since this heat is produced very locally and lasts only a very short time it may anneal rapidly the film without decomposing the molecules.

Outlooks

CT-AFM has demonstrated in many occasions to be a reliable method for surface characterization of inorganic and organic layers.[23-28] It in the field of surface biology and biophysics, however, that we can find the more exciting perspective applications of this technique.[156-157,178] In the following I am going to discuss the prospective application of CT-AFM to the electrophysiology of neurons, a field in which our laboratory has only recently been involved in.

Until now, this type of study has been carried out taking advantage of patch-clamp techniques.[179] A glass micro-pipette, containing a reference electrode immerse in saline solution, is placed into the cell membrane in order to create a conductive solution continuity between the electrode solution and the cell cytoplasm after membrane perforation. The membrane junction area is sealed from the external physiological solution thanks to a negative pressure applied inside the pipette.[179] Though patch-clamp is a well tested and almost standard technique, it presents some limitations due to the large size of the probe (compared with cellular dimensions) and the difficulty, in the standard implementation, to obtain different information than voltage stimulus response.

We plan to use our experience in electrical measurements by CT-AFM to open new directions in cell electrophysiology.

The simultaneous characterization of the surface morphology and the surface charge discontinuities distribution, with nanometric resolution, can be pursued together with voltage and chemical stimulations.

The development of a novel technique for electrophysiology of neurons *in vitro* may start from a CT-AFM based procedure instead of the standard apparatus used so far (patch-clamp).[180-182] This approach has the main advantage of combining together very high resolution surface topography imaging of the cell membrane and the intrinsic capability of the instrument to apply locally a voltage stimulus, detecting, at the same time, currents. There are two main difficulties in adapting CT-AFM technique to cell analysis in order to shrinking the scale of electrical measurements and stimulation inside neuronal cells.

The first is the obvious one of insulating the electrode (the AFM tip) from the saline, physiological solution, where cells are immersed during electrophysiology experiments. Different solutions are being considered to solve this problem, ranging from covering the usual conductive AFM tip with a layer of an insulating material (e.g. SiO_2 or a polymeric film), with the exception of the tip apex, to the use of a new generation of AFM tips manufactured starting from a nanometric sized glass capillary with a metallic contact inside. Analogous approach were used by other groups to develop ionic current scanning microscopes able to work in a similar manner based on classic STM using, instead of the tunneling current, a ionic current. However this technique is characterized by a very low spatial resolution and by the impossibility to have independent control over the applied force and the currents.[183]

The second difficulty regards the capability of making a very good seal at the interface between the outside surface of the insulated tip (or the AFM nanopipette) and the cell wall membrane. This is a critical but necessary goal in order to assure absence of electrical conduction between the extracellular physiological solution and the cell cytoplasm. While sufficient progress has been done recently in the area of nanofabrication and nanofluidics to make us confident that a solution to the first problem can be found we will need to apply our own, substantial, knowledge on interactions between monolayers to solve the second class of difficulties.

Starting from the extraordinary fact that neurons show an improvment in neuronal comunication when grown on a carbon nanotube (CNT) carpet,[184-185] we would like to investigate emerging neuronal network dynamics together with the manipulation of the substrate by nano-patterning specific functionalized-CNT on the surface. This will lead to the formation of specific neuronal pathways connections in vitro, or to faster synapse formation and plasticity at specific circuit-nodes. Nanografting,[62] can be used to directly manipulate selectively functionalized CNT, and to organize the latter in preferred orientation. We expect obtaining in this way precious information for improving our understanding of neuron growth while, at the same time, expanding the range of neurophysiology applications.

In order to bind CNTs to a gold surface the CNTs need to be functionalized, for istance with thiol-groups. Instead of a direct binding of functionalized CNTs to the Au surface, other strategies are viable: the original SAM can be nano-patterned with molecules capable to bind opportunely modified CNTs. One possibility is to modify CNTs by adding single stranded DNA (ssDNA) tags. Our laboratory has developed in the past-three years a deep knowledge on surface immobilization of ssDNA molecules to form nanopatches, and studied the subsequent hybridization with complementary strands as a function of ssDNA density. Fixing this complementary ssDNA to CNTs may allow for a systematic immobilization of these targets on the previously prepared nanopatches or nano-features.[30] Moreover, protein immobilization on well defined nanosized areas of gold surface was achieved in our group by using the well known NTA/Ni(II)/-Histidine linking chain.[186-187] In short, an NTA terminated molecule is nanografted into an ethylene glycol SAM. Ionic nickel, coming from a salt solution, is immobilized by the NTA termination and used to bind the histidine group of a protein that will be fixed above the nanopatch. An histidine functionalized CNT could then be immobilized following the same procedure. In this field, we are investigating the possibility to use CT-AFM as an electrochemical probe in order to control the amount of nickel and its localization on the surface instead of using a salt solution. This will increase the versatility of the technique allowing, at the same time, the immobilization of different targets.

References

[1] Nuzzo, R. G., Allara, D. L.. *Adsorption of Bifunctional Organic Disulfides on Gold Surfaces*. J. Am. Chem. Soc. 1983, **105**, 4481–4483.

[2] Ulman, A.. *Formation and Structure of Self-Assembled Monolayers*. Chem. Rev. 1996, **96**, 1533–1554.

[3] Love, J. C., Estroff, L. A., Kriebel, J. K., Nuzzo, R. G., Whitesides, G. M.. *Self-Assembled Monolayers of Thiolates on Metals as a Form of Nanotechnology*. Chem. Rev. 2005, **105**, 1103–1170.

[4] Geissler, M., Wolf, H., Stutz, R., Delamarche, E., Grummt, U. W., Michel, B., Bietsch, A.. *Fabrication of Metal Nanowires Using Microcontact Printing* . Langmuir 2003, **19**, 6301–6311.

[5] Manna, L., Scher, E. C., Alivisatos, A. P.. *Synthesis of Soluble and Processable Rod-, Arrow-, Teardrop-, and Tetrapod-Shaped CdSe Nanocrystals*. J. Am. Chem. Soc. 2000, **122**, 12700–12706.

[6] Xia, Y., Whitesides, G. M.. *Use of Controlled Spreading of Liquid Alkanethiol on the Surface of Gold to Modify the Size of Features Produced by Microcontact Printing*. J. Am. Chem. Soc. 1995, **117**, 3274.

[7] Colorado, R., Lee, T. R.. *Wettabilities of Self-Assembled Monolayers on Gold Generated from Progressively Fluorinated Alkanethiols*. Langmuir 2003, **19**, 3288–3296.

[8] Houston, J. E., Kim, H. I.. *Adhesion, Friction, and Mechanical Properties of Functionalized Alkanethiol Self-Assembled Monolayers* . Acc. Chem. Res. 2002, **35**, 547–553.

[9] Chaki, N. K., Vijayamohanan, K.. *Self-assembled monolayers as a tunable platform for biosensor applications*. Biosensors & Bioelectronics 2002, **17**, 1–12.

[10] Fan, F. F., Yang, J., Cai, L., Price, D. V., Dirk, S. M., Kosynkin, D. V., Yao, Y., Rawlett, R. M., Tour, J. M., Bard, A. J.. *Charge Transport through Self-Assembled Monolayers of Compounds of Interest in Molecular Electronics* . J. Am. Chem. Soc. 2002, **124**, 5550–5560.

[11] Kang, J. F., Zaccaro, J., Ulman, A., Myerson, A.. *Nucleation and Growth of Glycine Crystals on Self-Assembled Monolayers on Gold*. Langmuir 2000, **16**, 3791–3796.

[12] Whitesides, G. M., Laibinis, P. E.. *Wet chemical approaches to the characterization of organic surfaces: self-assembled monolayers, wetting, and the physical-organic chemistry of the solid-liquid interface*. Langmuir 1990, **6**, 87–96.

[13] Allara, D. L., Nuzzo, R. G.. *Spontaneously organized molecular assemblies. 2. Quantitative infrared spectroscopic determination of equilibrium structures of solution-adsorbed n-alkanoic acids on an oxidized aluminum surface* . Langmuir 1985, **1**, 52–66.

[14] Magnee, R., Maazouz, M., Doneux, C., Bodino, F., Rudolf, P., Teillet-Billy, D., Pireaux, J. -.. *Resonant Electron Scattering of 11-Mercaptoundecanoic Acid Self-Assembled Monolayer Adsorbed on Au (111)*. J. Phys. Chem. B 2003, **107**, 4567–4572.

[15] Genzer, J., Efimenko, K., Fischer, D. A.. *Molecular Orientation and Grafting Density in Semifluorinated Self-Assembled Monolayers of Mono-, Di-, and Trichloro Silanes on Silica Substrates* . Langmuir 2002, **18**, 9307–9311.

[16] Kanjilal, A., Ottaviano, L., Di Castro, V., Beccari, M., Betti, M. G., Mariani, C.. *Pentacene Grown on Self-Assembled Monolayer: Adsorption Energy, Interface Dipole, and Electronic Properties*. J. Phys. Chem. C 2007, **111**, 286–293.

[17] Wolf, K. V., Cole, D. A., Bernasek, S. L.. *High-Resolution TOF-SIMS Study of Varying Chain Length Self-Assembled Monolayer Surfaces*. Anal. Chem. 2002, **74**, 5009–5016.

[18] Abbott, N. L., Whitesides, G. M.. *Potential-Dependent Wetting of Aqueous Solutions on Self-Assembled Monolayers Formed from 15-(Ferrocenylcarbonyl)pentadecanethiol on Gold*. Langmuir 1994, **10**, 1493–1497.

[19] Badia, A., Cuccia, L., Demers, L., Morin, F., Lennox, R. B.. *Structure and Dynamics in Alkanethiolate Monolayers Self-Assembled on Gold Nanoparticles: A DSC, FT-IR, and Deuterium NMR Study*. J. Am. Chem. Soc. 1997, **119**, 2682–2692.

[20] Pflaum, J., Bracco, F., Schreiber, F., Colorado, R., Shmakora, O. E., Lee, T. R., Scoles, G., Kahn, A.. *Structure and electronic properties of CH_3- and CF_3- terminated alkanethiol monolayers on Au(111): A scanning tunneling microscopy, surface X-ray and helium scattering study*. Surf. Sci. 2002, **498**, 89–104.

[21] Chailapakul, O., Sun, L., Xu, C., Crooks, R. M.. *Interactions Between Organized, Surface-Confined Monolayers and Vapor-phase Probe Molecules. 7. Comparison of Self-assembling n-Alkanethiol Monolayers Deposited on Gold from Liquid and Vapor Phases*. J. Am. Chem. Soc. 1993, **115**, 12459–12467.

[22] Binnig, G., Rohrer, H., Gerber, C., Weiber, E.. *Surface Studies by Scanning Tunneling Microscopy* . Phys. Rev. Lett. 1982, **49**, 57–61.

[23] Panda, A. K., Manimaran, M., Mitra, A., Basu, S.. *AFM Surface Morphology and Magnetic Properties of Nanocrystalline Fe"7"1Nb"3"."7Cu"1Al"3Mn"0"."8Si"1"3"."5B"7 Ribbons*. Appl. Surf. Sci. 2004, **235**, 475–486.

[24] Leonenko, Z., Finot, E., Amrein, M.. *Adhesive Interaction Measured Between AFM Probe and Lung Epithelial Type II Cells*. Ultramicroscopy 2007, **107**, 948–953.

[25] Barrena, E., Ocal, C.. *Molecular packing changes of alkanethiols monolayers on Au(111) under applied pressure*. J. Chem. Phys. 2000, **113**, 2414–2418.

[26] Wold, D. J., Frisbie, C. D.. *Formation of Metal-Molecule-Metal Tunnel Junctions: Microcontacts to Alkanethiol Monolayers with a Conducting AFM Tip*. J. Am. Chem. Soc. 2000, **122**, 2970–2971.

[27] Takahashi, T., Kawamukai, T.. *Phase Detection of Electrostatic Force by AFM with a Conductive Tip*. Ultramicroscopy 2000, **82**, 63–68.

[28] Kim, P., Shi, L., Majumdar, A., McEuen, P. L.. *Mesoscopic Thermal Transport and Energy Dissipation in Carbon Nanotubes*. Phys. B: Cond. Matt. 2002, **323**, 67–70.

[29] Hoh, J. H., Engel, A.. *Friction effects on force measurements with an atomic force microscope*. Langmuir 1993, **9**, 3310–3312.

[30] Grunwald, C., Mirmomtaz, E., Bano, F., Castronovo, M., Scaini, D., Ensafi, A. A., Casalis, L., Scoles, G. (2008). *The Effect of Crowding on the Hybridization Efficiency of Surface-Bound DNA: Implications for DNA Nano-Arrays*. Under Review by Nature Nanotechnology

[31] Aviram, A., Ratner, M. A.. *Molecular rectifiers*. Chem. Phys. Lett. 1974, **29**, 277–283.

[32] Selzer, Y., Cabassi, M. A., Mayer, T. S., Allara, D. L.. *Temperature Effects on Conduction Through a Molecular Junction*. Nanotechnology 2004, **15**, S483–S488.

[33] Nitzan, A., Ratner, M. A.. *Electron Transport in Molecular Wire Junctions*. Science 2003, **300**, 1384–1389.

[34] Salomon, A., Cahen, D., Lindsay, S., Tomfohr, J., Engelkes, V. B., Frisbie, C. D.. *Comparison of Electronic Transport Measurements on Organic Molecules*. Adv. Mat. 2003, **15**, 1881–1890.

[35] Zhou, C., Deshpande, M. R., Reed, M. A., Jones II, L., Tour, J. M.. *Nanoscale Metal/-Self-assembled Monolayer/metal Heterostructures*. Appl. Phys. Lett. 1997, **71**, 611–613.

[36] Wang, W., Lee, T., Reed, M. A.. *Elastic and Inelastic Electron Tunneling in Alkane Self-Assembled Monolayers*. J. Phys. Chem. B 2004, **108**, 18398–18407.

[37] Selzer, Y., Salomon, A., Cahen, D.. *Effect of Molecule-Metal Electronic Coupling on Through-Bond Hole Tunneling across Metal-Organic Monolayer-Semiconductor Junctions*. J. Am. Chem. Soc. 2002, **124**, 2886–2887.

[38] Rampi, M. A., Schueller, O. J., Whitesides, G. M.. *Alkanethiol self-assembled monolayers as the dielectric of capacitors with nanoscale thickness* . Appl. Phys. Lett. 1998, **72**, 1781-1783.

[39] Reed, M. A., Zhou, C., Muller, C. J., Burgin, T. P., Tour, J. M.. *Conductance of a Molecular Junction*. Science 1997, **278**, 252–254.

[40] Xu, B., Tao, N. J.. *Measurement of Single-Molecule Resistance by Repeated Formation of Molecular Junctions*. Science 2003, **301**, 1221–1223.

[41] He, J., Sankey, O., Lee, M., Tao, N., Li, X., Lindsay, S.. *Measuring single molecule conductance with break junctions*. Faraday Discuss. 2006, **131**, 145–154.

[42] Tans, S. J., Verschueren, A. R., Dekker, C.. *Room-temperature transistor based on a single carbon nanotube*. Nature 1998, **393**, 49–52.

[43] Metzger, R. M.. *Electrical Rectification by a Molecule: The Advent of Unimolecular Electronic Devices*. Acc. Chem. Res. 1999, **32**, 950–957.

[44] Cui, X. D., Primak, A., Zarate, X., Tomfohr, J., Sankey, O. F., Moore, A. L., Moore, T. A., Gust, D., Harris, G., Lindsay, S. M.. *Reproducible Measurement of Single-Molecule Conductivity*. Science 2001, **294**, 571–574.

[45] Bumm, L. A., Arnold, J. J., Dunbar, T. D., Allara, D. L., Weiss, P. S.. *Electron Transfer through Organic Molecules*. J. Phys. Chem. B 1999, **103**, 8122–8127.

[46] Liang, J., Sun, Q., Selloni, A., Scoles, G.. *Side-by-Side Characterization of Electron Tunneling through Monolayers of Isomeric Molecules: A Combined Experimental and Theoretical Study*. J. Phys. Chem. B 2006, **110**, 24797–24801.

[47] Venkataraman, L., Klare, J. E., Tam, I. W., Nuckolls, C., Hybertsen, M. S., Steigerwald, M. L.. *Single-Molecule Circuits with Well-Defined Molecular Conductance*. Nano Lett. 2006, **6**, 458–462.

[48] Venkataraman, L., Park, Y. S., Whalley, A. C., Nuckolls, C., Hybertsen, M. S., Steigerwald, M. L.. *Electronics and Chemistry: Varying Single Molecule Junction Conductance Using Chemical Substituents*. Nano Lett. 2007, **7**, 502–506.

[49] Ishida, T., Mizutani, W., Choi, N., Akiba, U., Fujihira, M., Tokumoto, H.. *Structural Effects on Electrical Conduction of Conjugated Molecules Studied by Scanning Tunneling Microscopy*. J. Phys. Chem. B 2000, **104**, 11680–11688.

[50] Song, H., Lee, H., Lee, T.. *Intermolecular Chain-to-Chain Tunneling in Metal-Alkanethiol-Metal Junctions*. J. Am. Chem. Soc. 2007, **129**, 3806–3807.

[51] James, D. K., Tour, J. M.. *Electrical Measurements in Molecular Electronics*. Chem. Mater. 2004, **16**, 4423–4435.

[52] Kitagawa, K., Morita, T., Kimura, S.. *Electron Transfer in Metal-Molecule-Metal Junction Composed of Self-Assembled Monolayers of Helical Peptides Carrying Redox-Active Ferrocene Units*. Langmuir 2005, **21**, 10624–10631.

[53] Wold, D. J., Frisbie, C. D.. *Fabrication and Characterization of Metal-Molecule-Metal Junctions by Conducting Probe Atomic Force Microscopy*. J. Am. Chem. Soc. 2001, **123**, 5549–5556.

[54] Yasutake, Y., Shi, Z. J., Okazaki, T., Shinohara, H., Majima, Y.. *Single Molecular Orientation Switching of an Endohedral Metallofullerene*. Nano Lett. 2005, **5**, 1057–1060.

[55] Saito, N., Hayashi, K., Sugimura, H., Takai, O., Nakagiri, N.. *Surface potentials of patterned organosilane self-assembled monolayers acquired by Kelvin probe force microscopy and ab initio molecular calculation*. Chem. Phys. Lett. 2001, **349**, 172–177.

[56] Magoga, M., Joachim, C.. *Conductance of molecular wires connected or bonded in parallel*. Phys. Rev. B 1999, **59**, 16011–16021.

[57] Onipko, A.. *Analytical model of molecular wire performance: A comparison of π and σ electron systems*. Phys. Rev. B 1999, **59**, 9995–10006.

[58] Datta, S., Tian, W., Hong, S., Reifenberger, R., Henderson, J. I., Kubiak, C. P.. *Current-Voltage Characteristics of Self-Assembled Monolayers by Scanning Tunneling Microscopy*. Phys. Rev. Lett. 1997, **79**, 2530–2533.

[59] Gonzalez, C., Simón-Manso, Y., Batteas, J., Marquez, M., Ratner, M., Mujica, V.. *A Quasimolecular Approach to the Conductance of Molecule-Metal Junctions: Theory and Application to Voltage-Induced Conductance Switching*. J. Phys. Chem. B 2004, **108**, 18414–18420.

[60] Long, Y. T., Abu-Irhayem, E., Kraatz, H. B.. *Peptide Electron Transfer: More Questions than Answers*. Chem. Eur. J. 2005, **11**, 5186–5194.

[61] Xu, S., Laibinis, P. E., Liu, G. Y.. *Accelerating the Kinetics of Thiol Self-assembly on Gold - A Spatial Confinement Effect*. J. Am. Chem. Soc. 1998, **120**, 9356.

[62] Xu, S., Liu, G.. *Nanometer-Scale Fabrication by Simultaneous Nanoshaving and Molecular Self-Assembly*. Langmuir 1997, **13**, 127–129.

[63] Xu, S., Miller, S., Laibinis, P. E., Liu, G.. *Fabrication of Nanometer Scale Patterns within Self-Assembled Monolayers by Nanografting*. Langmuir 1999, **15**, 7244–7251.

[64] Ryu, S., Scgatz, G. C.. *Nanografting: Modeling and Simulation* . J. Am. Chem. Soc. 2006, **128**, 11563–11573.

[65] Liu, G., Xu, S., Qian, Y.. *Nanofabrication of Self-Assembled Monolayers Using Scanning Probe Lithography*. Acc. Chem. Res 2000, **33**, 457–466.

[66] Zhao, J., Uosaki, K.. *Formation of Nanopatterns of a Self-Assembled Monolayer (SAM) within a SAM of Different Molecules Using a Current Sensing Atomic Force Microscope* . Nano Lett. 2002, **2**, 137–140.

[67] Zhao, J., Uosaki, K.. *A Novel Nanolithography Technique for Self-Assembled Monolayers Using a Current Sensing Atomic Force Microscope*. Langmuir 2001, **17**, 7784–7788.

[68] Houston, J. E., Doelling, C. M., Vanderlick, T. K., Hu, Y., Scoles, G., Wenzl, I., Lee, T. R.. *Comparative Study of the Adhesion, Friction, and Mechanical Properties of CF_3- and CH_3-Terminated Alkanethiol Monolayers*. Langmuir 2005, **21**, 3926–3932.

[69] Case, M. A., McLendon, G. L., Hu, Y., Vanderlick, T. K., Scoles, G.. *Using Nanografting to Achieve Directed Assembly of de novo Designed Metalloproteins on Gold*. Nano Lett. 2003, **3**, 425–429.

[70] Liang, J., Rosa, L. G., Scoles, G.. *Nanostructuring, Imaging and Molecular Manipulation of Dithiol Monolayers on Au(111) Surfaces by Atomic Force Microscopy*. J. Phys. Chem. C 2007, **111**, 17275–17284.

[71] Castronovo, M., Bano, F., Raugei, S., Scaini, D., Dell'Angela, M., Hudej, R., Casalis, L., Scoles, G.. *Mechanical Stabilization Effect of Water on a Membrane-like System*. J. Am. Chem. Soc. 2007, **129**, 2636–2641.

[72] Scaini, D., Castronovo, M., Casalis, L., Scoles, G. (2008). *Electron Transfer Mediating Properties of Hydrocarbons as a Function of Chain Length: a Differential Scanning CT-AFM Investigation*. ACS Nano In Press

[73] Mazzarello, R., Cossaro, A., Verdini, A., Rousseau, R., Casalis, L., Danisman, M. F., Floreano, L., Scandolo, S., Morgante, A., Scoles, G.. *Structure of a CH_3 S Monolayer on Au(111) Solved by the Interplay between Molecular Dynamics Calculations and Diffraction Measurements*. Phys. Rev. Lett. 2007, **98**, 016012.

[74] Schreiber, F.. *Structure and Growth of Self-assembling Monolayers*. Prog. Surf. Sci. 2000, **65**, 151–256.

[75] Schwartz, D. K.. *Mechanism and Kinetics of Self-assembled Monolayer Formation*. Annu. Rev. Phys. Chem. 2001, **52**, 107–137.

[76] Lay, M. D., Varazo, K., Stickney, J. L.. *Formation of Sulfur Atomic Layers on Gold from Aqueous Solutions of Sulfide and Thiosulfate: Studies Using EC-STM, UHV-EC, and TLEC*. Langmuir 2003, **19**, 8416–8427.

[77] Speller, S., Rauch, T., Bömermann, J., Borrmann, P., Heiland, W.. *Surface structures of S on Pd(111)*. Surf. Sci. 1999, **441**, 107–116.

[78] Nuzzo, R. G., Zegarski, B. R., Dubois, L. H.. *Fundamental studies of the chemisorption of organosulfur compounds on gold(111). Implications for molecular self-assembly on gold surfaces*. J. Am. Chem. Soc. 1987, **109**, 733–740.

[79] Fischer, D., Curioni, A., Andreoni, W.. *Decanethiols on Gold: The Structure of Self-Assembled Monolayers Unraveled with Computer Simulations*. Langmuir 2003, **19**, 3567–3571.

[80] Lavrich, D. J., Wetterer, S. M., Bernasek, S. L., Scoles, G.. *Physisorption and Chemisorption of Alkanethiols and Alkyl Sulfides on Au(111)*. J. Phys. Chem. B 1998, **103**, 3456–3465.

[81] Bain, C. D., Troughton, E. B., Tao, Y. T., Evall, J., Whitesides, G. M., Nuzzo, R. G.. *Formation of monolayer films by the spontaneous assembly of organic thiols from solution onto gold*. J. Am. Chem. Soc. 1989, **111**, 321–335.

[82] Yang, G., Amro, N. A., Starkewolfe, Z. B., Liu, G. -.. *Molecular-Level Approach To Inhibit Degradations of Alkanethiol Self-Assembled Monolayers in Aqueous Media*. Langmuir 2004, **20**, 3995–4003.

[83] Schlenoff, J. B., Li, M., Ly, H.. *Stability and Self-Exchange in Alkanethiol Monolayers*. J. Am. Chem. Soc. 1995, **117**, 12528–12536.

[84] Poirier, G. E.. *Characterization of Organosulfur Molecular Monolayers on Au(111) using Scanning Tunneling Microscopy*. Chem. Rev. 1997, **97**, 1117–1127.

[85] Poirier, G. E., Taylor, M. J.. *The c(4X2) Superlattice of n-Alkanethiol Monolayers Self-Assembled on Au(111)*. Langmuir 1994, **10**, 2853–2856.

[86] Camillone, N., Chidsey, C. E., Liu, G. -., Scoles, G.. *Superlattice Structure at the Surface of a Monolayer of Octadecanethiol Self-assembled on Au(111)*. J. Chem. Phys. 1993, **98**, 3503–3511.

[87] Fenter, P., Schreiber, F., Berman, L., Scoles, G., Eisenberger, P., Bedzyk, M. J.. *On the structure and evolution of the buried S/Au interface in self-assembled monolayers: X-ray standing wave results*. Surf. Sci. 1998, **412-413**, 213–235.

[88] Sun, L., Crooks, R. M.. *Indirect visualization of defect structures contained within self-assembled organomercaptan monolayers: combined use of electrochemistry and scanning tunneling microscopy* . Langmuir 1993, **9**, 1951–1954.

[89] Amro, N. A., Xu, S., Liu, G.. *Patterning Surfaces Using Tip-Directed Displacement and Self-Assembly*. Langmuir 2000, **16**, 3006–3009.

[90] Chang, C. -., Franses, E. I.. *Adsorption dynamics of surfactants at the air/water interface: a critical review of mathematical models, data, and mechanisms*. Coll. Surf. A 1995, **100**, 1–45.

[91] Kaganer, V. M., Möhwald, H., Dutta, P.. *Structure and phase transitions in Langmuir monolayers* . Rev. Mod. Phys. 1999, **71**, 779–819.

[92] Xu, S., Cruchon-Dupeyrat, S. J., Garno, J. C., Liu, G. -., Jennings, G. K., Yong, T. -., Laibinis, P. E.. *In situ studies of thiol self-assembly on gold from solution using atomic force microscopy*. J. Chem. Phys. 1998, **108**, 5002–5012.

[93] Jung, L. S., Campbell, C. T.. *Sticking Probabilities in Adsorption from Liquid Solutions: Alkylthiols on Gold* . Phys. Rev. Lett. 2000, **84**, 5164–5167.

[94] Peterlinz, K. A., Georgiadis, R.. *In Situ Kinetics of Self-Assembly by Surface Plasmon Resonance Spectroscopy*. Langmuir 1996, **12**, 4731–4740.

[95] Dannenberger, O., Buck, M., Grunze, M.. *Self-Assembly of n-Alkanethiols: A Kinetic Study by Second Harmonic Generation*. J. Phys. Chem. 1999, **103**, 2202–2213.

[96] Debono, R. F., Loucks, G. D., Manna, D. D., Krull, U. J.. *Self-assembly of short and long-chain n-alkyl thiols onto gold surfaces: A real-time study using surface plasmon resonance techniques*. Can. J. Chem. 1996, **74**, 677–688.

[97] Schessler, H. M., Karpovich, D. S., Blanchard, G. J.. *Quantitating the Balance between Enthalpic and Entropic Forces in Alkanethiol/Gold Monolayer Self Assembly*. J. Am. Chem. Soc. 1996, **118**, 9645–9651.

[98] Yang, G., Liu, G. -.. *New Insights for Self-Assembled Monolayers of Organothiols on Au(111) Revealed by Scanning Tunneling Microscopy*. J. Phys. Chem. B 2003, **107**, 8746–8759.

[99] Bhatia, R., Garrison, B. J.. *Phase Transitions in a Methyl-Terminated Monolayer Self-Assembled on Au{111}* . Langmuir 1997, **13**, 765–769.

[100] Bhatia, R., Garrison, B. J.. *Structure of c(4×2) Superlattice in Alkanethiolate Self-Assembled Monolayers*. Langmuir 1997, **13**, 4038–4043.

[101] Zhang, Z. S., Wilson, O. M., Efremov, M. Y., Olson, E. A., Braun, P. V., Senaratne, W., Ober, C. K., Zhang, M., Allen, L. H.. *Heat capacity measurements of two-dimensional self-assembled hexadecanethiol monolayers on polycrystalline gold*. Appl. Phys. Lett. 2004, **84**, 5198.

[102] Fick, J., Steitz, R., Leiner, V., Tokumitsu, S., Himmelhaus, M., Grunze, M.. *Swelling Behavior of Self-Assembled Monolayers of Alkanethiol-Terminated Poly(ethylene glycol): A Neutron Reflectometry Study*. Langmuir 2004, **20**, 3848–3853.

[103] Venables, J. A. (2000). *Introduction to Surface and Thin Film Processes*. Cambridge: Cambridge University Press.

[104] Schlesinger, M., Paunovic, M. (2000). *Modern Electroplating*. New York: John Wiley & Sons.

[105] Pham, T., Jackson, J. B., Halas, N. J., Lee, T. R.. *Preparation and Characterization of Gold Nanoshells Coated with Self-Assembled Monolayers*. Langmuir 2002, **18**, 4915–4920.

[106] Binnig, G., Quate, C., Gerber, C.. *Atomic Force Microscope*. Phys. Rev. Lett. 1986, **56**, 930–933.

[107] Hegner, M., Wagner, P., Semenza, G.. *Ultralarge atomically flat template-stripped Au surfaces for scanning probe microscopy*. Surf. Sci. 1993, **291**, 39–46.

[108] Knarr, R. F., Quon, R. A., Vanderlick, T. K.. *Direct Force Measurements at the Smooth Gold/Mica Interface*. Langmuir 1998, **14**, 6414–6418.

[109] Losic, D., Shapter, J. G., Gooding, J. J.. *Atomically Flat Gold for Biomolecule Immobilization and Imaging*. Aust. J. Chem. 2001, **54**, 643–648.

[110] Gupta, P., Loos, K., Korniakov, A., Spagnoli, C., Cowman, M., Ulman, A.. *Facile Route to Ultraflat SAM-Protected Gold Surfaces by "Amphiphile Splitting"*. Angew. Chem. Int. Ed. 2004, **43**, 520–523.

[111] Dannenberger, O., Wolff, J. J., Buck, M.. *Solvent Dependence of the Self-Assembly Process of an Endgroup-Modified Alkanethiol* . Langmuir 1998, **14**, 4679–4682.

[112] Yamada, R., Sakai, H., Uosaki, K.. *Solvent Effect on the Structure of the Self-Assembled Monolayer of Alkanethiol*. Chem. Lett. 1999, **28**, 667.

[113] Schneider, T. M., Buttry, D. A.. *Electrochemical quartz crystal microbalance studies of adsorption and desorption of self-assembled monolayers of alkyl thiols on gold*. J. Am. Chem. Soc. 1993, **115**, 12391–12397.

[114] Morita, T., Lindsay, S.. *Determination of Single Molecule Conductances of Alkanedithiols by*
Conducting-Atomic Force Microscopy with Large Gold Nanoparticles. J. Am. Chem. Soc. 2007, **129**, 7262–7263.

[115] Piner, R. D., Zhu, J., Xu, F., Hong, S., Mirkin, C. A.. *"Dip-Pen" Nanolithography*. Science 1999, **283**, 661–663.

[116] Salmeron, M., Neubauer, G., Folch, A., Tomitori, M., Ogletree, D. F., Sautet, P.. *Viscoelastic and Electrical Properties of Self-assembled Monolayers on Gold (111) Films*. Langmuir 1993, **9**, 3600–3611.

[117] Bishop, A., Nuzzo, R. G.. *Self-assembled Monolayers: Recent Developments and Applications*. Curr. Opin.Colloid Interface Sci. 1996, **1**, 127.

[118] Kumar, A., Abbott, N. L., Kim, E., Biebuych, H. A., Whitesides, G. M.. *Patterned Self-assembled Monolayers and Mesoscale Phenomena*. Acc. Chem. Res. 1995, **28**, 219.

[119] Bumm, L. A., Arnold, J. J., Cygan, M. T., Dunbar, T. D., Burgin, T. P., Jones, L., Allara, D. L., Tour, J. M., Weiss, P. S.. *Are Single Molecular Wires Conducting?*. Science 1996, **271**, 1705.

[120] Bernard, A., Delamarche, E., Schmid, H., Michel, B., Bosshard, H. R., Biebuyck, H.. *Printing Patterns of Proteins*. Langmuir 1998, **14**, 2225.

[121] Wollman, E. W., Kang, D., Frisbie, C. D., Lorkovic, I. M., Wrighton, M. S.. *Photosensitive Self-assembled Monolayers on Gold: Photochemistry of Surface-Confined Aryl Azide and Cyclopentadienylmanganese Tricarbonyl*. J. Am. Chem.Soc. 1996, **116**, 4395.

[122] Sondag-Huethorst, J. A., Van Helleputte, H. R., Fokkink, L. G.. *Generation of Electrochemically Deposited Metal Patterns by Means of Electron-Beam Lithography of Self-assembled Monolayers Resists*. Appl. Phys. Lett. 1994, **64**, 285.

[123] Tamada, K., Hara, M., Sasabe, H., Knoll, W.. *Surface Phase Behavior of n-alkanethiol Self-assembled Monolayers Adsorbed on Au(111): An AFM Study*. Langmuir 1997, **13**, 1558.

[124] Hayes, W. A., Kim, H., Yue, X., Perry, S. S., Shannon, C.. *Nanometer-scale Patterning of Surfaces Using Self-assembley Chemistry*. Langmuir 1997, **13**, 2511.

[125] Hamers, R. J.. *Scanning Probe Microscopes in Chemistry*. J. Phys. Chem. 1996, **100**, 13103.

[126] Butt, H. J., Steifert, K., Bamberg, E.. *Imaging Molecular Defects in Alkanethiol Monolayers with an AFM*. J. Phys. Chem. 1993, **97**, 7316.

[127] Carpick, R. W., Salmeron, M.. *Scratching the Surface: Fundamental Investigations of Tribology with Atomic Force Microscopy*. Chem. Rev. 1997, **97**, 1163.

[128] Liu, G. Y., Salmeron, M. B.. *Reversible Displacement of Chemisorbed n-Alkanethiol Molecules on Au(111) Surface: An Atomic Force Microscopy Study*. Langmuir 1994, **10**, 367.

[129] Ishida, T., Mizutani, W., Aya, Y., Ogiso, H., Sasaki, S., Tokumoto, H.. *Electrical Conduction of Conjugated Molecular SAMs Studied by Conductive Atomic Force Microscopy*. J. Phys. Chem. B 2002, **106**, 5886–5892.

[130] Munuera, C., Barrena, E., Ocal, C.. *Scanning Force Microscopy Three-Dimensional Modes Applied to Conductivity Measurements Through Linear-Chain Organic SAMs*. Nanotechnology 2007, **18**, 125505–125512.

[131] Barrena, E., Kopta, S., Ogletree, D. F., Charych, D. H., Salmeron, M.. *Relationship between Friction and Molecular Structure: Alkylsilane Lubricant Films under Pressure*. Phys. Rev. Lett. 1999, **82**, 2880–2883.

[132] Sun, Q., Selloni, A., Scoles, G.. *Electronic Structure of Metal/Molecule//Metal Junctions: A Density Functional Theory Study of the Influence of the Molecular Terminal Group*. J. Phys. Chem. B 2006, **110**, 3493–3498.

[133] Sze, S. M. (1981). *Physics of Semiconductor Devices*. New York: Wiley.

[134] Chen, J., Calvet, L. C., Reed, M. A., Carr, D. W., Grubisha, D. S., Bennett, D. W.. *Electronic Transport Through Metal–1,4-phenylene Diisocyanide–Metal Junctions*. Chem. Phys. Lett. 1999, **313**, 741–748.

[135] Ratner, M. A., Davis, B., Kemp, M., Mujica, V., Roitberg, A., Yaliraki, S. (1998). *Molecular Electronics: Science and Technology*. In A. Aviram & M. Ratner (Ed.), *Annals of the New York Accademy of Science* (pp. 176). New York: New York Accademy of Science.

[136] Boulas, C., Davidovits, J. V., Rondelez, F.. *Suppression of Charge Carrier Tunneling through Organic Self-Assembled Monolayers*. Phys. Rev. Lett. 1996, **76**, 4797–4800.

[137] Bumm, L. A., Arnold, J. J., Charles, L. F., Dunbar, T. D., Allara, D. L., Weiss, P. S.. *Directed Self-Assembly to Create Molecular Terraces with*
Molecularly Sharp Boundaries in Organic Monolayers. J. Am. Chem. Soc. 1999, **121**, 8017–8021.

[138] Franz, W. (1956). *Handbuch der Physik*. Berlin: Springer-Ver lag.

[139] Lewicki, G., Mead, C. A.. *Experimental Determination of E-k Relationship in Electron Tunneling*. Phys. Rev. Lett. 1966, **16**, 939–941.

[140] Joachim, C., Magoga, M.. *The Effective Mass of an Electron When Tunneling Through a Molecular Wire*. Chem. Phys. 2002, **281**, 347–352.

[141] Simmons, J. G.. *Generalized Formula for the Electric Tunnel Effect between Similar Electrodes Separated by a Thin Insulating Film*. J. Appl. Phys. 1963, **34**, 1793–1803.

[142] Simmons, J. G.. *Electric Tunnel Effect between Disimilar Electrodes Separated by a Thin Insulating Film*. J. Appl. Phys. 1963, **34**, 2581–2590.

[143] Holmlin, R., Haag, R., Chabinyc, M. L., Ismagilov, R. V., Cohen, A. E., Terfort, A., Rampi, A., Whitesides, G. M.. *Electron Transport through Thin Organic Films in Metal-Insulator-Metal Junctions Based on Self-Assembled Monolayers*. J. Am. Chem. Soc. 2001, **123**, 5075–5085.

[144] Wang, W., Lee, T., Reed, M. A.. *Mechanism of Electron Conduction in Self-assembled Alkanethiol Monolayer Devices*. Phys. Rev. B 2003, **68**, 035416.

[145] Tomfohr, J. K., Sankey, O. F.. *Complex Band Structure, Decay Lengths, and Fermi Level Alignment in Simple Molecular Electronic Systems*. Phys. Rev. B 2002, **65**, 245105.

[146] Guiducci, C., Stagni, C., Zuccheri, G., Bogliolo, A., Benini, L., Samorì, B., Riccò, B.. *DNA detection by integrable electronics*. Biosens. Bioelectron. 2004, **19**, 781–787.

[147] Fritz, J., Cooper, E. B., Gaudet, S., Sorger, P. K., Manalis, S. R.. *Electronic detection of DNA by its intrinsic molecular charge*. PNAS 2002, **99**, 14142–14146.

[148] Pourmand, N., Karhanek, M., Persson, H. H., Webb, C. D., Lee, T. H., Zahradníková, A., Davis, R. W.. *Direct electrical detection of DNA synthesis*. PNAS 2006, **103**, 6466–6470.

[149] Chang, T., Tsai, C., Sun, C., Chen, C., Kuo, L., Chen, P.. *Ultrasensitive electrical detection of protein using nanogap electrodes and nanoparticle-based DNA amplification*. Biosens. Bioelecton. 2007, **22**, 3139–3145.

[150] Bandiera, L., Cellere, G., Cagnin, S., De Toni, A., Zanoni, E., Lanfranchi, G., Lorenzelli, L.. *A fully electronic sensor for the measurement of cDNA hybridization kinetics*. Biosens. Bioelectron. 2007, **22**, 2108–2114.

[151] Ghosh, A. W., Damle, P. S., Datta, S., Nitzan, A.. *Molecular Electronics: Theory and Device Prospects*. MRS Bulletin 2004, **29**, 391–395.

[152] Israelachvili, J. N. (1991). *Intermolecular & Surface Forces*. London: Academic Press.

[153] Engelkes, V. B., Beebe, J. M., Frisbie, C. D.. *Analysis of the Causes of Variance in Resistance Measurements on Metal-Molecule-Metal Junctions Formed by Conducting-Probe Atomic Force Microscopy*. J. Phys. Chem. B 2005, **109**, 16801–16810.

[154] Weiss, E. A., Chiechi, R. C., Kaufman, G. K., Kriebel, J. K., Li, Z., Duati, M., Rampi, M. A., Whitesides, G. M.. *Influence of Defects on the Electrical Characteristics of Mercury-Drop Junctions: Self-Assembled Monolayers of n-Alkanethiolates on Rough and Smooth Silver* . J. Am. Chem. Soc. 2007, **129**, 4336–4349.

[155] Poirier, G. E., Fitts, W. P., White, J. M.. *Two-Dimensional Phase Diagram of Decanethiol on Au(111)*. Langmuir 2001, **17**, 1176–1183.

[156] Kienberger, G., Ebner, A., Gruber, H. J., Hinterdorfer, P.. *Molecular Recognition Imaging and Force Spectroscopy of Single Biomolecules*. Acc. Chem. Res. 2006, **39**, 29–36.

[157] Fernandez, J. M., Li, H. B.. *Force-Clamp Spectroscopy Monitors the Folding Trajectory of a Single Protein*. Science 2004, **303**, 1674–1678.

[158] Sheng, S., Czajkowsky, D. M., Shao, Z.. *AFM Tips: How Sharp Are They?*. J. Microscopy 1999, **196**, 1–5.

[159] Hutter, J. L., Bechhoefer, J.. *Calibration of Atomic-Force Microscope Tips*. Rev. Sci. Instrum. 1993, **64**, 1868.

[160] Mazeran, P. A., Odoni, L., Loubet, J. L.. *Curvature Radius Analysis for Scanning Probe Microscopy*. Surf. Sci. 2005, **585**, 25–37.

[161] Joachim, C., Gimzewski, K. J., Aviram, A.. *Electronics Using Hybrid-Molecular and Mono-Molecular Devices*. Nature 2000, **408**, 541–548.

[162] Sabatani, E., Cohne-Boulakia, J., Bruening, M., Rubinstein, I.. *Thioaromatic Monolayers on Gold: a New Family of Self-Assembling Monolayers*. Langmuir 1993, **9**, 2974–2981.

[163] Tao, T. Y., J., C. C., Eu, Y. W., Lin, L. W., Wu, C. K., Chen, C.. *Structure Evolution of Aromatic-Derivatized Thiol Monolayers on Evaporated Gold*. Langmuir 1997, **13**, 4018–4023.

[164] Leung, B. T., Schwartz, P., Scoles, G., Schreiber, F., Ulman, A.. *Structure and Growth of 4-methyl-4'-mercaptobiphenyl Monolayers on Au(111): a Surface Diffraction Study*. Surf. Sci. 2000, **458**, 34–52.

[165] Dhirani, A. A., Zehner, W. R., Hsung, P. R., Guyot-Sionnest, P.. *Self-assembly of Conjugated Molecular Rods: A High Resolution STM Study*. J. Am. Chem. Soc. 1996, **118**, 3319–3320.

[166] Chen, J., Reed, E. M., Rawlett, M. A., Tour, M. J.. *Large On-Off Ratios and Negative Differential Resistance in a Molecular Electronic Device*. Science 1999, **286**, 1550–1552.

[167] Leatherman, G., Durantini, N. E., Gust, D., Moore, A. T., Moore, L. A., Stone, S., Zhou, Z., Lez, P., Liu, Z. Y., Lindsay, M. S.. *Carotene as a Molecular Wire: Conducting Atomic Force Microscopy*. J. Phys. Chem. B 1999, **103**, 4006–4010.

[168] Jin, Q., Rodriguez, J. A., Li, C. Z., Darici, Y., Tao, N. J.. *Self-assembly of Aromatic Thiols on Au(111).* Surf. Sci. 1999, **425**, 101–111.

[169] Tomfohr, J., Sankey, O. F.. *Theoretical Analysis of Electron Transport Through Organic Molecules*. J. Chem. Phys. 2004, **120**, 1542–1554.

[170] Paulsson, M., Zahid, F., Datta, S. (2003). *Nanoscience, Engineering and Technology Handbook*. West Lafayette, IN: CRC Press 2003.

[171] Staii, C., Wood, D. W., Scoles, G.. *Verification of Biochemical Activity for Proteins Nanografted on Gold Surfaces*. J. Am. Chem. Soc. 2008, **130**, 640–646.

[172] Tinland, B., Pluen, A., Sturm, J., Weill, G.. *Persistence Lenth of Single-Stranded DNA*. Macromolecules 1997, **30**, 5763–5765.

[173] Zhu, Z., Daniel, T. A., Maitani, M., Cabarcos, O. M., Allara, D. L., Winograd, N.. *Controlling Gold Atom Penetration through Alkanethiolate Self-Assembled Monolayers on Au{111} by Adjusting Terminal Group Intermolecular Interactions*. J. Am. Chem. Soc. 2006, **128**, 13710–13719.

[174] Zamborini, F. P., Crooks, R. M.. *In-Situ Electrochemical Scanning Tunneling Microscopy (ECSTM) Study of Cyanide-Induced Corrosion of Naked and Hexadecyl Mercaptan-Passivated Au(111).* Langmuir 1997, **13**, 122–126.

[175] Li, Y. -., Chailapakul, O., Crooks, R. M.. *Electrochemical Scanning Tunneling Microscopy Study of the Electrochemical Behavior of Naked and n-Alkanethiol-modified Au(111) Surfaces in F^- – and CN^- – Containing Electrolyte Solutions*. Vac. Sci. Technol. B 1995, **13**, 1300–1306.

[176] Porter, M. D., Bright, T. B., Allara, D. L., Chidsey, C. E.. *Spontaneously Organized Molecular Assemblies. 4. Structural Characterization of n-Alkyl Thiol Monolayers on Gold by Optical Ellipsometry, Infrared Spectroscopy, and Electrochemistry* . J. Am. Chem. Soc. 1987, **109**, 3559–3568.

[177] Fenter, P., Eberhardt, A., Eisenberger, P.. *Self-Assembly of n-Alkyl Thiols as Disulfides on Au(111).* Science 1994, **266**, 1216–1218.

[178] Alessandrini, A., Facci, P.. *AFM: a versatile tool in biophysics*. Meas. Sci. Technol. 2005, **16**, R65–R92.

[179] Hamitl, O. P., Marty, A., Sakrnarm, E., Sigworth, F. J.. *Improved patch-clamp techniques for high-resolution current recording from cells and cell-free membrane patches.* Pfügers Arch. - Eur. J. Physiol. 1981, **391**, 85–100.

[180] Bakker, E., Pretsch, E.. *Modern Potentiometry*. Angew. Chem. Int. Ed. 2007, **46**, 5660–5668.

[181] Danker, T., Mazzanti, M., Tonini, R., Rakowska, A., Oberleithner, H.. *Using Atomic Force Microscopy to Investigate Patch-Clamped Nuclear Membrane*. Cell Biol. Int. 1997, **21**, 747–757.

[182] Lehmann-Horn, F., Jurkat-Rott, K.. *Nanotechnology for neuronal ion channels*. J. Neurol. Neurosurg. Psychiatry 2003, **74**, 1466–1475.

[183] Sun, P., Laforge, F. O., Mirkin, M. V.. *Scanning electrochemical microscopy in the 21st century*. Phys. Chem. Chem. Phys. 2007, **9**, 802–823.

[184] Lovat, V., Pantarotto, D., Lagostena, L., Cacciari, B., Grandolfo, M., Righi, M., Spalluto, G., Prato, M., Ballerini, L.. *Carbon Nanotube Substrates Boost Neuronal Electrical Signaling*. Nano Lett. 2005, **5**, 1107–1110.

[185] Mazzatenta, A., Giugliano, M., Campidelli, S., Gambazzi, L., Businaro, L., Markram, H., Prato, M., Ballerini, L.. *Interfacing Neurons with Carbon Nanotubes: Electrical Signal Transfer and Synaptic Stimulation in Cultured Brain Circuits*. J. Neurosci. 2007, **27**, 6931–6936.

[186] Benson, D. E., Conrad, D. W., de Lorimier, R. M., Trammell, S. A., Hellinga, H. W.. *Design of bioelectronic interfaces by exploiting hinge-bending motions in proteins*. Science 2001, **293**, 1641–1644.

[187] Blankespoor, R., Limoges, B., Schöllhorn, B., Syssa-Magalé, J. -., Yazidi, D.. *Dense Monolayers of Metal-Chelating Ligands Covalently Attached to Carbon Electrodes Electrochemically and Their Useful Application in Affinity Binding of Histidine-Tagged Proteins*. Langmuir 2005, **21**, 3362–3375.

List of Figures

Chapter 3

List of Tables